arXiv:0904.3507v1 [astro-ph.SR] 22 Apr 2009

A Large Sample Study of Red Giants in the Globular Cluster Omega Centauri (NGC 5139)

Christian I. Johnson[1], Catherine A. Pilachowski[1], R. Michael Rich[2], and Jon P. Fulbright[3,4]

ABSTRACT

We present abundances of several light, α, Fe–peak, and neutron–capture elements for 66 red giant branch (RGB) stars in the Galactic globular cluster Omega Centauri (ω Cen). Our observations lie in the range 12.0<V<13.5 and focus on the intermediate and metal–rich RGBs. Abundances were determined using equivalent width measurements and spectrum synthesis analyses of moderate resolution (R≈18,000) spectra obtained with the Blanco 4m telescope and Hydra multifiber spectrograph. Combining these data with previous work, we find that there are at least four peaks in the metallicity distribution function at [Fe/H]=–1.75, –1.45, –1.05, and –0.75, which correspond to about 55%, 30%, 10%, and 5% of our sample, respectively. Additionally, the most metal–rich stars are the most centrally located. Na and Al are correlated despite exhibiting star–to–star dispersions of more than a factor of 10, but the distribution of those elements appears to be metallicity dependent and are divided at [Fe/H]≈–1.2. About 40–50% of stars with [Fe/H]<–1.2 have Na and Al abundances consistent with production solely in Type II supernovae and match observations of disk and halo stars at comparable metallicity. The remaining metal–poor stars are enhanced in Na and Al compared to their disk and halo counterparts and are mostly consistent with predicted yields from >5 $M_\odot$ asymptotic giant branch (AGB) stars. At [Fe/H]>–1.2, more than 75% of the stars are Na/Al enhanced and may have formed almost exclusively from AGB ejecta. Most of these stars

[1]Department of Astronomy, Indiana University, Swain West 319, 727 East Third Street, Bloomington, IN 47405–7105, USA; cijohnson@astro.indiana.edu; catyp@astro.indiana.edu

[2]Department of Physics and Astronomy, UCLA, 430 Portola Plaza, Box 951547, Los Angeles, CA 90095-1547, USA; rmr@astro.ucla.edu

[3]Department of Physics and Astronomy, Johns Hopkins University, Baltimore, MD 21218, USA; jfulb@skysrv.pha.jhu.edu

[4]Visiting astronomer, Cerro Tololo Inter–American Observatory, National Optical Astronomy Observatory, which are operated by the Association of Universities for Research in Astronomy, under contract with the National Science Foundation.

are enhanced in Na by at least 0.2 dex for a given Al abundance than would be expected based on "normal" globular cluster values. All stars in our sample are α–rich with $\langle$[Ca/Fe]$\rangle$=+0.36 (σ=0.09) and $\langle$[Ti/Fe]$\rangle$=+0.23 (σ=0.14). The Fe–peak elements give solar–scaled abundances and similarly small dispersions with $\langle$[Sc/Fe]$\rangle$=+0.09 (σ=0.15) and $\langle$[Ni/Fe]$\rangle$=–0.04 (σ=0.09). Europium does not vary extensively as a function of metallicity and has $\langle$[Eu/Fe]$\rangle$=+0.19 (σ=0.23). However, [La/Fe] varies from about –0.4 to +2 and stars with [Fe/H]$\gtrsim$–1.5 have [La/Eu] values indicating domination by the s–process. A quarter of our sample have [La/Eu]$\geq$+1 and may be the result of mass transfer in a binary system. We conclude that the metal–rich population must be at least 1–2 Gyr younger than the metal–poor stars, owing to the long timescales needed for strong s–process enrichment and the development of a large contingent of mass transfer binaries.

Subject headings: stars: abundances, globular clusters: general, globular clusters: individual (ω Centauri, NGC 5139). stars: Population II

1. INTRODUCTION

Among all of the known Galactic globular clusters, Omega Centauri (ω Cen) is unique in the extent of its chemical enrichment. The cluster exhibits huge star–to–star abundance variations that are not limited solely to the light elements, as is the case for most "normal" globular clusters. Instead, ω Cen stars have [X/Fe][1] dispersions of 0.5 to more than 1.0 dex for many elements and span a metallicity range from [Fe/H]$\approx$–2.2 to nearly –0.5 (e.g., Norris & Da Costa 1995; Suntzeff & Kraft 1996; Smith et al. 2000; Johnson et al. 2008). Additionally, ω Cen's red giant branch (RGB) and subgiant branch (SGB) show 4–5 discrete populations in concert with multiple main sequences (Lee et al. 1999; Hilker & Richtler 2000; Pancino et al. 2000; van Leeuwen et al. 2000; Ferraro et al. 2004; Rey et al. 2004; Stanford 2004, 2006; Sollima et al. 2005a; Villanova et al. 2007). These data, along with the apparent age dispersion at the main sequence turnoff, suggest ω Cen underwent extensive self–enrichment and star formation over >1 Gyr.

While ω Cen has an estimated mass of $\sim$2–7$\times10^6$ $M_\odot$ (Richer et al. 1991; Meylan et al. 1995; van de Ven et al. 2006), it does not appear to have a particularly deep potential well compared to other lower mass clusters (Gnedin et al. 2002). Combined with the cluster's

[1]We make use of the standard spectroscopic notations where [A/B]$\equiv\log(N_A/N_B)_{star}-\log(N_A/N_B)_\odot$ and $\log\epsilon(A)\equiv\log(N_A/N_H)+12.0$ for elements A and B.

retrograde orbit and short disk crossing time ($\sim$1–2$\times10^8$ yrs; Dinescu et al. 1999), it seems unlikely that star formation could have occurred over several Gyrs in the cluster's current configuration. A proposed scenario is that ω Cen was once the nucleus of a dwarf spheroidal galaxy that was accreted and stripped apart via gravitational interaction with the Milky Way (e.g., Bekki & Norris 2006). If this is true, then the cluster was probably much more massive in the past.

Until recently, ω Cen was the only known globular cluster with multiple populations, but new observations (e.g., Piotto 2008) have indicated several of the more massive clusters in the Galaxy host at least two SGBs and/or main sequences despite being monometallic. These anomalous sequences are often interpreted as having large He enhancements ranging from Y$\sim$0.30–0.38, compared to the canonical He abundance of Y$\sim$0.25. This assumption applies to the blue main sequence in ω Cen as well, which is roughly 0.3 dex more metal–rich than the red main sequence and requires Y$\sim$0.38 to match the observations in this paradigm (Bedin et al. 2004; Norris 2004; Piotto et al. 2005). However, the important caveat remains that while the metallicity difference is *measured*, the He difference is only *inferred*. The source of these potential He enhancements remains unknown, but the most likely candidates include: 3–8 $M_\odot$ asymptotic giant branch (AGB) stars, super–AGB stars ($\sim$8–10 $M_\odot$), massive rotating stars, and population III stars (e.g., see Renzini 2008 for a review of this topic). Each of these scenarios poses a unique set of obstacles, but the basic problem is the difficulty in producing a discrete *population* of He–enriched stars while satisfying other chemical, age, and IMF constraints.

Globular cluster stars appear to have a more complex chemical history than their halo counterparts of similar metallicities, particularly with respect to the light elements oxygen through aluminum. In moderately metal–poor halo stars ($-2.0\lesssim$[Fe/H]$\lesssim-1.0$), these elements closely mimic the trends predicted for stars forming primarily out of gas polluted by core collapse supernovae (SNe; e.g., Timmes et al. 1995; Samland 1998; Nomoto et al. 2006). That is, the α elements remain enhanced at [α/Fe]$\sim$+0.40, but Na and Al, due to their secondary (i.e., metal–dependent) production, slowly increase relative to Fe with increasing metallicity. This is contrasted with the ubiquitous trends observed in globular clusters, which have stars with similar abundance patterns (the so–called "primordial" population) *and* stars showing signs of varying degrees of high temperature proton–capture processing (the "intermediate" and "extreme" populations; e.g., Kraft 1994; Gratton et al. 2004; Carretta et al. 2008). These tell–tale signs of additional processing are evidenced by the pervasive O–Na and Mg–Al anticorrelations along with the Na–Al correlation observed in all well–studied clusters to date, and are the result of processing in the ON, NeNa, and MgAl cycles (e.g., Gratton et al. 2004). Since these trends are observed in main sequence and turnoff stars (Cannon et al. 1998; Gratton et al. 2001; Cohen et al. 2002; Briley et al. 2004a; 2004b;

Boesgaard et al. 2005) as well as RGB stars, it seems likely that the chemical patterns were already imprinted in the gas from which the current generation of stars formed. The source of these abundance patterns is unknown, but intermediate mass AGB stars, which undergo hot bottom burning (HBB) at temperatures exceeding 80–100$\times10^6$ K and experience third dredgeup, are a popular choice because they do not alter [Fe/H], have low velocity ejecta, and produce large quantities of He, thus possibly alleviating some of the He enhancement issues mentioned above. While AGB stars are a qualitatively attractive solution, many problems arise in quantitative analyses and the ejecta yields are highly model dependent (e.g., Denissenkov & Herwig 2003; Fenner et al. 2004; Choi & Yi 2008; Ventura & D'Antona 2008). Other potential polluters include fast rotating massive stars (Decressin et al. 2007) and previous generations of slightly more massive RGB stars (Denissenkov & Weiss 2004); *In situ* deep mixing may also still play a role in highly evolved RGB stars.

In terms of chemical properties, ω Cen behaves similarly to Galactic globular cluster populations (aside from the large metallicity spread) in that the various light element relations and α enhancements are present in nearly all subpopulations analyzed so far (e.g., Norris & Da Costa 1995; Smith et al. 2000), but the cluster hosts stars of considerable Na/Al enrichment and O depletion. Unlike the field and disk populations that exhibit lower [α/Fe] ratios at [Fe/H]>–1, presumably due to the contributions of Type Ia SNe, the overwhelming majority of ω Cen stars at the same metallicity are α enhanced. This suggests that Type Ia SNe have played only a minor role in the cluster's chemical enrichment for all but perhaps the most metal–rich stars (Pancino et al. 2002; but see also Cunha et al. 2002). If ω Cen is the remnant of a former dwarf spheroidal galaxy then it has evolved much differently than present day dwarf galaxies because they do not show extreme light element enhancements/depletions and often exhibit subsolar [α/Fe] abundances (e.g., see review by Geisler et al. 2007). However, ω Cen does share the stronger s–process component seen in many dwarf spheroidal stars, except that the cluster stars more metal–rich than [Fe/H]$\sim$–1.5 show s–/r–process ratios indicating complete s–process dominance whereas the dwarf galaxies experienced much weaker s–process enrichment. This is in direct contradiction to globular clusters, which are r–process rich. Lower mass AGB stars ($\sim$1–4 M$_\odot$), which are thought to produce most of the s–process elements, have therefore had a much more significant effect on ω Cen's chemical evolution than is seen in dwarf spheroidals and globular clusters.

In this paper we present spectroscopic analyses of numerous light, α, Fe–peak, and neutron–capture elements for 66 stars spanning ω Cen's full metallicity range, with an emphasis on the lesser studied intermediate and metal–rich populations. We combine our results with those from the literature and compare ω Cen to the Galactic thin and thick disk, halo, bulge, other globular clusters, and nearby dwarf spheroidals in an attempt to disentangle the evolution of these very different populations and perhaps isolate chemical signatures that

are unique to each subpopulation in ω Cen.

2. OBSERVATIONS AND REDUCTIONS

All observations were taken at the Cerro Tololo Inter-American Observatory on 2006 May 26 and 2006 May 27 using the Blanco 4m telescope and Hydra multifiber spectrograph. In each configuration we used the "large" 300μm (2$''$) fibers and obtained spectra with two different bench spectrograph setups. The first setup was centered near 6670 Å and spanned approximately 6530–6800 Å while the second setup was centered on 6125 Å and ranged from 6000–6250 Å. Both spectrograph setups employed the 100μm slit mask along with the 400 mm Bench Schmidt Camera and 316 line mm^{-1} echelle grating to achieve a resolving power of R($\lambda/\Delta\lambda$)$\approx$18,000 (0.35 Å FWHM).

Target stars, coordinates, photometry, and membership probabilities were taken from the proper motion study by van Leeuwen et al. (2000). The targets were chosen to be on the upper third of the giant branch and all have V<14.0, but priority was given to those with larger B–V indices (i.e., more metal–rich) in the Hydra assignment code. Stars with membership probabilities <70% were excluded from the fiber assignment process. While we did not measure radial velocities for the target stars, cluster members were easily discerned from the field star population because of ω Cen's comparatively large radial velocity ($\langle V_R \rangle \sim$232 km s^{-1}; Reijns et al. 2006).

We obtained 3, 1800 second exposures for each spectrograph setup with 92 fibers placed on targets. The co–added signal–to–noise (S/N) ratios of the spectra ranged from $\sim$25–200, but we only analyzed stars for which the S/N was $\gtrsim$50. The final sample includes 66 stars and are shown in Figure 1 along with the data from Johnson et al. (2008) and the full sample of van Leeuwen et al. (2000).

Since ω Cen exhibits such a large range in metallicity and the various giant branches contain stars in different ratios, selection effects may be more prominent than for typical globular clusters. In Figure 2 we show the observed completion fractions of our current data combined with Johnson et al. (2008) as a function of both V magnitude and B–V color. While there was little increase in the completion fraction for stars with 11.0<V<12.0, those with 12.0<V<13.5 increased $\sim$5-10% and similar additions are seen in B–V ranging from 1.15 to 1.55. We now have data that are at least uniformly representative across a wide range of temperatures and luminosities; however, the sample is still weighted towards observing more stars in the most metal–poor population. Since the new observations preferentially target stars with metallicities in the range –1.50$\lesssim$[Fe/H]$\lesssim$–0.50, the increased H$^-$ opacity

and line blocking with increasing metallicity causes these stars to have lower flux in the spectral regions of interest than their more metal–poor counterparts. As a result, stars observed in progressively more metal–rich branches are, on average, more evolved with our magnitude cutoff.

There is some evidence for the presence of a radial metallicity gradient in the cluster (Norris et al. 1996, 1997; Suntzeff & Kraft 1996; Hilker & Richtler 2000; Pancino et al. 2000; Rey et al. 2004; Johnson et al. 2008), and it is important to observe stars at various radii to measure the true metallicity distribution. In Figures 3 and 4 we plot the positions of our program stars and show a normalized cumulative distribution as a function of distance from the cluster center, defined by van Leeuwen et al. (2000) as $13^{h}26^{m}45.9^{s}$, $-47°28'37.0''$ (J2000). Both figures indicate our combined sample from this study and Johnson et al. (2008) mostly covers stars between $\sim$5–15′ from the center, which is equivalent to roughly 3.5 to 10.5 core radii where the core radius is 1.40′ (Harris 1996; rev. 2003 February). Fiber positioning limitations and increasing stellar densities near the cluster core prevent us from obtaining copious observations inside $\sim$1–2′ from the center, but we have observed nearly 30–40% of all bright giants inside 10–20′.

Data reductions were carried out using various tasks provided in standard IRAF[2] packages. We used *ccdproc* to trim the overscan region and apply the bias level corrections. Flat–field corrections, ThAr lamp wavelength calibrations, cosmic ray removal, subtraction of scattered light and sky spectra, and extraction of the one–dimensional spectra were performed using the *dohydra* package. The resultant spectra were then corrected for telluric contamination, continuum flattened, and combined.

3. Analysis

We have derived abundances for nine different elements using local thermodynamic equilibrium (LTE) equivalent width and spectrum synthesis analyses in the combined spectral regions of 6000–6250 Å and 6530–6800 Å. Spectrum synthesis was used for determining all Al abundances because of the potential for CN contamination in metal–rich and CN–strong stars. Model atmosphere parameters including effective temperatures (T_{eff}), surface gravities (log g), and microturbulence (V_t) were estimated based on published photometry and the empirical V_t–T_{eff} relation given in Johnson et al. (2008).

[2]IRAF is distributed by the National Optical Astronomy Observatories, which are operated by the Association of Universities for Research in Astronomy, Inc., under cooperative agreement with the National Science Foundation.

3.1. Model Stellar Atmospheres

Effective temperatures were estimated via empirical calibrations of V and 2MASS photometry based on the infrared flux method (Blackwell & Shallis 1977). To improve accuracy, we averaged the T_{eff} values obtained through the color–temperature relations of Alonso et al. (1999; 2001) and Ramírez & Meléndez (2005) for V–J, V–H, and V–K color indices. The photometry was corrected for interstellar reddening and extinction using the corrections recommended by Harris (1996) of E(B–V)=0.12 and McCall (2004) for E(V–J)/E(B–V)=2.25, E(V–H)/E(B–V)=2.55, and E(V–K)/E(B–V)=2.70. Evidence for differential reddening is mainly concentrated near the core (Calamida et al. 2005; van Loon et al. 2007), but the well defined evolutionary sequences seen in Villanova et al. (2007) suggest significant differential reddening is unlikely. Therefore, we have applied a uniform reddening correction to all stars. The temperatures derived from each color index are in very good agreement with an average offset of 21 K (σ=6 K). Our adopted T_{eff} values are probably accurate to within ±50 K, and are consistent with the star–to–star scatter seen in the calibrations of both studies. Plotting Fe abundance versus excitation potential did not reveal any trends and our adopted photometric temperatures satisfied excitation equilibrium.

Surface gravity was determined by T_{eff} and absolute bolometric magnitude (M_{bol}) through the standard relation,

$$log(g_*) = 0.40(M_{bol.} - M_{bol.\odot}) + log(g_\odot) + 4(log(T/T_\odot)) + log(M/M_\odot). \quad (1)$$

We applied the bolometric correction to M_V from Alonso et al. (1999) and used a distance modulus of $(m–M)_V$=13.7 (van de Ven et al. 2006). As mentioned in §1, an age spread of ∼1–4 Gyr is likely present in the cluster, but the difference in mass between the oldest and youngest stars is only of order ∼0.05 $M_\odot$, which is negligible for surface gravity determinations. Norris et al. (1996) argue that 20–40% of stars on the RGB may be AGB stars with M∼0.60 $M_\odot$, but this would only lead to abundance uncertainties of order 0.10 dex for species residing in the dominant ionization state (e.g., Fe II). Similar surface gravity and abundance effects may be expected for He–rich stars, which have slightly lower RGB masses due to their shorter lifetimes compared to He–normal stars (e.g., Newsham & Terndrup 2007).

Since we only had a limited number of singly ionized lines available for analysis relative to the number of neutral lines, we relied on the photometric surface gravity estimate instead of ionization equilibrium. In the top panel of Figure 5, we show the differences in derived abundance for neutral and singly ionized species of Fe, Sc, and Ti. For Fe, the average offset between log ϵ(Fe I) and log ϵ(Fe II) is –0.09 (σ=0.12), but this is based on a highly discrepant number of lines between the two species and thus may not accurately reflect a systematically

low gravity. Sc shares a similar pattern with an average difference of –0.16 dex (σ=0.22), but these are based on only one line a piece for each species and reliable hyperfine structure information for these transitions is sparse. Ti I and II lines give an average difference of –0.01 dex (σ=0.18). Overall, the difference between abundances derived from both species is –0.07 dex (σ=0.17), which is comparable to measurement and model uncertainties. In the bottom panel of Figure 5, we show photometric log g values compared with estimates based on spectroscopic gravity calibrations of globular clusters provided by Kučinskas et al. (2006). The average offset between the two systems is +0.04 dex (σ=0.17), and is comparable to the uncertainty found by examining ionization equilibrium. This leads us to believe our surface gravity estimates are not in serious error.

We obtained a rough estimate of [Fe/H] using the [Ca/H] calibration based on V and B–V given in van Leeuwen et al. (2000; their equation 15) and assumed [Ca/Fe]$\sim$+0.30. Likewise, an initial microturbulence value was calculated from the V_t–T_{eff} relation given in Johnson et al. (2008) for luminous giants. Our determined T_{eff}, log g, [Fe/H], and V_t values were used to generate model atmospheres (without convective overshoot) via interpolation within the ATLAS9[3] grid (Castelli et al. 1997). We iteratively adjusted the microturbulence of the model until Fe abundances were independent of line strength following the method described in Magain (1984). Lastly, the model's metallicity was adjusted to match the derived Fe abundance of each star. A complete list of our adopted model atmosphere parameters along with star identifiers, published photometry, membership probabilities, and S/N estimates for each spectrum are provided in Table 1.

3.2. Derivation of Abundances

3.2.1. Equivalent Width Analysis

For all elements except Al, final abundances were determined using equivalent width analyses and the *abfind* driver in the LTE line analysis code MOOG (Sneden 1973). Equivalent widths were measured by interactively fitting multiple Gaussians to isolated and blended line profiles. Suitable lines were identified using the solar and Arcturus atlases[4]. Our adopted log gf values were determined by measuring equivalent widths in the solar atlas and then modified until all lines yielded abundances consistent with the photospheric values given in

[3]The model atmosphere grids can be downloaded from http://cfaku5.cfa.harvard.edu/grids.html.

[4]The atlases can be downloaded from the NOAO Digital Library at http://www.noao.edu/dpp/library.html.

Anders & Grevesse (1989). A summary of our line list and measured equivalent widths is given in Tables 2a–2f and the final abundances are in Table 3. Note that all abundance ratios in Table 3 are relative to $[Fe/H]_{avg.}$, which is the average of [Fe I/H] and [Fe II/H] or just [Fe I/H] if Fe II lines are not available. We did not determine [X/Fe] ratios by matching ionization states because many stars did not have reliable Fe II transitions, our typical measured [Fe I/H] values are based on more than 25 lines versus 1 or 2 for [Fe II/H], and ⟨[Fe I/H]–[Fe II/H]⟩ is approximately equal to the line–to–line dispersion seen in our [Fe I/H] determinations. Giving [X/Fe] ratios relative to $[Fe/H]_{avg.}$ is an attempt to minimize the effects of overionization.

Many line profiles for the odd–Z Fe–peak and neutron capture elements suffer from hyperfine splitting, but the necessary atomic data for several of these transitions are not currently available in the literature. A standard equivalent width analysis will produce an overabundance if this effect is not properly taken into account. Since the error caused by hyperfine splitting increases with line strength, we do not expect our abundances, which are based on unsaturated and generally weak lines, to be strongly affected.

The elements here that may be affected by hyperfine splitting are Sc, La, and Eu. Our Sc abundances are based on the 6210.67 Å Sc I line and 6604.60 Å Sc II line. While hyperfine structure estimates have been produced for Sc II (Prochaska & McWilliam 2000), there is no available information for the Sc I line and neither of these transitions is included in Zhang et al. (2008). Therefore, we have not applied the correction to Sc II, but the offset is probably not too large given that the average equivalent width for the Sc I/II lines is ∼60 mÅ. Similarly, no hyperfine data exist for the 6774.27 Å La II line and therefore we accept the derived abundances at face value. Europium is slightly more complicated because, in addition to hyperfine splitting, it has two stable, naturally occurring isotopes (^{151}Eu and ^{153}Eu) that are present in nearly equal proportions. For all Eu abundances, we have applied a hyperfine and isotopic line list provided by C. Sneden (2006, private communication). Lacking *a priori* knowledge of the r–/s–process contributions for La and Eu in ω Cen, we have assumed a solar mix such that the ratio for La is 25/75% (Sneden et al. 2008) and for Eu 97/3% (Sneden et al. 1996), respectively.

3.2.2. Spectrum Synthesis Analysis

While all other abundances were determined using equivalent width analyses, we derived Al abundances via spectrum synthesis because of the non–trivial contamination from CN lines seen in many of the cooler, more metal–rich stars. For consistency, spectrum synthesis was performed even in cases where CN contamination was not an issue. In Figure 6 we show

two sample syntheses for a case with strong (top panel) and weak (bottom panel) CN lines in order to illustrate the line blanketing effects from molecular absorption. For stars where the CN lines were present, we found that a straight–forward equivalent width analysis led to an over estimate of log ϵ(Al) by as much as 0.1–0.2 dex compared to spectrum synthesis, but the two methods agreed to within <0.1 dex in spectra without strong CN features. The Al lines are designated by "synth" in Tables 2a–2f.

We created the molecular line list by combining the Kurucz online database[5] with one provided by B. Plez (private communication, 2007; see also Hill et al. 2002). Since the C, N, and ^{12}C/^{13}C abundances are unknown, we fixed [C/Fe]=–0.5 and ^{12}C/^{13}C=4, which are consistent with Norris & Da Costa (1995) and Smith et al. (2002) for ω Cen giants. Without accurate C, N, and O data, it is impossible to constrain the molecular equilibrium equations and derive true C and/or N abundances for CN. Therefore, we treated the nitrogen abundance as a free parameter and adjusted it to obtain a best fit to the CN lines. Other metal lines surrounding the Al doublet have excitation potentials $\gtrsim$5 eV and are not important contributors in these cool stars.

3.2.3. Abundance Comparison to Other Studies

Although ω Cen has been the subject of many spectroscopic studies, here we restrict comparison to those measuring abundances using moderately high resolution (R$\gtrsim$15,000) spectroscopy. The only two previous works for which we have several stars in common are Norris & Da Costa (1995) and Johnson et al. (2008). In the case of Norris & Da Costa, the average difference in measured [Fe/H] for the 7 common stars is –0.02 dex (σ=0.05), in the sense present minus Norris & Da Costa. The results are similar for most of the other elements with average differences of order ±0.10 dex ($\sigma\sim$0.15), and La is the only exception with an average offset of +0.34 (σ=0.12). This discrepancy is likely due to the difficulty in obtaining accurate La abundances. In comparison to Johnson et al. (2008), the difference in [Fe/H] based on 21 stars in common is –0.10 dex (σ=0.05) and 0.00 dex (σ=0.22) for [Al/Fe]. These results are consistent with the small deviations in adopted atmospheric parameters found by Johnson et al. (2008; see their Figures 8–9) comparing that study to other spectroscopic surveys in the literature.

[5]The Kurucz line lists can be accessed at: http://kurucz.harvard.edu/linelists.html.

3.3. Abundance Sensitivity to Model Atmosphere Parameters

In Table 4, we show the results of our tests regarding abundance sensitivity to uncertainties in adopted model atmosphere parameters for all elements studied here. We examined how the various log ϵ(X) values changed when altering $T_{eff}\pm100$ K, log g±0.30 cm s^{-2}, [M/H]±0.30 dex, and $V_t\pm0.30$ km s^{-1}. In general, we find that the neutral species tend to be more strongly affected by changes in temperature, but the singly ionized species are influenced by surface gravity changes because of their dependence on electron pressure. However, abundances taken from singly ionized transitions tend to have a larger dependence on T_{eff} with increasing metallicity while the effects on neutral lines are mitigated. Similarly, only the ionized species have a significant dependence on the model atmosphere's overall metallicity because their line–to–continuous opacity ratios are more sensitive to changes in the H^- abundance. For stars with [Fe/H]$\lesssim$–1, microturbulence uncertainties have very little influence on the derived abundance because the lines are weak and lie further down the linear portion of the curve of growth, but even in the most metal–rich stars the effects are typically no larger than $\pm$0.10–0.15 dex. The lanthanum line is an exception because the more metal–rich ω Cen stars are very s–process rich and thus the La II lines typically have equivalent widths $\gtrsim$75 mÅ. Although each element has a slightly different dependence on these physical parameters, the important point is that the element–to–iron ratio should be mostly invariant. Instead, only the log ϵ(X) values should be sensitive to model parameter variations.

As mentioned in §1, it has been argued that several of the intermediate and perhaps metal–rich stars in this cluster may have strong He enhancements extending as large as Y$\sim$0.38. We do not expect our analysis to be severely altered (see Girardi et al. 2007) and the [X/Fe] ratios should be mostly independent of the adopted He abundance; however, [Fe/H] may be systematically higher in the He–rich stars. To test the effects of He enhancement, we created synthetic spectra using He–normal (Y=0.27) and He–rich (Y=0.35) ATLAS9 models of comparable temperature and metallicity to our stars. We found the line strength differences between the two sets to be much less than 1%, with the He–rich model producing stronger lines because of decreased continuous H^- opacity. This result is consistent with Piotto et al. (2005) and leads us to believe our abundances are robust against possible He variations.

4. RESULTS

4.1. Light elements: Na & Al

The odd–Z elements Na and Al are particularly important because they are among the heaviest elements thought to be produced via proton–capture nucleosynthesis in low and intermediate mass stars. This makes them useful probes for deciphering which processes, in addition to Type II SN production, may have been dominant during various epochs of star formation. Previous large sample, high resolution spectroscopic studies of ω Cen giants (e.g., Norris & Da Costa 1995; Smith et al. 2000; Johnson et al. 2008) have shown that Na and Al (in addition to C, N, O, and Mg) exhibit very large star–to–star [X/Fe] variations while preserving the Na–Al correlation seen in other Galactic globular clusters. The top two panels of Figure 7 illustrate this point by demonstrating the stark contrast in Na and Al line strengths for stars with similar temperatures and metallicities. Since we can compare stars of similar evolutionary state and metallicity, we can safely assume departures from LTE are not the cause of the observed abundance variations. No NLTE corrections have been applied to our Na and Al results because there are no "standard" values available in the literature and those that are available disagree in magnitude and sign. However, Na and Al abundances determined from the non–resonance, subordinate transitions used here typically have corrections of order $\lesssim$0.20 dex for stars with –2.5<[Fe/H]<–0.5 (e.g., Gratton et al. 1999; Gehren et al. 2004).

First considering our Na results, we find that there is a general increase in $\langle$[Na/Fe]$\rangle$ as a function of increasing metallicity accompanied by a decrease in the star–to–star scatter. The dominant metallicity group of stars (–1.8$\lesssim$[Fe/H]$\lesssim$–1.6) have $\langle$[Na/Fe]$\rangle$=+0.03 (σ=0.32) with a full range of 1.29 dex while the next population of stars (–1.5$\lesssim$[Fe/H]$\lesssim$–1.3) have $\langle$[Na/Fe]$\rangle$=+0.20 (σ=0.21) and a full range of 0.67 dex, which is smaller by about a factor of 4. However, there is a noticeable change in the distribution of [Na/Fe] for RGB stars in the higher metallicity populations. At [Fe/H]$\gtrsim$–1.2, 95% (18/19) of the stars are very Na–rich with $\langle$[Na/Fe]$\rangle$=+0.86 (σ=0.12). The strong enrichment of this population is in agreement with Norris & Da Costa (1995) who find that at least 75% (6/8) of stars in that metallicity range are Na–rich and at least 50% are O–poor. A two–sample Kolmogorov–Smirnov (K–S) test (Press et al. 1992) shows that the population of stars with [Fe/H]<–1.2 is drawn from a different parent population than the [Fe/H]>–1.2 group at the 99% level.

By combining our current data with that of Johnson et al. (2008), we have a homogeneous set of [Al/Fe] abundances determined for more than 200 RGB stars. In Figure 8 we show the results of our combined samples for [Al/Fe] and log ϵ(Al) as a function of metallicity. Although the sample sizes between Na and Al differ by a factor of 3.5, some key

differences standout in the Al data set: (1) there appear to be 2 or 3 different populations of stars, (2) the star–to–star dispersion stays mostly constant until [Fe/H]$\sim$–1.2, and (3) stars with [Fe/H]$\gtrsim$–1.2 show a roughly constant log ϵ(Al)$\approx$6.22 (σ=0.18) as a function of increasing [Fe/H]. However, there are some interesting similarities: (1) the Al data show a clear change in the abundance pattern for stars with [Fe/H]$\gtrsim$–1.2, (2) the metal–rich RGB stars are predominantly Al–rich, and (3) log $\epsilon(\mathrm{Na})_{\mathrm{max}}\approx$log $\epsilon(\mathrm{Al})_{\mathrm{max}}$. It should be noted that despite the large abundance scatter, the Na–Al correlation is present in our data.

We define the three different Al populations as those having [Al/Fe]<+0.60, +0.60$\leq$[Al/Fe]<+1.0, and [Al/Fe]$\geq$+1.0. First considering only stars with [Fe/H]<–1.2, the subpopulations break down into $\langle$[Al/Fe]$\rangle$=+0.34 (σ=0.14), $\langle$[Al/Fe]$\rangle$=+0.82 (σ=0.10), and $\langle$[Al/Fe]$\rangle$=+1.17 (σ=0.11), respectively. These represent 50% (83/166), 30% (49/166), and 20% (34/166) of the cluster stars in this metallicity regime. Extending this break down to the entire sample gives a similar distribution of 48% (96/202), 34% (69/202), and 18% (37/202), respectively. This distribution is perhaps tied to the "primordial", "intermediate", and "extreme" populations of the O–Na anticorrelation (Carretta et al. 2008). However, only the intermediate Al subpopulation is present at all metallicities. The very enhanced Al stars ([Al/Fe]>+1) are only found at [Fe/H]$\lesssim$–1.2, and the sequence of low–Al stars ([Al/Fe]<+0.60) essentially terminates at about the same metallicity cut–off (this is particularly evident in the bottom panel of Figure 8). A two–sample K–S test confirms the same result as the Na case, which is that the [Al/Fe] distribution for stars with [Fe/H]>–1.2 and [Fe/H]<–1.2 are different at the 94% level.

These data suggest that ω Cen's metal–rich populations may be significantly more chemically homogeneous than the metal–poor (and presumably older) populations, but the gas from which the metal–rich stars formed was enhanced in light elements at a level beyond what is thought to be possible from Type II SNe (e.g., Woosley & Weaver 1995; Chieffi & Limongi 2004). Evidently, at high metallicity it is possible to produce Na in greater quantities than Al.

4.2. α elements

The α elements are often used to gauge the relative contributions from Type II SNe, which are efficient producers of α elements, and Type Ia SNe, which produce mostly Fe–peak elements. Predicted stellar yields from core collapse SNe weighted by a Salpeter initial mass function (IMF; x=1.35) produce [α/Fe]$\sim$+0.30 to +0.50 across a broad range of metallicities (e.g., Chieffi & Limongi 2004). Therefore, values of [α/Fe]$\sim$+0.10 or less suggest Type Ia SNe have contributed some portion of the Fe–peak elements. The most commonly measured α

elements are O, Mg, Si, Ca, and Ti; however, Ti is more complicated because it has multiple production sources. In globular clusters, a large portion of the stars have had their O and Mg abundances altered by proton–capture nucleosynthesis and therefore these elements cannot be treated as "pure" α elements. This restricts discussions regarding α enhancement to the heavier elements.

Previous studies of ω Cen and other globular clusters have shown nearly all stars to be α enhanced at [α/Fe]$\sim$+0.40 with very small star–to–star scatter (e.g., see review by Gratton et al. 2004). Our results are consistent with previous work and give $\langle$[Ca/Fe]$\rangle$=+0.36 (σ=0.09). Although Ti may straddle being classified as an α or Fe–peak element, the stars in our sample are mostly Ti–enhanced with $\langle$[Ti/Fe]$\rangle$=+0.23 (σ=0.14). We do not find any stars to be α–poor and our lowest derived value is [Ca/Fe]=+0.17, but a handful of α–poor stars have been found in this cluster (e.g., Norris & Da Costa 1995; Smith et al. 1995, 2000; Pancino et al. 2002). We do not find any trend in [Ca/Fe] with [Fe/H], which is in contrast to the results of Pancino et al. (2002) who find the most metal–rich stars to be α–poor. However, there is real scatter in [α/Fe] in this cluster as is evident in the Si and Ca line strength variations seen in the top panel of Figure 7. In any case, larger sample sizes are required to settle this issue, but it seems that the majority of ω Cen stars are α–rich and thus Type Ia SNe have not contributed much to the [X/Fe] ratios. This is a significant problem from a chemical evolution standpoint because either the ejecta from Type Ia SNe were preferentially lost or their presence was suppressed despite a several Gyr timespan in star formation.

4.3. Fe & Fe–peak elements

As mentioned above, Fe–peak elements are produced in both Type II and Type Ia SNe in copious amounts and are the most commonly used tracers of metallicity in stars. These elements are produced in similar conditions during the late stages of stellar evolution and as a result often track together as a function of overall metallicity. Aside from Fe, the other Fe–peak elements analyzed here reproduce this trend with $\langle$[Sc/Fe]$\rangle$=+0.09 (σ=0.15) and $\langle$[Ni/Fe]$\rangle$=–0.04 (σ=0.09). In both cases, there is no trend in [X/Fe] with [Fe/H]. However, since ω Cen hosts multiple stellar populations, the behavior of [Fe/H] is not as simple as most monometallic globular clusters.

Large sample spectroscopic and photometric observations of ω Cen (e.g., Norris & Da Costa 1995; Suntzeff & Kraft 1996; van Leeuwen et al. 2000; Rey et al. 2004; Sollima et al. 2005a; Villanova et al. 2007; Johnson et al. 2008) have shown that the cluster hosts multiple populations of stars with almost no stars being more metal–poor than [Fe/H]=–2,

more than half having [Fe/H]≈–1.7, and the rest forming a high metallicity tail extending to [Fe/H]∼–0.5. Again combining our new results with those from Johnson et al. (2008), we have a homogeneous set of spectroscopically determined [Fe/H] abundances for 228 RGB stars. In Figure 9 we show a histogram of our combined sample and our results are consistent with the cluster having multiple peaks in the metallicity distribution function at [Fe/H]=–1.75, –1.45, –1.05, and –0.75. These peaks constitute roughly 55%, 30%, 10%, and 5% of our observations, respectively. The percentage of stars contained in each population is nearly identical between our entire sample and a subset having the highest completion fraction (V≤12.5). This leads us to believe our full sample is representative of the entire cluster population.

In addition to ω Cen being chemically diverse, there is some evidence for a cluster metallicity gradient such that the inner regions contain most of the metal–rich stars (e.g., Suntzeff & Kraft 1996; Norris et al. 1996 Hilker & Richtler 2000; Pancino et al. 2003; Johnson et al. 2008). These results are confirmed in photometric studies (e.g., Rey et al. 2004), which show that the anomalous, metal–rich RGB (RGB–a) is found only near the core of the cluster. In Figure 10, we plot log ϵ(Fe) versus distance from the cluster center. We find that the most metal–rich stars are mostly located inside 10′, but the metal–poor stars are located uniformly throughout the cluster. The inset plot in Figure 10 shows that the median metallicity stays constant at about log ϵ(Fe)=6.0 ([Fe/H]≈–1.5) at all radii, but the metallicity interquartile and full ranges decrease at large radii. There has been speculation that, in addition to these spatial anomalies, the various cluster populations may exhibit unique kinematic signatures as the result of the cluster formation process (e.g., Norris et al. 1997; Sollima et al. 2005b). However, recent larger sample studies seem to indicate none of ω Cen's subpopulations exhibit rotational, proper motion, or radial velocity anomalies (Reijns et al. 2006; Pancino et al. 2007; Johnson et al. 2008; Bellini et al. 2009). These new results seem to negate the merger and background cluster superposition scenarios.

4.4. Neutron–capture elements

Most elements heavier than the Fe–peak are produced via successive neutron captures on seed nuclei, but a limited number of these elements have optical atomic transitions. In the metallicity regime considered here, Ba and La are often the primary tracers of the main s–process component and Eu the primary tracer of the r–process. As previously mentioned, nearly all globular clusters are r–process rich with [Eu/Ba,La]≈+0.25 (e.g., Gratton et al. 2004), but previous studies have shown that ω Cen has very strong s–process enhancement, especially at [Fe/H]$\gtrsim$–1.5 (e.g., Francois et al. 1988; Norris & Da Costa 1995; Smith et al.

1995, 2000). We find in agreement with previous studies that most ω Cen stars more metal–rich than [Fe/H]$\sim$–1.7 are strongly s–process enriched based on [La/Eu] ratios approaching and exceeding +0.8. While the most metal–poor stars have $\langle$[La/Eu]$\rangle$=–0.02, this value rises to $\langle$[La/Eu]$\rangle$=+0.49 by [Fe/H]$\sim$–1.4 meaning that [La/Eu] increases by more than a factor of 3 during a span in which [Fe/H] increases by a factor of 2. However, we find that $\langle$[La/Fe]$\rangle$ does not increase appreciably at metallicities exceeding [Fe/H]$\sim$–1.2 (excluding possible Ba–stars), but all stars in our sample with [Fe/H]>–1.2 have [La/Fe]>+0.5 and abundance patterns dominated by the s–process. This trend is not shared by Eu, which remains mostly constant at $\langle$[Eu/Fe]$\rangle$=+0.19 (σ=0.23) at all metallicities. We have also found that 25% (15/60) of our sample may qualify as Ba–stars with [La/Fe]$\geq$+1.0. The most extreme case is star LEID 45358, which has [La/Fe]=+2.03 and [La/Eu]=+1.81. For stars in common between the two samples, van Loon et al. (2007) found these to have large Ba4554 indices indicating they are Ba–rich as well.

5. DISCUSSION

5.1. Chemical Enrichment in ω Cen

Spectroscopic and photometric analyses of ω Cen stars have revealed a system hosting a complex past. The cluster metallicity apparently increased from [Fe/H]$\approx$–2.2 to [Fe/H]$\approx$–0.5 over roughly 2–4 Gyrs (e.g., Stanford et al. 2006) and ω Cen has experienced a handful of discrete star formation events. The metallicity distribution peaks in our data agree with those found in the literature and correspond to the "MP" ([Fe/H]$\sim$–1.7), "MINT2" ([Fe/H]$\sim$–1.4), "MINT3" ([Fe/H]$\sim$–1.0), and "SGB–a" ([Fe/H]$\sim$–0.6) populations found on the SGB by Sollima et al. (2005b). However, these classifications are not as well–defined on the main sequence and show considerable complexity (e.g., Bedin et al. 2004; Piotto et al. 2005; Villanova et al. 2007). The apparent kinematic homogeneity of the various stellar populations (e.g. Pancino et al. 2007; Bellini et al. 2009) suggests most, if not all, of the cluster's chemical enrichment is the result of internal processes rather than a product of multiple merger events. However, the paucity of stars more metal–poor than [Fe/H]$\sim$–2 means the nascent gas from which the primary population formed was already considerably polluted by massive star ejecta. One of the most striking results discovered so far is that the second most metal–poor stellar population ([Fe/H]$\sim$–1.4; and perhaps the subsequent more metal–rich stars) may have experienced both a huge increase in He content (dY/dZ$\sim$70; Piotto et al. 2005) and an equally impressive increase in s–process element abundances compared to the primary population ([Fe/H]$\sim$–1.7), which contains more than half of all ω Cen stars. Somehow these events took place while preserving the various light element

correlations observed in other globular clusters that do not (in general) have large He and metallicity variations and lack strong s–process signatures. Since the combined Johnson et al. (2008) and current data sets allow us to probe various production sources, we turn now to what our current data add to ω Cen's puzzling past.

5.1.1. Supernova Pollution

The majority of elements heavier than Li are produced during various quiescent and explosive nucleosynthetic events in $\gtrsim$11 $M_\odot$ stars (Woosley & Weaver 1995). These processes, which occur within $\lesssim 20\times10^6$ years after the onset of star formation, are known to produce an overabundance of α elements by about a factor of two relative to the solar α/Fe ratio. In addition, massive stars also produce varying amounts of the odd–Z light elements (e.g., C through Al) with metallicity dependent yields of $-0.5\lesssim$[X/Fe]$\lesssim+0.3$ in the metallicity regime covered by ω Cen stars (e.g., Woosley & Weaver 1995; Chieffi & Limongi 2004; Nomoto et al. 2006). Although the final abundances of Fe–peak elements are dependent on the explosion energy and mass–cut, they generally track closely to Fe. These stars inevitably produce some neutron capture elements as well, but only the lower mass SNe ($\sim$8–11 $M_\odot$) are believed to be significant r–process contributors (e.g., Mathews & Cowan 1990; Cowan et al. 1991; Wheeler et al. 1998), while low mass AGB stars ($\sim$1–4 $M_\odot$) seem the best candidates for s–process production (e.g., Busso et al. 1999).

In contrast, mass transfer Type Ia SNe may take anywhere from 500×10^6 to more than 3×10^9 years to evolve (e.g., Yoshii et al. 1996) and could have difficulty forming in low metallicity ([Fe/H]<-1) environments (Kobayashi et al. 1998). Nucleosynthesis calculations have shown that these SNe predominantly produce Fe–peak elements and only trace amounts of α and light elements (Nomoto et al. 1997). It is estimated that Type Ia SNe have produced at least 50% of the total ^{56}Fe in the Galaxy and their onset is believed to be the primary cause for the decline in [α/Fe] at [Fe/H]>-1 in the disk and halo populations. It is for this reason that the [α/Fe] ratio is often used as a diagnostic to test the presence of Type Ia SNe in a stellar system.

While there have been some α–poor stars found in ω Cen's most metal–rich population (Pancino et al. 2002), the general trend of enhancement in the α elements suggests a majority of the cluster's chemical evolution occurred before Type Ia SNe had time to evolve. Determining whether or not Type Ia SNe can form in metal–poor environments could help place additional constraints on ω Cen's evolutionary timescale. If the lower limit of [Fe/H]~-1 estimated by Kobayashi et al. (1998) is correct and only the most metal–rich population in the cluster is affected by Type Ia SNe ejecta, then this would imply an age difference

between the [Fe/H]$\sim$–1 and [Fe/H]$\sim$–0.7 groups of $\lesssim$1 Gyr. However, if this limit is at a much lower metallicity, then the cluster would have had to evolve on a much shorter time scale.

In Figures 11–13 we show the evolution of all elements measured in this study as a function of [Fe/H] along with those available in the literature for ω Cen, the Galactic disk, bulge, halo, globular clusters, and nearby dwarf spheroidal galaxies (see Table 5 for data references). From these data we have confirmed: (1) a more than 1.0 dex spread exists for [Na/Fe] and [Al/Fe] and the two elements are correlated, (2) the α elements are enhanced by about a factor of two at all metallicities with small star–to–star scatter, (3) there are at least four different metallicity peaks (see also Figure 9) at [Fe/H]=–1.75, –1.45, –1.05, –0.75 with internal dispersions of $\sim$0.10 dex in each subpopulation, and (4) there is a large s–process component that manifests itself in the intermediate and metal–rich populations of the cluster. As is the case for other globular clusters, the larger star–to–star variations seen in the light and neutron–capture elements versus the α and Fe–peak elements suggest additional production (or destruction) sources other than core collapse SNe. We know that, at least for the light elements, the observed inhomogeneity is not due to incomplete mixing of SN ejecta because the Na/Al enhanced stars are also O–poor (e.g., Norris & Da Costa 1995; Smith et al. 2000).

If massive stars cannot account for all of the observed abundance anomalies in ω Cen, then how much can they account for? At least in stars with [Fe/H]<–1, Type II SNe are responsible for producing nearly all of the α and Fe–peak elements. However, IMF weighted theoretical yields of SNe with initial metallicities in the range –2<[Fe/H]<–0.5 (e.g., Woosley & Weaver 1995; Chieffi & Limongi 2004; Nomoto et al. 2006) produce values roughly consistent with those observed in the disk, halo, and bulge (i.e., $\langle$[Na/Fe]$\rangle\sim$0; $\langle$[Al/Fe]$\rangle\sim$+0.3), but ω Cen (and other globular cluster) stars can reach [Na/Fe]$\sim$+1.0 and [Al/Fe]$\sim$+1.4. Using the Al data in Figure 11 to trace the percentage of stars with light element abundance patterns matching those observed in the other Galactic populations at comparable metallicity ([Al/Fe]$\leq$+0.5), we find 42% (84/202) of our sample fall into this category. It is more difficult to quantify this with the Na data because the sample size is more than a factor of three smaller, but it appears that at least a significant fraction of the stars in Figure 11 with [Fe/H]<–1.2 show [Na/Fe] ratios consistent with the disk, halo, and bulge, but nearly all of the more metal–rich stars are enhanced in Na. This further solidifies the claim that although Type II SNe have had a significant impact on all ω Cen stars, they are not the only significant nucleosynthesis site. Assuming our data are representative, roughly half of all ω Cen stars appear to have formed in an environment that was polluted with the ejecta from sources other than Type II SNe.

Further inspection of Figure 11 reveals an interesting trend in Na and Al as a function of [Fe/H]. As noted in §4.2, there is a clear lack of stars showing Na and Al abundances consistent with being polluted solely by Type II SNe at [Fe/H]$\gtrsim$–1.2. Only 6% (1/17) of ω Cen giants are "Na–normal" ([Na/Fe]$\sim$0), and this trend is present in both the Norris & Da Costa (1995) and Smith et al. (2000) data as well. A similar result is observed in the larger sample of Al data in that only 22% (8/36) are "Al–normal" ([Al/Fe]$\lesssim$+0.3). While there appears to be a down turn in the maximum [Al/Fe] attained at [Fe/H]>–1.2, the rise in [Na/Fe] and [La/Fe] coupled with the stability of [α/Fe] and [Eu/Fe] in the same metallicity range indicates this artifact is not the result of Type Ia SNe adding Fe but instead a decrease in the [Al/Fe] ratio being added to the cluster's ISM by the production source. What is perhaps most intriguing is that despite a (possible) huge increase in He between the [Fe/H]=–1.7 and –1.4 groups, the light element trends are very similar. It would seem that whichever stars are the source of the high He abundances do not produce abnormally large [Na/Fe] and [Al/Fe] ratios because similar enhancements in Na and Al are found in globular clusters that do not show signs of such extreme He variations.

If Eu production can be attributed mostly to 8–10 $M_\odot$ stars, then we know from those data alone that chemical enrichment had to have occurred in ω Cen over more than $\sim 200\times10^6$ years because there are at least four subpopulations with different [Fe/H] and [Eu/Fe] is roughly constant (with some scatter). However, [Eu/Fe] is, on average, consistently at least 0.1–0.2 dex underabundant relative to the other populations shown in Figure 13. The reason for this is not clear, but it could be that the ratio of 8–10 $M_\odot$ versus higher mass stars was anomalously low in ω Cen relative to other systems.

5.1.2. Intermediate Mass AGB Stars

The discovery of significant star–to–star scatter in light elements coupled with the O–Na anticorrelation in stars on the main sequence and subgiant branches of globular clusters seems to indicate that the various relations among the elements O through Al were already imprinted on the gas from which the current generations of stars formed. As discussed in §1, HBB occurring in intermediate mass ($\sim$5–8 $M_\odot$) AGB stars is currently favored as a likely location for producing the light element trends. These stars have the advantages of preserving their initial [Fe/H] envelope abundances, ejecting enriched material at low velocities, experiencing few third dredge–up episodes (negligible s–process production), and reaching envelope temperatures $>70\times10^6$ K that activate the NeNa and MgAl proton–capture cycles. However, current AGB stellar models are highly sensitive to the adopted treatment of convection and mass loss and it has been pointed out that these scenarios do not explain

the role of super–AGB stars (those that ignite core carbon but not neon burning) nor 1–4 $M_\odot$ AGB stars (Prantzos & Charbonnel 2006). Models using standard mixing length theory (e.g., Fenner et al. 2004; Karakas & Lattanzio 2007) are unable to reproduce the large O depletions ([O/Fe]<–0.6) found in some globular cluster stars (including ω Cen) and show large enhancements in [C+N+O/Fe], which conflict with observations that the CNO sum is constant (Pilachowski 1988; Dickens et al. 1991; Norris & Da Costa 1995; Smith et al. 1996; Ivans et al. 1999). On the other hand, models adopting the full spectrum of turbulence treatment of convection (e.g., Ventura & D'Antona 2008) show fewer third dredge–up episodes and thus keep the CNO sum roughly constant while explaining some of the C through Al abundance trends seen in globular clusters. Neither case is able to fully explain all light element anomalies, in particular the super O–poor stars and Mg isotopic ratios, which may require a hybrid scenario that includes *in situ* deep mixing and HBB in $\gtrsim$5 $M_\odot$ AGB stars (e.g., D'Antona & Ventura 2007) in addition to improvements in key nuclear reaction rates.

Can these stars reproduce what we observe in ω Cen? Our data have shown that only about half of the stars in our sample are consistent with being formed from gas predominantly polluted by Type II SNe (i.e., the stars are not particularly enhanced in Na and Al compared to disk and halo stars of comparable metallicity). Since >5 $M_\odot$ AGB stars likely do not alter the abundances of any elements heavier than Al, we will restrict the discussion to those elements. First turning to the populations with [Fe/H]<–1.2, the stars with [Na/Fe]>0 and [Al/Fe]>+0.5 have envelope material that was likely exposed to high temperature proton–capture processing in an external environment. Although the light element yields are sensitive to both model parameters and nuclear reaction rates, the Ventura & D'Antona (2008) results indicate intermediate metallicity 5–6.5 $M_\odot$ AGB stars can produce +0.30<[Na/Fe]<+0.60 and [Al/Fe]$\sim$+1.0, while the Fenner et al. (2004) data predict somewhat higher Na and lower Al abundances. These values are consistent with the "intermediate" Al population that has $\langle$[Al/Fe]$\rangle$=+0.82 (σ=0.10) and suggest intermediate mass AGB stars could be responsible for the enhancements seen in these stars. However, about 20% of the stars with [Fe/H]<–1.2 have [Al/Fe]>+1 and [Na/Fe]>+0.5. These stars are not accounted for by current AGB models and may have undergone additional *in situ* deep mixing or require pollution from another unknown source.

As can be seen in the top panel of Figure 14, halo, disk, and bulge stars exhibit a roughly constant [Na/Al]$\approx$–0.2 from [Fe/H]=–2 to –0.6, while ω Cen, dwarf spheroidal, and globular cluster stars display a wide range from [Na/Al]=–1 to +0.4 and show a general increase in $\langle$[Na/Al]$\rangle$ with increasing metallicity. Since the final abundances of Na and Al in SN ejecta scale similarly with neutron excess and metallicity (Arnett 1971), the Na/Al ratio is mostly insensitive to metallicity changes and is consistently near [Na/Al]$\sim$–0.2 (e.g., Woosley & Weaver 1995). The overproduction of Al at low metallicities and underproduction

at higher metallicities is consistent with the observed trends in AGB models (e.g., Ventura & D'Antona 2008) due to lower temperatures at the bottom of the convective envelope and shallower mixing in more metal–rich stars. This trend is nearly identically reproduced in globular cluster stars of varying metallicity (bottom panel of Figure 14) and likely indicates the same stars that are responsible for the globular cluster light element anomalies are also prevalent in ω Cen. Since the same trend is also observed in dwarf spheroidal stars, which are not believed to be strongly enriched in Type II SN ejecta, this may strengthen the case for HBB in intermediate mass AGB stars (or some equivalent H–burning environment) to be the source of light element abundance trends different than those seen in the disk and halo. It is interesting that these two systems share the rise in [Na/Al] versus [Fe/H] with globular clusters because, as their low [α/Fe] ratios indicate, star formation has proceeded much differently in dwarf spheroidals despite having comparable main sequence turnoff age ranges with ω Cen.

The paucity of stars with [Al/Fe]>+1 at [Fe/H]>–1.2 is also consistent with the predictions of *in situ* deep mixing at higher metallicities where the increased μ–gradient is expected to inhibit dredge–up of ON, NeNa, and MgAl cycled material into the stellar envelope via meridional circulation (e.g., Sweigart & Mengel 1979). While the range in Na and Al data track closely to that of other globular clusters at low and intermediate metallicity, the more metal–rich ω Cen stars show surprising Na enhancements and decreased star–to–star scatter that are not seen in globular clusters of comparable metallicity. This is true even for M4 ([Fe/H]$\sim$–1.1), which is suspected of having a second, more enriched population without a large spread in Fe (Marino et al. 2008). Although the range of M4's Al abundances are consistent with the values we find here, the *average* [Na/Fe] ratio in ω Cen giants of comparable metallicity is about 0.3 dex larger than the highest [Na/Fe] abundance found by either Ivans et al. (1999) or Marino et al. (2008) in M4. It would seem that there was an additional source of Na in the more metal–rich ω Cen populations or that hardly any unenriched gas remained to dilute the AGB ejecta. Figure 15 illustrates this point in that the stars with [Fe/H]>–1.2 and [Al/Fe]>+0.5 have [Na/Fe] ratios that lie above the range expected for a given Al abundance based on typical globular cluster values. The identity of the Na source is only speculative, but if the progenitor AGB population that polluted the gas from which the [Fe/H]>–1.2 stars formed was He–rich, the higher temperatures and possible deeper mixing in regions where the NeNa cycle was operating may have contributed to the increased Na abundances. It may also be possible that lower mass, He–rich AGB stars, which evolve more quickly than He–normal stars (and produce more Na and less Al), could have a larger impact than in normal globular clusters. However, $\lesssim$4 M$_\odot$ AGB stars are not believed to strongly deplete O and would have to already be O–poor to reproduce the sub–solar [O/Fe] ratios found in many ω Cen giants with [Fe/H]$\gtrsim$–1.5.

5.1.3. Low Mass AGB Stars

Lower mass, thermally pulsing AGB stars ($\sim$1–4 $M_\odot$), which evolve over 150×10^6 to 2.5×10^9years (Schaller et al. 1992), are thought to be the primary producers of the main s–process component in the Galaxy at metallicities found in ω Cen (e.g., Busso et al. 2001). Smith et al. (2000) showed that the [Rb/Zr] ratio in ω Cen was consistent with the s–process being produced in 1.5–3.0 $M_\odot$ AGB stars, implying a monotonic, total evolutionary timescale of $\sim$2–3 Gyrs. This is consistent with most other estimates (e.g., Stanford et al. 2006; but see also Villanova et al. 2007). Since these stars have the longest formation timescale, the presence of their chemical signatures sets a lower limit on relative age estimates.

The halo and disk populations are known to exhibit a steady rise in the contribution of s–process elements at [Fe/H]>–2.5 (e.g., Simmerer et al. 2004), but globular cluster heavy element abundances are dominated by the r–process (e.g., Gratton et al. 2004) and are indicative of the rather rapid chemical evolution timescales of normal globular clusters compared to the disk and halo. Interestingly, dwarf spheroidal stars tend to have a stronger s–process component than any of the Galactic populations (e.g., Geisler et al. 2007), but one that is much smaller than that seen in ω Cen. This, along with the evidence for Type Ia SN pollution, implies dwarf spheroidal galaxies evolve much differently than most other Galactic stellar systems and do so with a rather subdued star formation rate (e.g., Mateo 2008).

However, the Galactic bulge is believed to have formed rapidly, as constrained by turnoff photometry (Ortolani et al. 1995; Kuijken & Rich 2002; Zoccali et al. 2003; Clarkson et al. 2008) as well as by measured high [α/Fe] (e.g., McWilliam & Rich 1994; Fulbright et al. 2006; Lecureur et al. 2007). Theoretical studies argue for timescales significantly less than 10^9 yrs (e.g., Elmegreen 1999; 2008; Ballero et al. 2007). Yet despite a metallicity that is high compared to the halo and ω Cen, (e.g., Fulbright et al. 2006, Zoccali et al. 2008) the s–process elements are seen to exhibit Solar [X/Fe] ratios (McWilliam & Rich 1994) that would appear to require low and intermediate mass stars to have provided significant input to the bulge's chemical evolution.

In Figure 13 we show the evolution of [La/Fe], [Eu/Fe], and [La/Eu] as a function of [Fe/H] for ω Cen and other stellar populations. Since all but the most metal–poor group of ω Cen stars show significant enhancement in the s–process element La (and the [La/Eu] ratio), we find in agreement with previous studies that at least 10^9 years had to have passed between the formation of the primary population at [Fe/H]=–1.7 and the final population at [Fe/H]=–0.7 to allow the low mass progenitor populations enough time to evolve. A significant percentage (25%) of stars in our sample have [La/Fe]$\geq$+1.0 and may be the result of binary mass transfer from a <4 $M_\odot$ AGB companion. However, none of these stars

are present in the dominant, most metal–poor population but are found at [Fe/H]>–1.5 with most being present at [Fe/H]>–1. It is unknown whether the prevalence of such stars at higher metallicities is a result of the longer formation timescales needed for one of the companions to evolve, an anomalous increase in the binary fraction at higher metallicity, or a sample selection effect. If the result is not a selection effect, then this may be a clear indication that the more metal–rich stars are at least 1–2$\times10^9$ years older than the metal–poor population.

Figures 15 and 16 show [Na/Fe] and [La/Fe] versus [Al/Fe], which could be a useful indicator regarding the relative importance of low versus intermediate mass AGB stars. In most globular clusters there is little evidence of light elements showing any correlation with heavy neutron–capture elements on top of the correlations seen among the various light elements (e.g., Smith 2008), which implies the elements lighter than Al are produced in a different astrophysical site over different timescales than those produced via the s–process and r–process. This may mean that the current generation of globular cluster stars have abundance signatures strongly weighted towards pollution from more massive AGB stars compared to those $\lesssim$4 M$_\odot$. On the contrary, ω Cen exhibits a mild correlation between La and Al (as well as Na) and as stated above shows [La/Fe] ratios well in excess of the roughly [La/Fe]$\sim$+0.5 maximum found in globular cluster stars, especially at [Fe/H]>–1.5. Current AGB nucleosynthesis models (e.g., Ventura & D'Antona 2008) suggest that this correlation is unlikely to be the result of $\sim$1–4 M$_\odot$ stars dominating the chemical enrichment of ω Cen because AGB stars in that mass range are shown to produce Na without significantly depleting O, which contradicts the O–Na anticorrelation observed in the cluster giants and prevalence of O–poor stars at higher metallicities (e.g., Norris & Da Costa 1995). For the other populations shown in Figure 16, only the bulge data show any hint of a Na–Al correlation, but that is not believed to be the result of the same mechanism at work in globular clusters (Lecureur et al. 2007). However, the current lack of heavy element data in the bulge makes it difficult to draw conclusions regarding the impact of low mass AGB stars in that environment. Since none of the other populations show any correlation between La and Al (or Na), it appears that ω Cen is (as always) a special case where both low and intermediate mass AGB stars have had significant influence on the cluster's chemical evolution.

In this paper and previous studies, it has been shown that ω Cen is an extremely complex object with an intriguing formation history. Nearly all aspects of its past remain a mystery and although it has been shown that the cluster experienced multiple star formation episodes (and probably significant mass loss), there is evidence both for and against simple monotonic chemical enrichment (i.e., metal–poor stars are older than more metal–rich stars). It appears that ω Cen shares many chemical characteristics with a variety of systems that

formed under widely different conditions and the cluster exhibits signs of both rapid and extended star formation. One of the interesting issues raised by our data is the significance of the apparent transition in light element abundance trends at [Fe/H]≈–1.2. It seems as if the stars with [Fe/H]>–1.2 were made almost entirely out of AGB ejecta, but the populations with [Fe/H]<–1.2 contain groups of stars that likely formed both with and without the presence of AGB pollution in nearly equal proportions. The lack of α–poor stars in all but perhaps the most metal–rich population poses a serious problem and ω Cen's enrichment history challenges the paradigm of chemical evolution that for timescales >1 Gyr, Type Ia SNe contribute Fe–peak and α–poor material that drive down the [α/Fe] ratio to near solar composition. It may be that the cluster lost too much mass before the onset of Type Ia SNe or the ejecta were located too far outside the core to be retained. This may be corroborated by evidence that there is no radial preference in the location of X–ray binaries in ω Cen due to a lack of mass segregation (e.g., Gendre et al. 2003). While the observation of large numbers of RGB, SGB, and main sequence stars are needed to understand the full picture of ω Cen's evolution, the large fluctuations in light element abundances such as Na and Mg, which are often used as metallicity tracers, make low resolution or integrated light studies difficult to decipher. However, future large sample, high resolution studies spanning both the giant branches and main sequences should help further isolate the chemical signatures of each subpopulation and allow more quantitative analyses.

6. SUMMARY

We have determined abundances of several light, α, Fe–peak, and neutron–capture elements for 66 RGB stars in the globular cluster ω Cen using moderate resolution (R≈18,000) spectra. Two different Hydra spectrograph setups were employed spanning 6000–6250 Å and 6530–6800 Å, yielding co–added S/N ratios of about 50–200. The observations covered the full cluster metallicity regime with an emphasis on the intermediate and metal–rich populations. The elemental abundances were determined using either equivalent width analyses or spectrum synthesis, with the addition of hyperfine structure data when available.

The light elements Na and Al show large abundance inhomogeneities that span more than a factor of 10 and the elements are correlated. The Al data set was supplemented with that from Johnson et al. (2008) and yielded [Fe/H] and [Al/Fe] abundances for more than 200 RGB stars. From these data we find evidence for the existence of possibly three different populations of stars with distinct [Al/Fe] patterns. The three sequences segment into those with $\langle$[Al/Fe]$\rangle$=+0.34 (σ=0.14), $\langle$[Al/Fe]$\rangle$=+0.82 (σ=0.10), and $\langle$[Al/Fe]$\rangle$=+1.17 (σ=0.11) and represent 48%, 34%, and 18% of our sample, respectively. These may be inherently tied

to the "primordial," "intermediate," and "extreme" populations found in normal globular clusters that exhibit varying degrees of O depletion and Na enhancement. However, there appears to be a break in the distribution of both Na and Al at [Fe/H]≈–1.2. Stars with [Fe/H]<–1.2 have abundances in the range –0.1≲[Al/Fe]≲+1.4 and –0.5≲[Na/Fe]≲+0.6 with at least half of the stars exhibiting light element abundances consistent with the disk and halo populations, but more than 75% of stars with [Fe/H]>–1.2 are enhanced in Na and Al with values exceeding those found in the disk, halo, and even some globular clusters. None of the stars with [Al/Fe]>+1.0 are found at [Fe/H]>–1.2. A two–sided K–S test reveals the Na and Al abundances on either side of the [Fe/H]=–1.2 cutoff to have a >90% probability of being drawn from different parent populations.

All of our program stars are enhanced in α elements with $\langle$[Ca/Fe]$\rangle$=+0.36 (σ=0.09) and $\langle$[Ti/Fe]$\rangle$=+0.23 (σ=0.14), despite showing a range of more than a factor of 30 in [Fe/H]. The Fe–peak elements share the same small range in star–to–star scatter but give roughly solar–scaled values of $\langle$[Sc/Fe]$\rangle$=+0.09 (σ=0.15) and $\langle$[Ni/Fe]$\rangle$=–0.04 (σ=0.09). Our results are in agreement with previous studies as we find multiple peaks in the metallicity distribution function at [Fe/H]=–1.75, –1.45, –1.05, and –0.75 and few stars with [Fe/H]<–1.8. These populations represent about 55%, 30%, 10%, and 5% of our sample, respectively. Additionally, we find evidence supporting the idea that the most metal–rich stars are more centrally concentrated, and there appears to be a decrease in the star–to–star metallicity dispersion as a function of increasing distance from the cluster core.

The neutron–capture elements La and Eu yield abundances indicative of strong s–process enrichment in all but the most metal–poor stars. We find that nearly all ω Cen stars with [Fe/H]>–1.5 have [La/Eu]≳+0.5, which contradicts the generally r–process dominated nature of normal globular cluster stars that have $\langle$[La/Eu]$\rangle$≈–0.25. Despite the sharp rise in [La/Fe], the Eu abundance remains fairly constant across all metallicities with [Eu/Fe]=+0.19 (σ=0.23). However, 25% of our sample contains stars with [La/Fe]≥+1.0 that are possibly the result of mass transfer in a binary system. These stars are also known to have large Ba4554 indices and are predominantly found at [Fe/H]>–1.3.

Comparing these results with the abundance trends observed in the Galactic halo, disk, bulge, globular clusters, and nearby dwarf spheroidal galaxies indicates the current generation of ω Cen stars share many chemical characteristics found in each of those populations but contain key differences. The elevated [α/Fe] and solar–scaled Fe–peak abundances suggest that Type II SNe have dominated the production of metals in the cluster with almost no contribution from Type Ia SNe. However, we find that at least 40–50% of stars in our sample have [Na/Fe] and [Al/Fe] ratios that exceed the yields expected from moderately metal–poor SNe. Previous studies have shown that the Na and Al enhanced stars are also

O–poor, which implies that these stars were polluted by material that has been exposed to high temperature proton–capture burning. This is corroborated by examining the behavior of [Na/Al] as a function of metallicity. Type II SNe are expected to produce a nearly metallicity independent yield of [Na/Al]$\sim$–0.2 over –2<[Fe/H]<–0.5, which matches observations of disk and halo stars, but ω Cen, normal globular cluster, and dwarf spheroidal stars span a range of –1$\lesssim$[Na/Al]$\lesssim$+0.4. Therefore, our data strongly support the idea of an additional source of light elements in these environments.

HBB occurring in intermediate mass AGB stars is a favored location for producing Na and Al while destroying O. Current AGB nucleosynthesis models predict our observed trends, that more Al is produced at low metallicity and more Na produced at high metallicity, and may explain stars with +0.5<[Al/Fe]<+1.0. However, they may not be adequate to reproduce the $\sim$20% of metal–poor stars with [Al/Fe]>+1, which may require some other source (e.g., *in situ* mixing or massive rotating stars). What is perhaps most intriguing is that we find evidence for two different subpopulations separated as being either more metal–poor or metal–rich than [Fe/H]$\approx$–1.2. Most of the stars with [Fe/H]>–1.2 appear to have formed almost entirely out of AGB ejecta and have [Na/Fe] and [Al/Fe] abundances well above those found in the disk and halo at similar metallicity, while those at [Fe/H]<–1.2 show more of a continuum between strong SN pollution and AGB pollution. Since we did not choose targets based on known chemical properties (e.g., CN strength), it seems that the prevalence of Na and Al enhanced stars at higher metallicity is likely not a selection effect. Interestingly, although all ω Cen giants exhibit the same Na–Al correlation found in other globular clusters, the ω Cen stars with [Fe/H]>–1.2 have more Na for a given Al abundance by >0.2 dex compared to what is expected based on the trend seen in normal globular clusters. There is also a mild correlation between La and both Na and Al, but it is unclear how La relates to these elements. The decreasing maximum value of [Al/Fe] at [Fe/H]>–1.2 is not shared by Na and La and suggests a decrease in the [Al/Fe] abundance being added to the cluster's ISM rather than an increase in Fe due to Type Ia SNe.

The sharp increase in the abundance of [La/Fe] and [La/Eu] with increasing metallicity coupled with the relatively long lifetimes of stars thought to produce most of the s–process elements is consistent with the generally adopted chemical evolution timescale of $\sim$2–4 Gyr. However, other stellar systems that evolved over >1 Gyr exhibit the characteristic downturn in [α/Fe], but this trend is mostly absent in ω Cen stars. Even though it is highly probable that ω Cen did not evolve as a closed box, the apparent preferential retention of Type II versus Type Ia SN ejecta or even the suppression of Type Ia SNe at [Fe/H]>–1 at timescales exceeding 1–2 Gyrs remains an important problem.

This publication makes use of data products from the Two Micron All Sky Survey,

which is a joint project of the University of Massachusetts and the Infrared Processing and Analysis Center/California Institute of Technology, funded by the National Aeronautics and Space Administration and the National Science Foundation. This research has made use of NASA's Astrophysics Data System Bibliographic Services. RMR acknowledges support from grant AST–0709479 from the National Science Foundation. Support of the College of Arts and Sciences and the Daniel Kirkwood fund at Indiana University Bloomington for CIJ is gratefully acknowledged. We would like to thank the referee for his/her thoughtful comments that led to improvement of the manuscript.

Facilities: CTIO

REFERENCES

Alonso, A., Arribas, S., & Martínez-Roger, C. 1999, A&AS, 140, 261

Alonso, A., Arribas, S., & Martínez-Roger, C. 2001, A&A, 376, 1039

Anders, E., & Grevesse, N. 1989, Geochim. Cosmochim. Acta, 53, 197

Arnett, W. D. 1971, ApJ, 166, 153

Ballero, S. K., Matteucci, F., Origlia, L., & Rich, R. M. 2007, A&A, 467, 123

Bedin, L. R., Piotto, G., Anderson, J., Cassisi, S., King, I. R., Momany, Y., & Carraro, G. 2004, ApJ, 605, L125

Bekki, K., & Norris, J. E. 2006, ApJ, 637, L109

Bellini, A., et al. 2009, A&A, 493, 959

Bensby, T., Feltzing, S., & Lundström, I. 2003, A&A, 410, 527

Bensby, T., Feltzing, S., Lundström, I., & Ilyin, I. 2005, A&A, 433, 185

Blackwell, D. E., & Shallis, M. J. 1977, MNRAS, 180, 177

Boesgaard, A. M., King, J. R., Cody, A. M., Stephens, A., & Deliyannis, C. P. 2005, ApJ, 629, 832

Briley, M. M., Cohen, J. G., & Stetson, P. B. 2004a, AJ, 127, 1579

Briley, M. M., Harbeck, D., Smith, G. H., & Grebel, E. K. 2004b, AJ, 127, 1588

Busso, M., Gallino, R., & Wasserburg, G. J. 1999, ARA&A, 37, 239

Busso, M., Gallino, R., Lambert, D. L., Travaglio, C., & Smith, V. V. 2001, ApJ, 557, 802

Calamida, A., et al. 2005, ApJ, 634, L69

Cannon, R. D., Croke, B. F. W., Bell, R. A., Hesser, J. E., & Stathakis, R. A. 1998, MNRAS, 298, 601

Carretta, E., Gratton, R. G., Bragaglia, A., Bonifacio, P., & Pasquini, L. 2004, A&A, 416, 925

Carretta, E., Bragaglia, A., Gratton, R. G., & Lucatello, S. 2008, arXiv:0811.3591

Castelli, F., Gratton, R. G., & Kurucz, R. L. 1997, A&A, 318, 841

Cavallo, R. M., Suntzeff, N. B., & Pilachowski, C. A. 2004, AJ, 127, 3411

Chieffi, A., & Limongi, M. 2004, ApJ, 608, 405

Choi, E., & Yi, S. K. 2008, MNRAS, 386, 1332

Clarkson, W., et al. 2008, ApJ, 684, 1110

Cohen, J. G., Briley, M. M., & Stetson, P. B. 2002, AJ, 123, 2525

Cowan, J. J., Thielemann, F.-K., & Truran, J. W. 1991, Phys. Rep., 208, 267

Cunha, K., Smith, V. V., Suntzeff, N. B., Norris, J. E., Da Costa, G. S., & Plez, B. 2002, AJ, 124, 379

D'Antona, F., & Ventura, P. 2007, MNRAS, 379, 1431

Decressin, T., Meynet, G., Charbonnel, C., Prantzos, N., & Ekström, S. 2007, A&A, 464, 1029

Denissenkov, P. A., & Herwig, F. 2003, ApJ, 590, L99

Denissenkov, P. A., & Weiss, A. 2004, ApJ, 603, 119

Dickens, R. J., Croke, B. F. W., Cannon, R. D., & Bell, R. A. 1991, Nature, 351, 212

Dinescu, D. I., Girard, T. M., & van Altena, W. F. 1999, AJ, 117, 1792

Elmegreen, B. G. 1999, ApJ, 517, 103

Elmegreen, B. G., Bournaud, F., & Elmegreen, D. M. 2008, ApJ, 688, 67

Fenner, Y., Campbell, S., Karakas, A. I., Lattanzio, J. C., & Gibson, B. K. 2004, MNRAS, 353, 789

Ferraro, F. R., Sollima, A., Pancino, E., Bellazzini, M., Straniero, O., Origlia, L., & Cool, A. M. 2004, ApJ, 603, L81

Francois, P., Spite, M., & Spite, F. 1988, A&A, 191, 267

Fulbright, J. P. 2000, AJ, 120, 1841

Fulbright, J. P., McWilliam, A., & Rich, R. M. 2006, ApJ, 636, 821

Fulbright, J. P., McWilliam, A., & Rich, R. M. 2007, ApJ, 661, 1152

Gehren, T., Liang, Y. C., Shi, J. R., Zhang, H. W., & Zhao, G. 2004, A&A, 413, 1045

Geisler, D., Wallerstein, G., Smith, V. V., & Casetti-Dinescu, D. I. 2007, PASP, 119, 939

Gendre, B., Barret, D., & Webb, N. A. 2003, A&A, 400, 521

Girardi, L., Castelli, F., Bertelli, G., & Nasi, E. 2007, A&A, 468, 657

Gnedin, O. Y., Zhao, H., Pringle, J. E., Fall, S. M., Livio, M., & Meylan, G. 2002, ApJ, 568, L23

Gratton, R. G., Carretta, E., Eriksson, K., & Gustafsson, B. 1999, A&A, 350, 955

Gratton, R. G., et al. 2001, A&A, 369, 87

Gratton, R., Sneden, C., & Carretta, E. 2004, ARA&A, 42, 385

Harris, W. E. 1996, AJ, 112, 1487

Hilker, M., & Richtler, T. 2000, A&A, 362, 895

Hill, V., et al. 2002, A&A, 387, 560

Ivans, I. I., Sneden, C., Kraft, R. P., Suntzeff, N. B., Smith, V. V., Langer, G. E., & Fulbright, J. P. 1999, AJ, 118, 1273

Ivans, I. I., Kraft, R. P., Sneden, C., Smith, G. H., Rich, R. M., & Shetrone, M. 2001, AJ, 122, 1438

James, G., François, P., Bonifacio, P., Carretta, E., Gratton, R. G., & Spite, F. 2004, A&A, 427, 825

Johnson, C. I., Kraft, R. P., Pilachowski, C. A., Sneden, C., Ivans, I. I., & Benman, G. 2005, PASP, 117, 1308

Johnson, C. I., Pilachowski, C. A., Simmerer, J., & Schwenk, D. 2008, ApJ, 681, 1505

Karakas, A., & Lattanzio, J. C. 2007, Publications of the Astronomical Society of Australia, 24, 103

Kobayashi, C., Tsujimoto, T., Nomoto, K., Hachisu, I., & Kato, M. 1998, ApJ, 503, L155

Kraft, R. P. 1994, PASP, 106, 553

Kuijken, K., & Rich, R. M. 2002, AJ, 124, 2054

Kučinskas, A., Hauschildt, P. H., Brott, I., Vansevičius, V., Lindegren, L., Tanabé, T., & Allard, F. 2006, A&A, 452, 1021

Lecureur, A., Hill, V., Zoccali, M., Barbuy, B., Gómez, A., Minniti, D., Ortolani, S., & Renzini, A. 2007, A&A, 465, 799

Lee, J.-W., Carney, B. W., & Habgood, M. J. 2005, AJ, 129, 251

Magain, P. 1984, A&A, 134, 189

Marino, A. F., Villanova, S., Piotto, G., Milone, A. P., Momany, Y., Bedin, L. R., & Medling, A. M. 2008, A&A, 490, 625

Mateo, M. 2008, The Messenger, 134, 3

Mathews, G. J., & Cowan, J. J. 1990, Nature, 345, 491

McCall, M. L. 2004, AJ, 128, 2144

McWilliam, A. 1997, ARA&A, 35, 503

McWilliam, A., & Rich, R. M. 1994, ApJS, 91, 749

Meylan, G., Mayor, M., Duquennoy, A., & Dubath, P. 1995, A&A, 303, 761

Newsham, G., & Terndrup, D. M. 2007, ApJ, 664, 332

Nomoto, K., Tominaga, N., Umeda, H., Kobayashi, C., & Maeda, K. 2006, Nuclear Physics A, 777, 424

Norris, J. E., & Da Costa, G. S. 1995, ApJ, 447, 680

Norris, J. E., Freeman, K. C., & Mighell, K. J. 1996, ApJ, 462, 241

Norris, J. E., Freeman, K. C., Mayor, M., & Seitzer, P. 1997, ApJ, 487, L187

Ortolani, S., Renzini, A., Gilmozzi, R., Marconi, G., Barbuy, B., Bica, E., & Rich, R. M. 1995, Nature, 377, 701

Pancino, E., Ferraro, F. R., Bellazzini, M., Piotto, G., & Zoccali, M. 2000, ApJ, 534, L83

Pancino, E., Pasquini, L., Hill, V., Ferraro, F. R., & Bellazzini, M. 2002, ApJ, 568, L101

Pancino, E., Seleznev, A., Ferraro, F. R., Bellazzini, M., & Piotto, G. 2003, MNRAS, 345, 683

Pancino, E., Galfo, A., Ferraro, F. R., & Bellazzini, M. 2007, ApJ, 661, L155

Pilachowski, C. A. 1988, ApJ, 326, L57

Piotto, G., et al. 2005, ApJ, 621, 777

Piotto, G. 2008, Memorie della Societa Astronomica Italiana, 79, 334

Prantzos, N., & Charbonnel, C. 2006, A&A, 458, 135

Press, W. H., Teukolsky, S. A., Vetterling, W. T., & Flannery, B. R. 1992, Numerical Recipes in FORTRAN: The Art of Scientific Computing (2nd ed.; Cambridge: Cambridge Univ. Press)

Prochaska, J. X., & McWilliam, A. 2000, ApJ, 537, L57

Ramírez, S. V., & Cohen, J. G. 2002, AJ, 123, 3277

Ramírez, I., & Meléndez, J. 2005, ApJ, 626, 465

Reddy, B. E., Tomkin, J., Lambert, D. L., & Allende Prieto, C. 2003, MNRAS, 340, 304

Reddy, B. E., Lambert, D. L., & Allende Prieto, C. 2006, MNRAS, 367, 1329

Reijns, R. A., Seitzer, P., Arnold, R., Freeman, K. C., Ingerson, T., van den Bosch, R. C. E., van de Ven, G., & de Zeeuw, P. T. 2006, A&A, 445, 503

Renzini, A. 2008, MNRAS, 391, 354

Rey, S.-C., Lee, Y.-W., Ree, C. H., Joo, J.-M., Sohn, Y.-J., & Walker, A. R. 2004, AJ, 127, 958

Richer, H. B., Fahlman, G. G., Buonanno, R., Fusi Pecci, F., Searle, L., & Thompson, I. B. 1991, ApJ, 381, 147

Samland, M. 1998, ApJ, 496, 155

Sbordone, L., Bonifacio, P., Buonanno, R., Marconi, G., Monaco, L., & Zaggia, S. 2007, A&A, 465, 815

Schaller, G., Schaerer, D., Meynet, G., & Maeder, A. 1992, A&AS, 96, 269

Shetrone, M. D., & Keane, M. J. 2000, AJ, 119, 840

Shetrone, M. D., Côté, P., & Sargent, W. L. W. 2001, ApJ, 548, 592

Shetrone, M., Venn, K. A., Tolstoy, E., Primas, F., Hill, V., & Kaufer, A. 2003, AJ, 125, 684

Simmerer, J., Sneden, C., Cowan, J. J., Collier, J., Woolf, V. M., & Lawler, J. E. 2004, ApJ, 617, 1091

Smith, V. V., Cunha, K., & Lambert, D. L. 1995, AJ, 110, 2827

Smith, G. H., Shetrone, M. D., Bell, R. A., Churchill, C. W., & Briley, M. M. 1996, AJ, 112, 1511

Smith, V. V., Suntzeff, N. B., Cunha, K., Gallino, R., Busso, M., Lambert, D. L., & Straniero, O. 2000, AJ, 119, 1239

Smith, G. H. 2008, PASP, 120, 952

Sneden, C. 1973, ApJ, 184, 839

Sneden, C., McWilliam, A., Preston, G. W., Cowan, J. J., Burris, D. L., & Armosky, B. J. 1996, ApJ, 467, 819

Sneden, C., Kraft, R. P., Shetrone, M. D., Smith, G. H., Langer, G. E., & Prosser, C. F. 1997, AJ, 114, 1964

Sneden, C., Kraft, R. P., Guhathakurta, P., Peterson, R. C., & Fulbright, J. P. 2004, AJ, 127, 2162

Sneden, C., Cowan, J. J., & Gallino, R. 2008, ARA&A, 46, 241

Sollima, A., Ferraro, F. R., Pancino, E., & Bellazzini, M. 2005a, MNRAS, 357, 265

Sollima, A., Pancino, E., Ferraro, F. R., Bellazzini, M., Straniero, O., & Pasquini, L. 2005b, ApJ, 634, 332

Stanford, L. M., Da Costa, G. S., Norris, J. E., & Cannon, R. D. 2004, Memorie della Societa Astronomica Italiana, 75, 290

Stanford, L. M., Da Costa, G. S., Norris, J. E., & Cannon, R. D. 2006, ApJ, 647, 1075

Suntzeff, N. B., & Kraft, R. P. 1996, AJ, 111, 1913

Sweigart, A. V., & Mengel, J. G. 1979, ApJ, 229, 624

Timmes, F. X., Woosley, S. E., & Weaver, T. A. 1995, ApJS, 98, 617

van de Ven, G., van den Bosch, R. C. E., Verolme, E. K., & de Zeeuw, P. T. 2006, A&A, 445, 513

van Leeuwen, F., Le Poole, R. S., Reijns, R. A., Freeman, K. C., & de Zeeuw, P. T. 2000, A&A, 360, 472

van Loon, J. T., van Leeuwen, F., Smalley, B., Smith, A. W., Lyons, N. A., McDonald, I., & Boyer, M. L. 2007, MNRAS, 382, 1353

Ventura, P., & D'Antona, F. 2008, MNRAS, 385, 2034

Villanova, S., et al. 2007, ApJ, 663, 296

Wheeler, J. C., Cowan, J. J., & Hillebrandt, W. 1998, ApJ, 493, L101

Woolley, R. R. 1966, Royal Observatory Annals, 2, 1

Woosley, S. E., & Weaver, T. A. 1995, ApJS, 101, 181

Yoshii, Y., Tsujimoto, T., & Nomoto, K. 1996, ApJ, 462, 266

Zhang, H. W., Gehren, T., & Zhao, G. 2008, A&A, 481, 489

Zoccali, M., et al. 2003, A&A, 399, 931

Zoccali, M., Hill, V., Lecureur, A., Barbuy, B., Renzini, A., Minniti, D., Gómez, A., & Ortolani, S. 2008, A&A, 486, 177

This preprint was prepared with the AAS LaTeX macros v5.2.

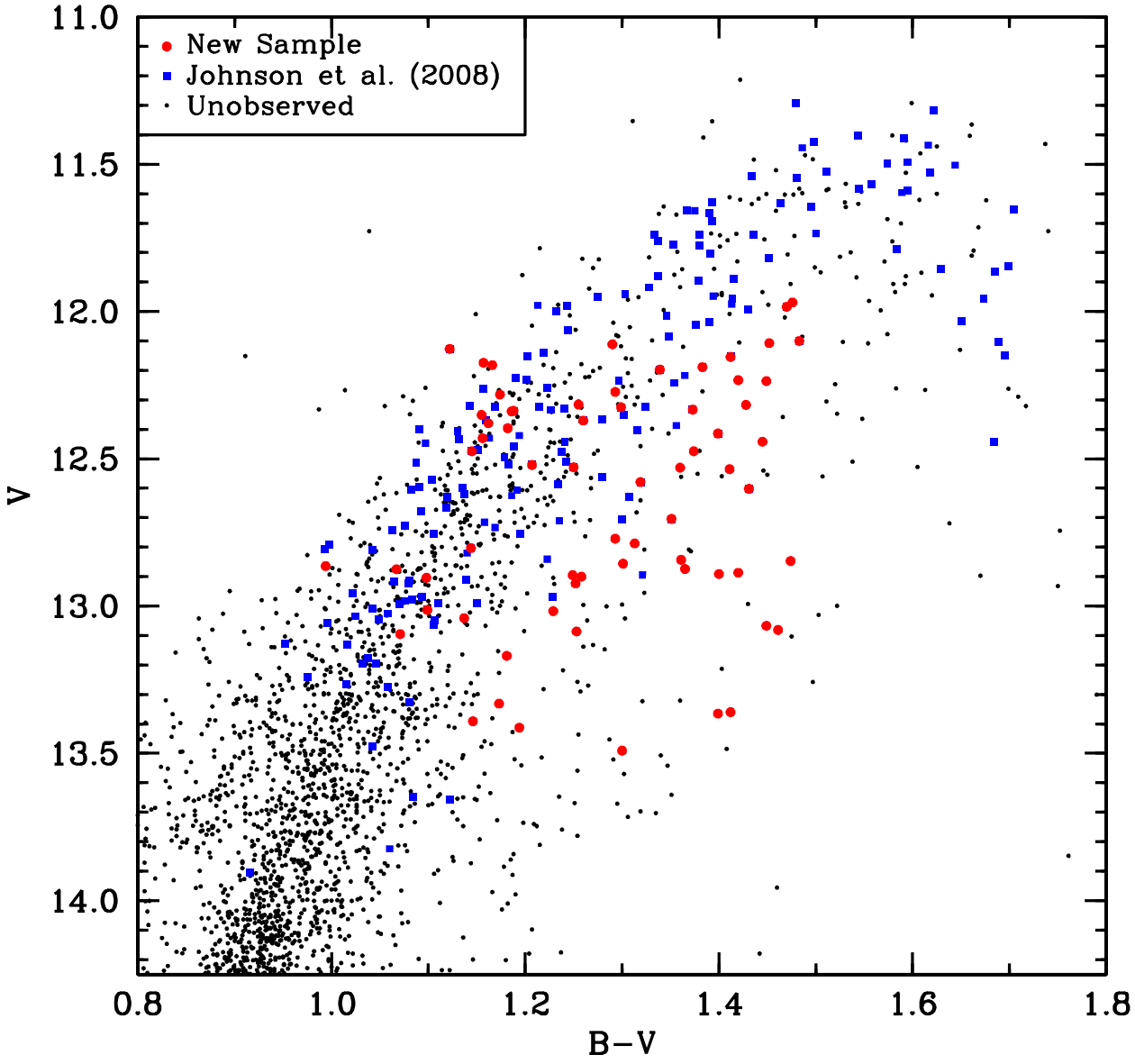

Fig. 1.— Color–magnitude diagram of ω Cen's RGB. The filled red circles represent the stars observed for this study and the filled blue squares show the stars observed for Johnson et al. (2008). There are 22 stars which overlap with Johnson et al. and those are also indicated by filled red circles. The complete sample, including stars not observed here, are from van Leeuwen et al. (2000).

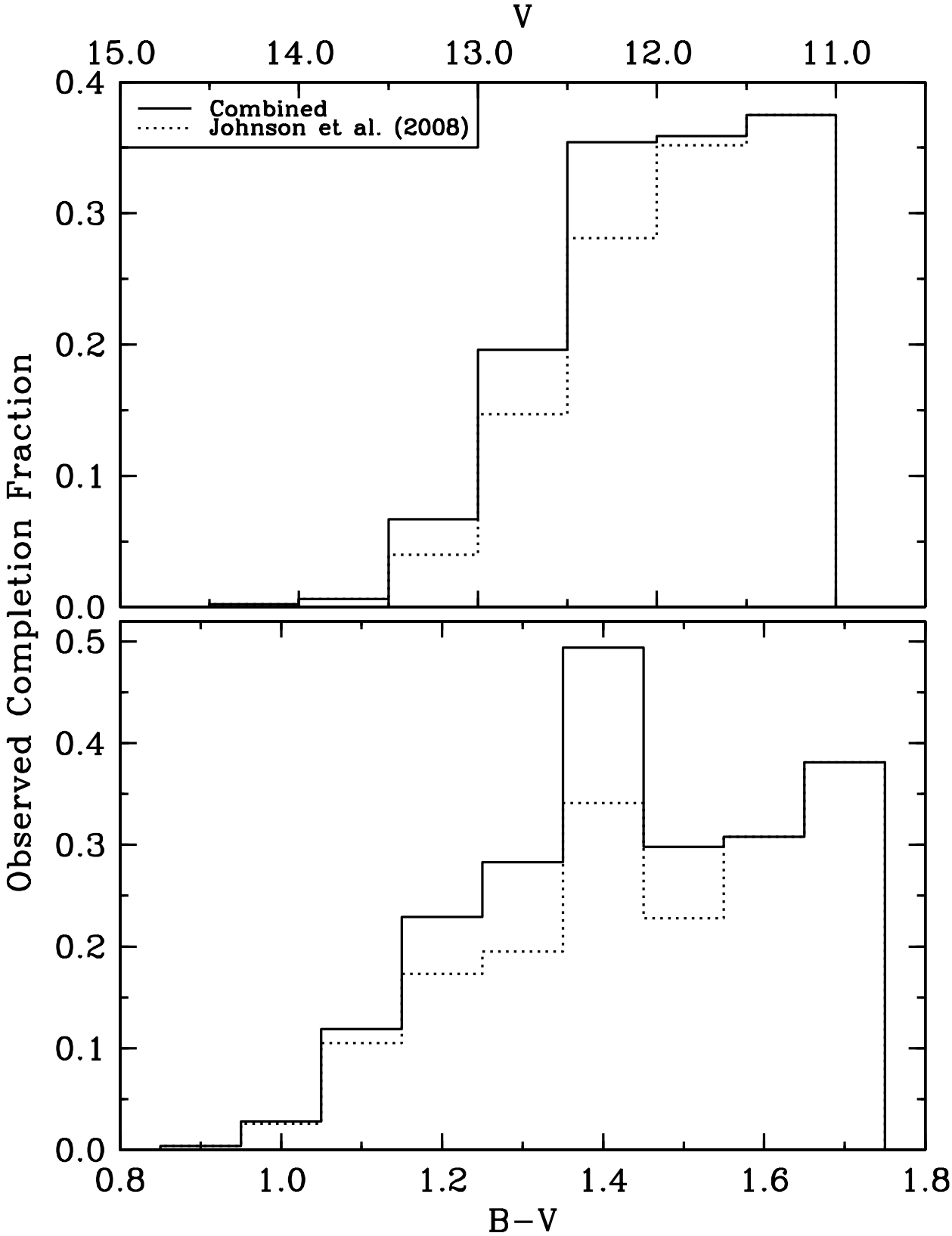

Fig. 2.— Histogram showing the observed completion fraction of this study combined with the data of Johnson et al. (2008). The top panel shows the completion fraction as a function of V magnitude and the bottom panel shows the completion fraction as a function of B–V color.

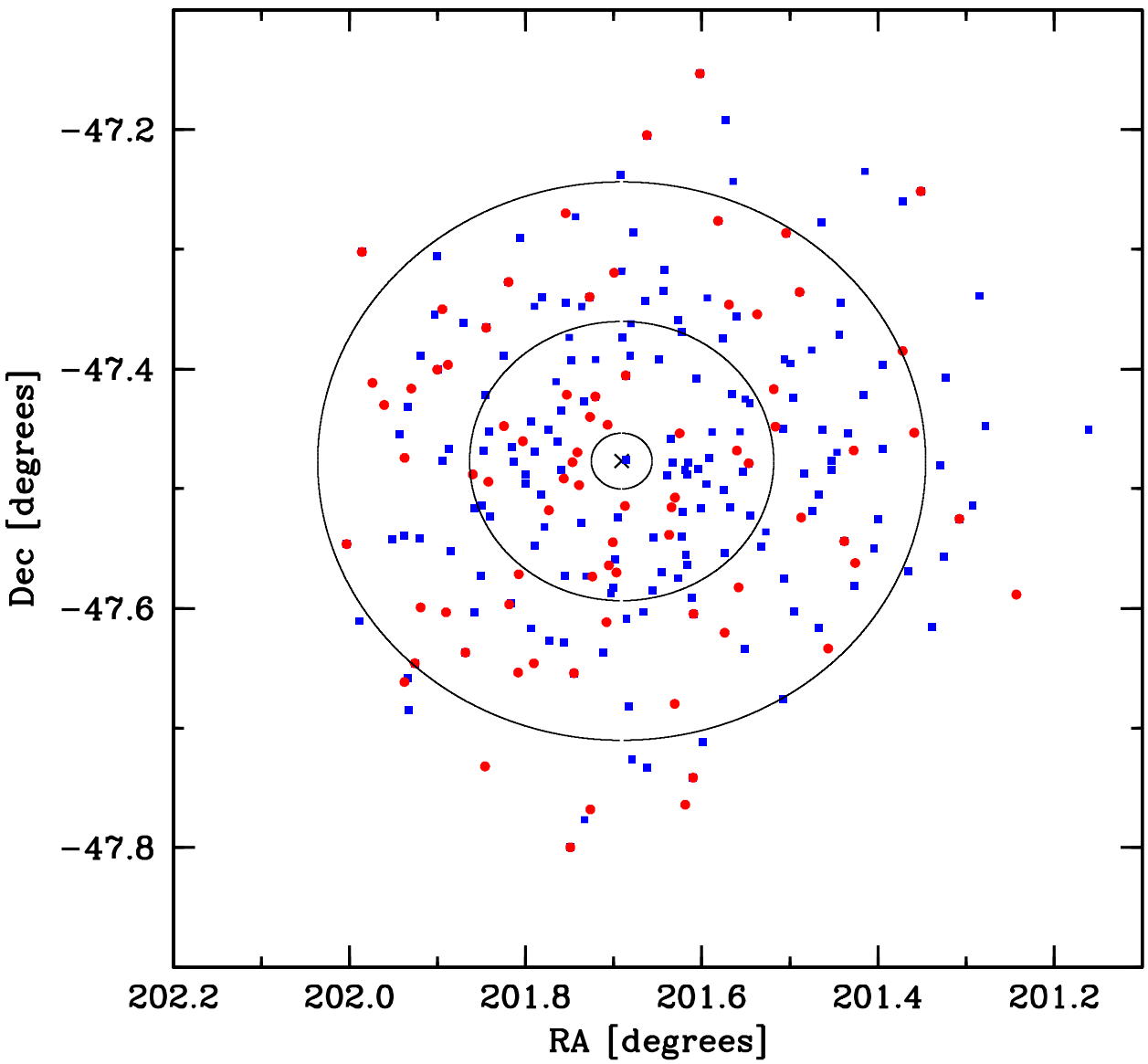

Fig. 3.— Program stars are shown in terms of position in the field. The symbols are the same as in Figure 1. The cross indicates the field center at 201.691°, –47.4769° (J2000) ($13^{h}26^{m}45.9^{s}$, –47°28′37.0″) and the ellipses indicate 1, 5, and 10 times the core radius of 1.40′.

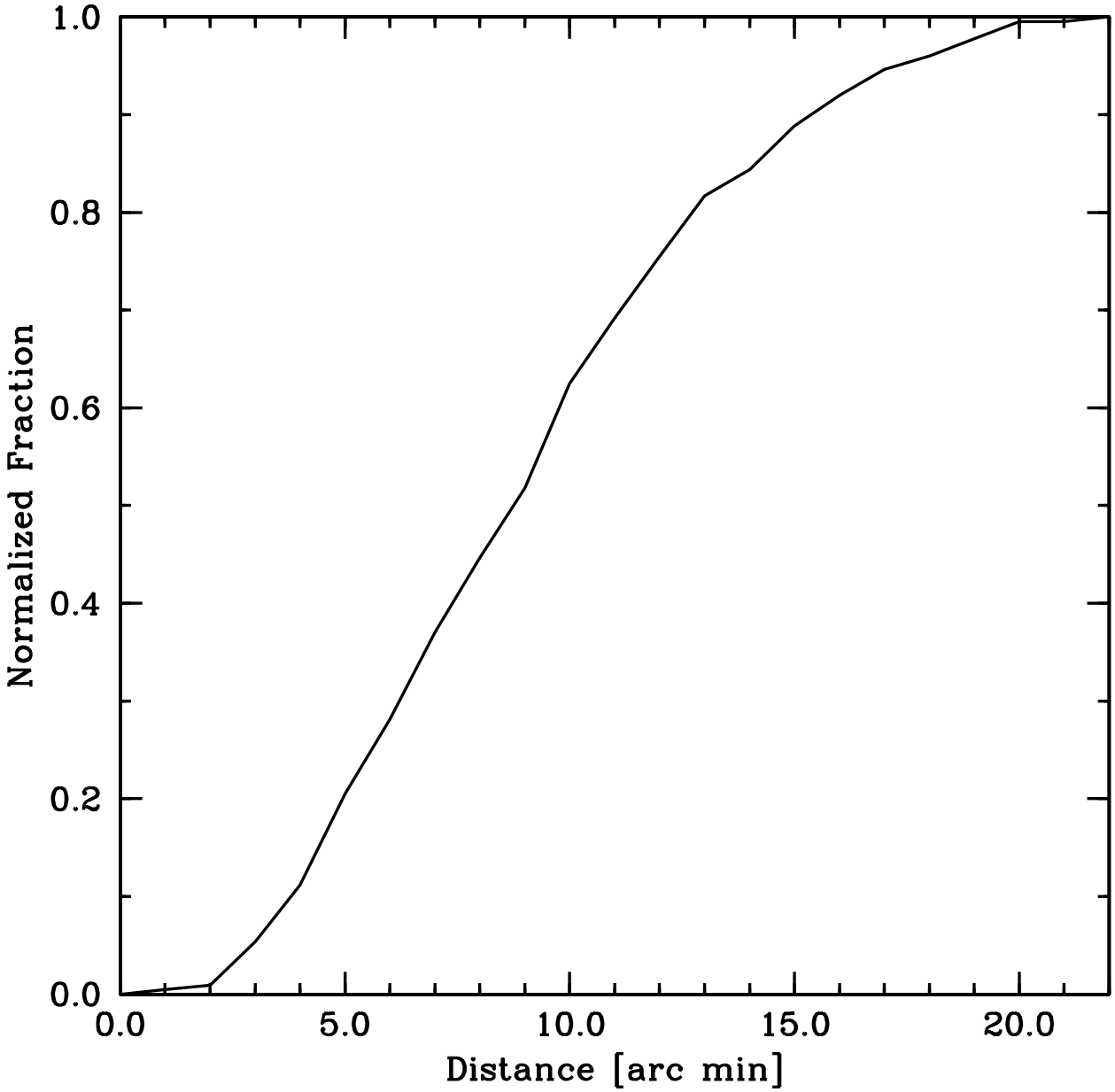

Fig. 4.— Normalized cumulative distribution for our combined sample as a function of distance from the cluster center. This plot shows the fraction of our total sample observed inside a given radius. The cluster center reference is the same as in Figure 3.

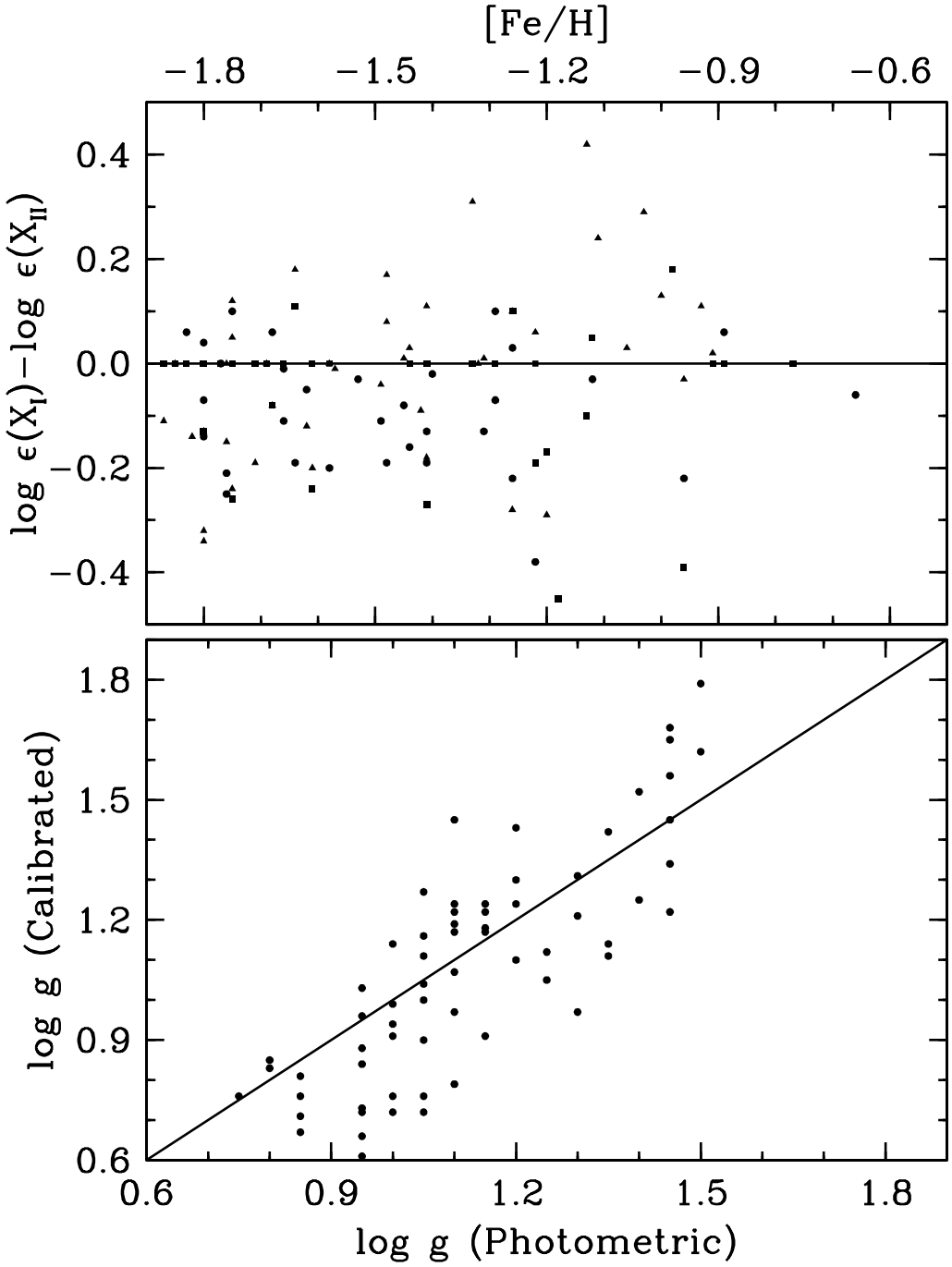

Fig. 5.— The top panel shows a plot of the difference in abundance as derived from both neutral and singly ionized species as a function of [Fe/H]. The filled circles represent Fe, the filled boxes are Sc, and the filled triangles are Ti. The bottom panel shows the log g values adopted from photometry versus the calibrated T_{eff}–log g relation from Kučinskas et al. (2006). In both panels the straight line indicates perfect agreement.

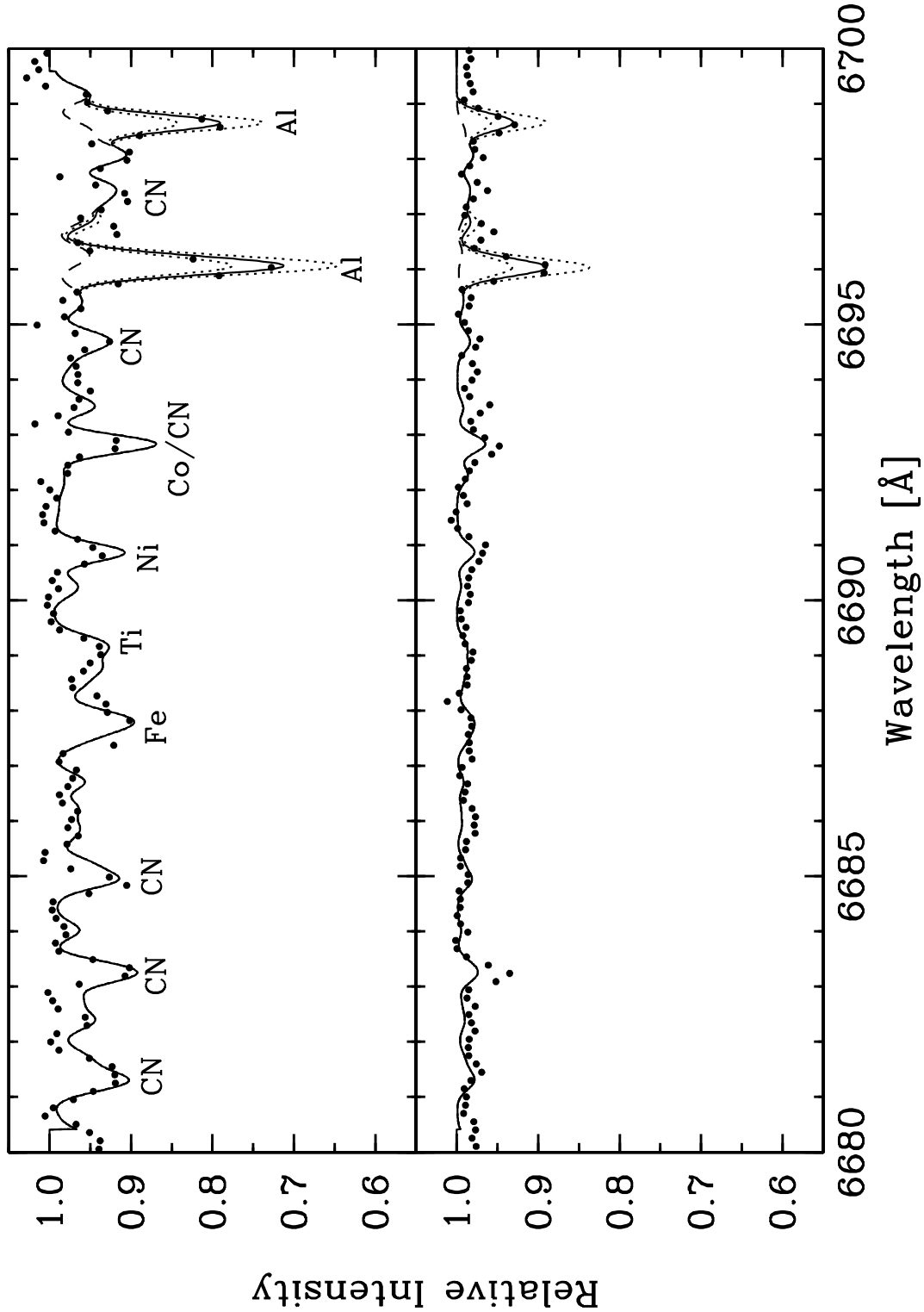

Fig. 6.— Sample spectrum syntheses are shown for two stars of varying T_{eff}, [Fe/H], and CN strength, but similar [Al/Fe] ratios. The relative intensity scales are the same in both figures. The solid line shows the best fit to the observed spectrum, the dotted lines illustrate deviations ±0.30 dex, and the dashed line indicates how the spectrum would appear if Al were absent.

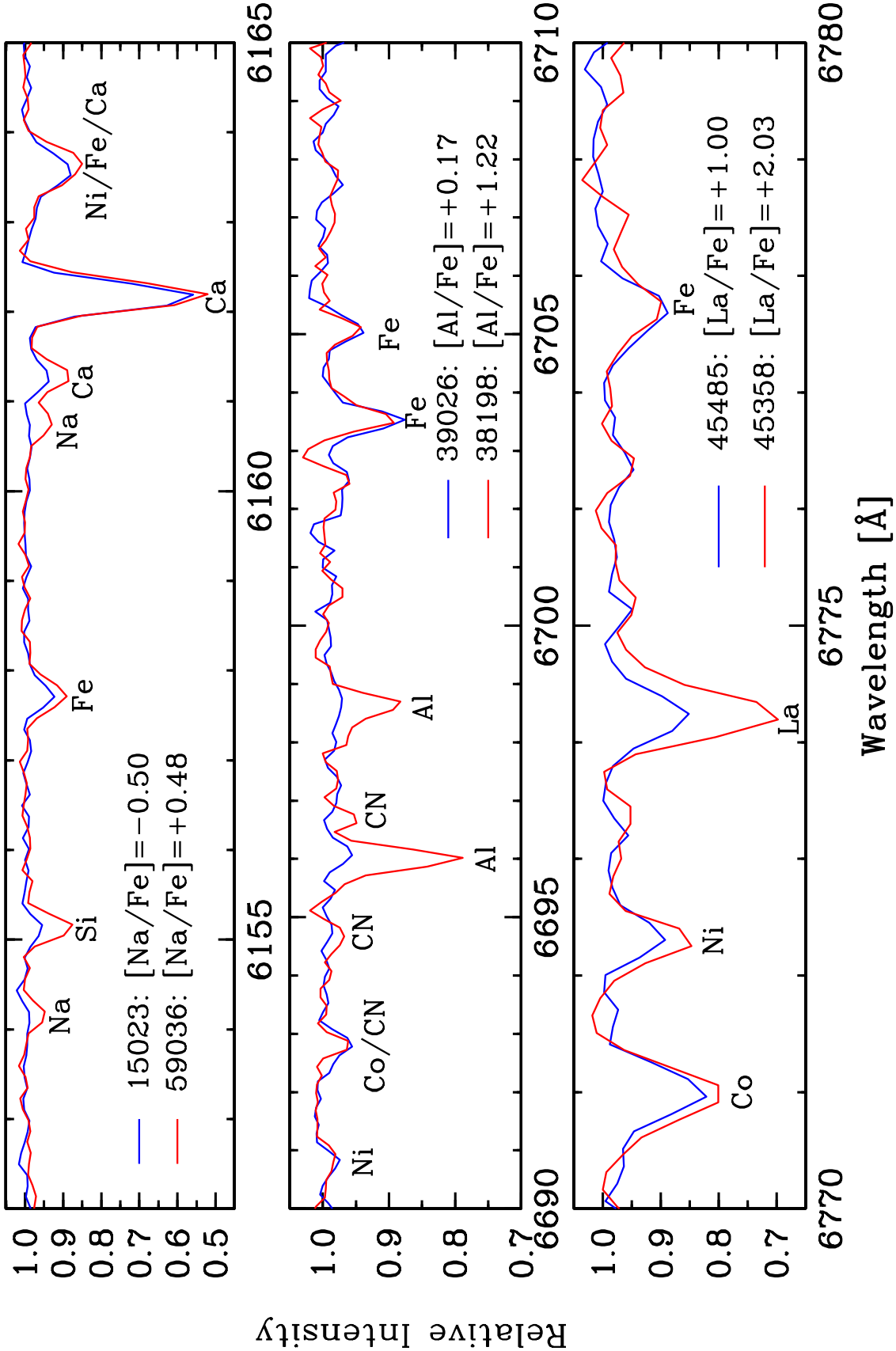

Fig. 7.— Sample spectra are shown in three different wavelength regions to highlight the line strength differences seen in Na, Al, and La. Each panel contains stars of roughly the

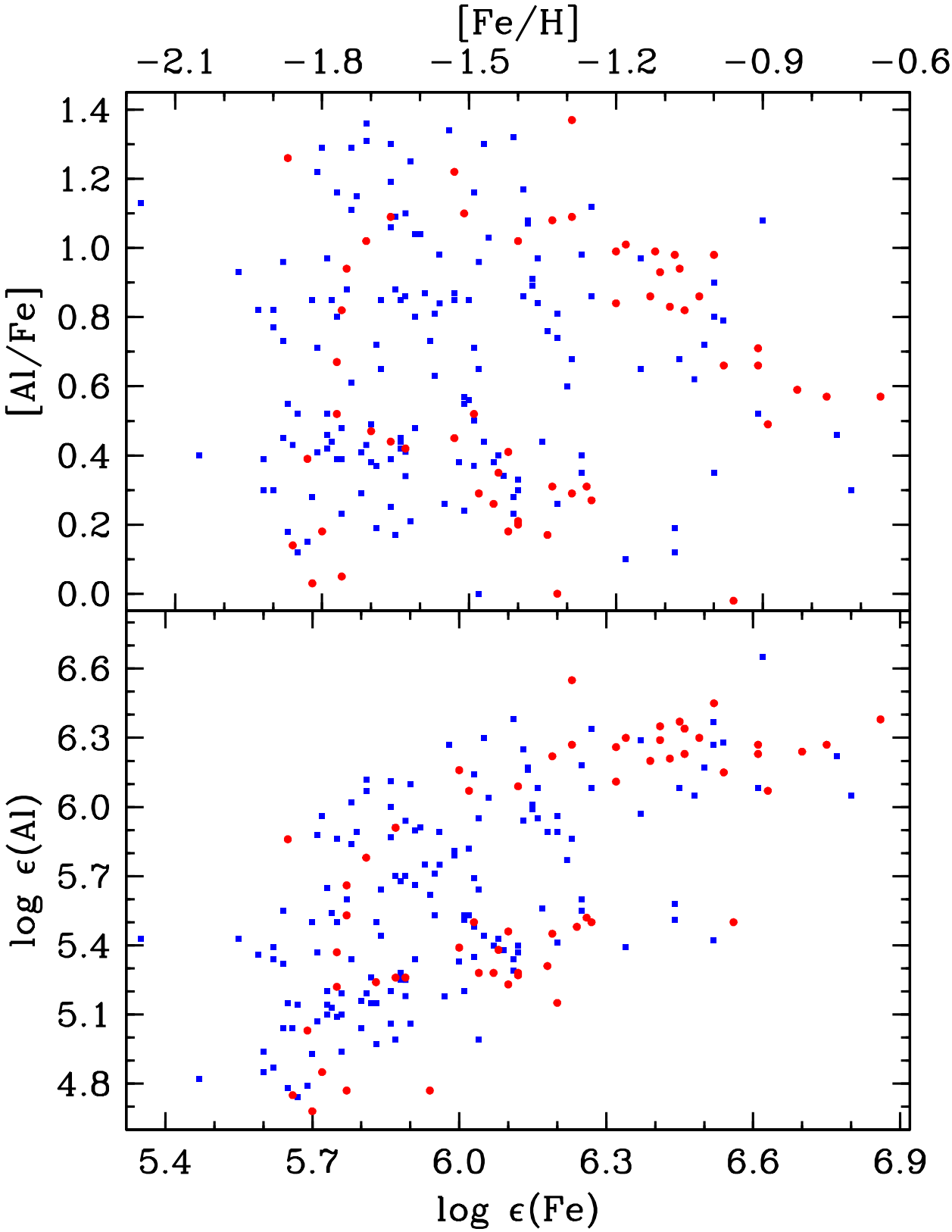

Fig. 8.— The top panel shows [Al/Fe] plotted as a function of [Fe/H] and the bottom panel shows log ϵ(Al) plotted as a function of log ϵ(Fe). The symbols are the same as those in Figure 1.

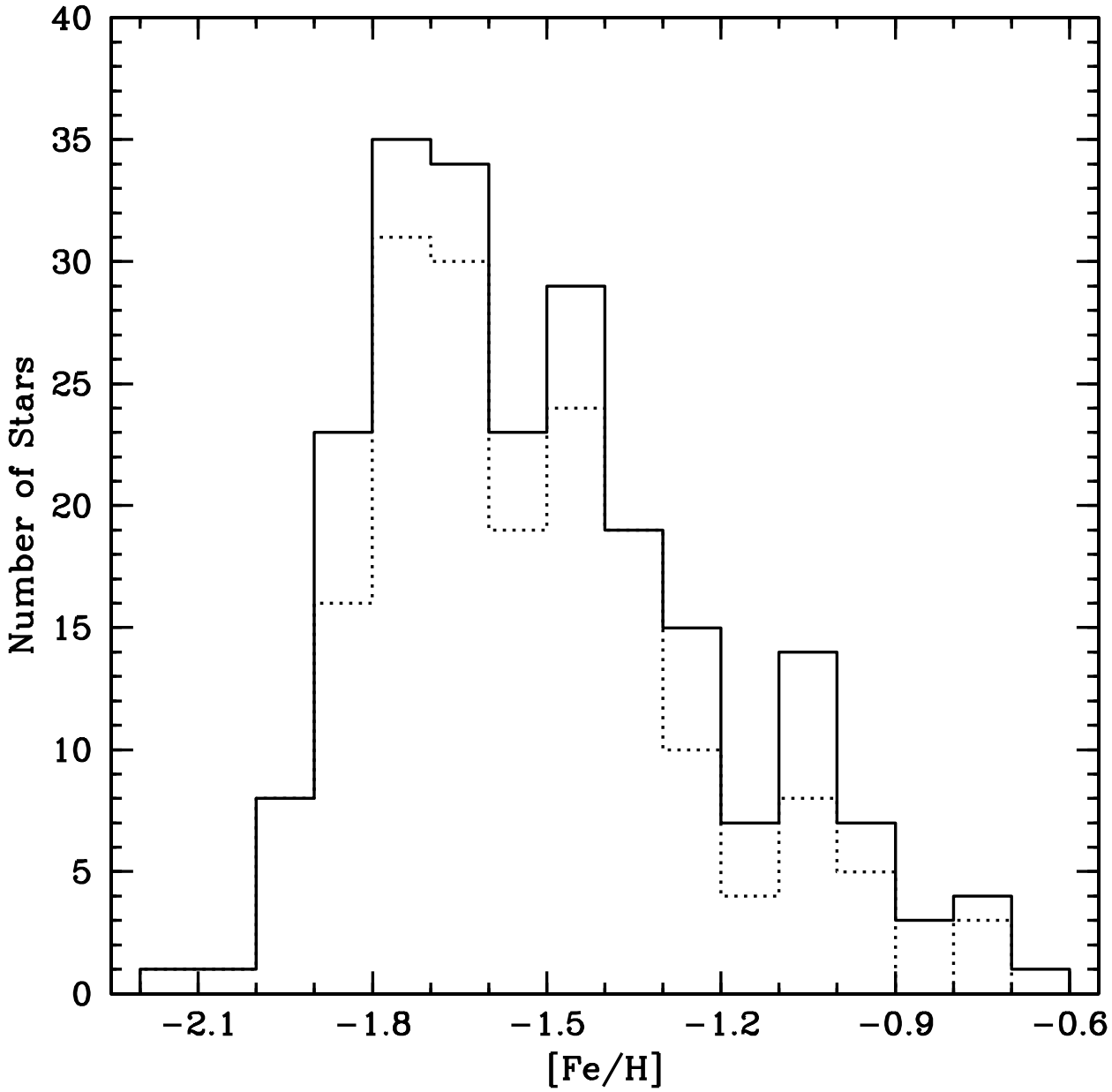

Fig. 9.— Histogram of derived [Fe/H] values for the combined sample of this study and Johnson et al. (2008) with bin sizes of 0.10 dex. The dashed line histogram shows the results from Johnson et al. (2008).

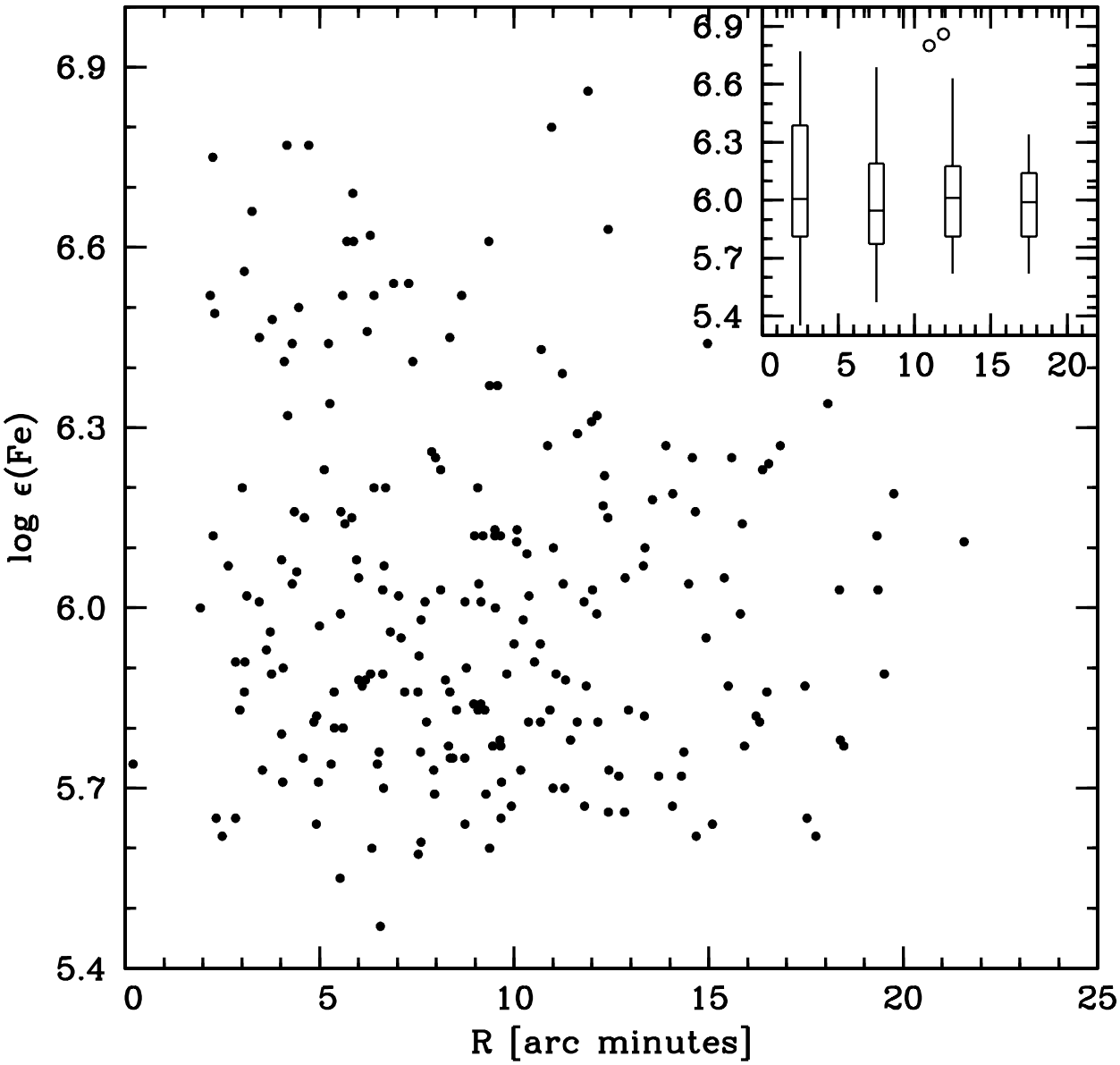

Fig. 10.— Fe is plotted as a function of distance from the cluster center. The points show the data from both this study and Johnson et al. (2008). We have averaged the Fe abundances for stars observed in both studies. The inset plot shows the mean and quartile distributions in 5′ bins. The vertical lines represent the full data range (except outliers) and open circles indicate mild outliers between 1.5 and 3.0 times the interquartile range.

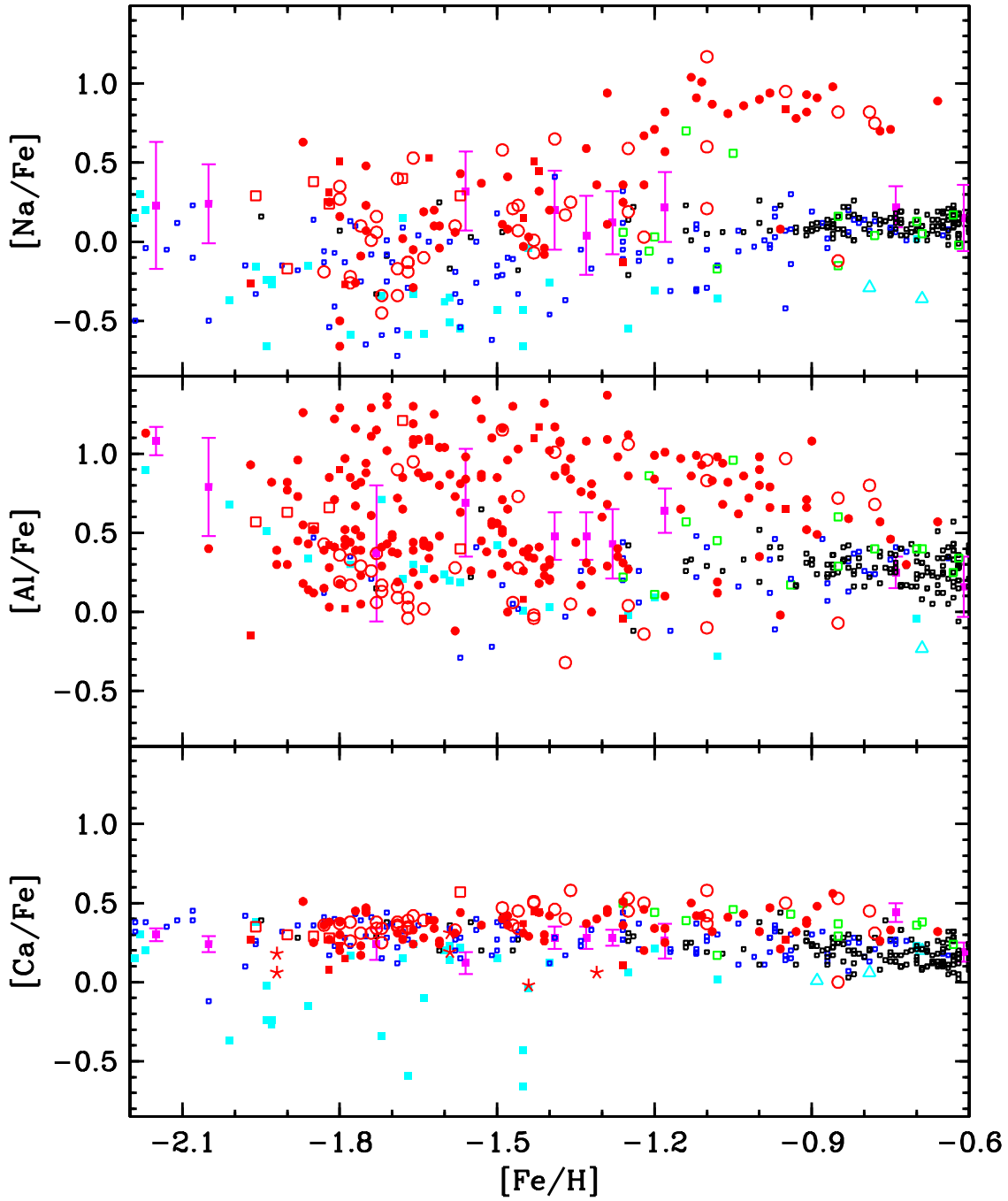

Fig. 11.— Plots of [Na/Fe], [Al/Fe], and [Ca/Fe] versus [Fe/H] are shown with data from this study and the literature. The filled circles are values from the combined sample of this study and Johnson et al. (2008), the open circles are from Norris & Da Costa (1995), the filled squares are from Smith et al. (2000), the open squares are from Francois et al. (1988), and the stars are from Smith et al. (1995). Literature values are provided for the thin/thick disk (open black boxes), halo (open blue boxes), bulge (open green boxes), dwarf spheroidals (filled cyan boxes), globular clusters with 1σ bars (filled magenta boxes), and the Sagittarius dwarf spheroidal (open cyan triangles). References are given in Table 5.

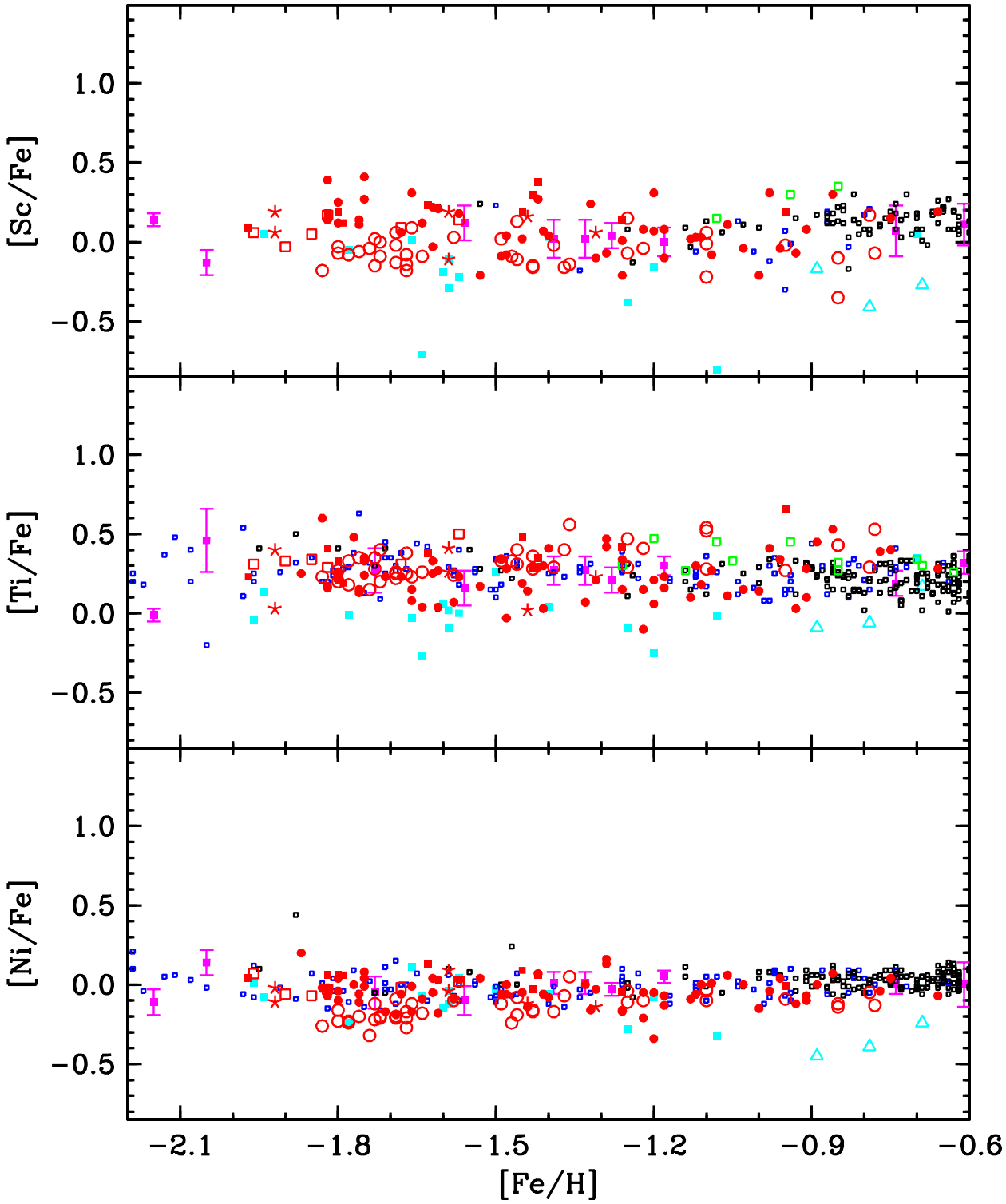

Fig. 12.— Plots of [Sc/Fe], [Ti/Fe], and [Ni/Fe] versus [Fe/H] are shown with data from this study and the literature. The symbols and [X/Fe] scales are the same as in Figure 11.

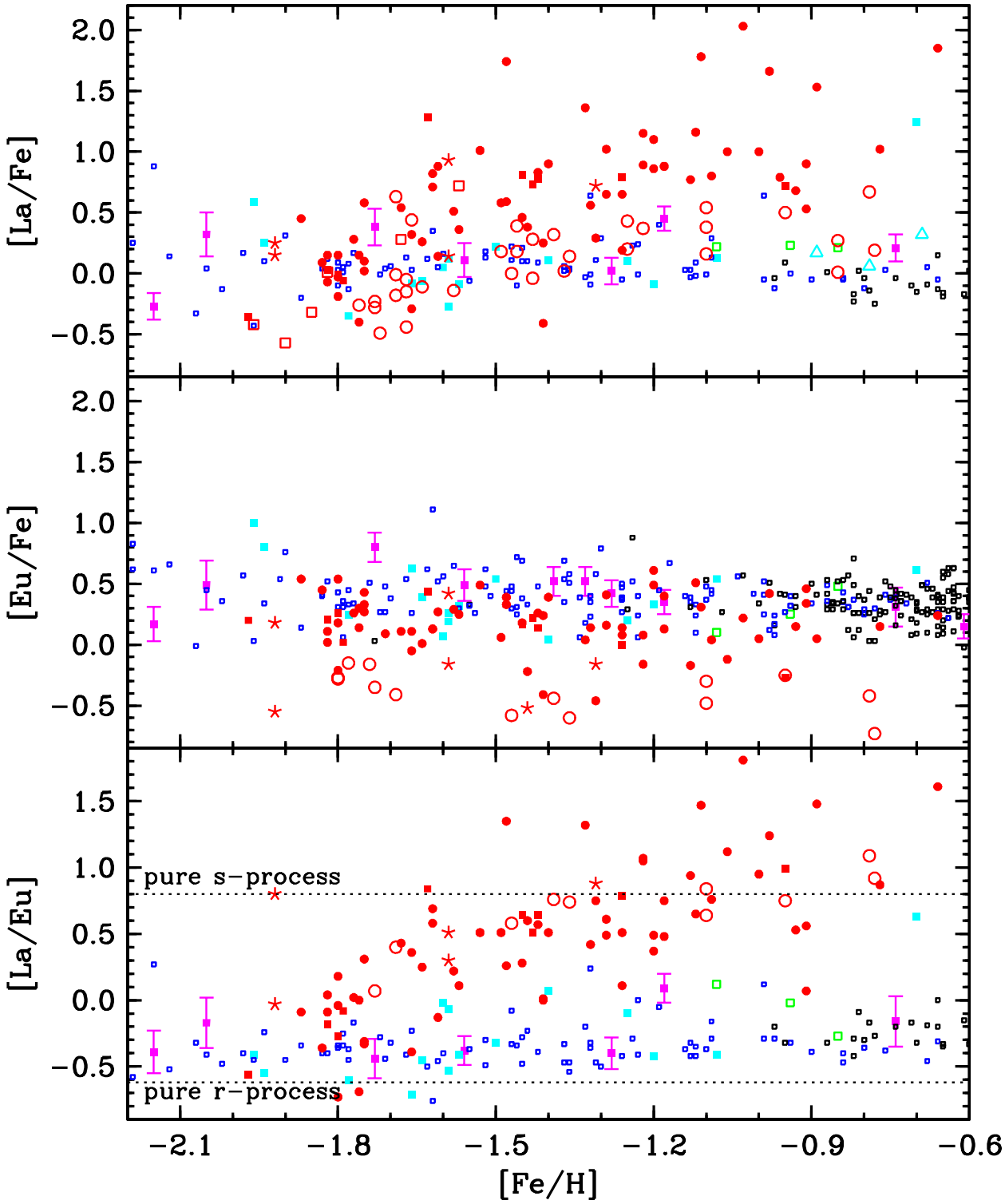

Fig. 13.— Plots of [La/Fe], [Eu/Fe], and [La/Eu] versus [Fe/H] are shown with data from this study and the literature. The symbols are the same as in Figure 11. The dashed lines indicating pure s–process and r–process abundance ratios are taken from McWilliam (1997).

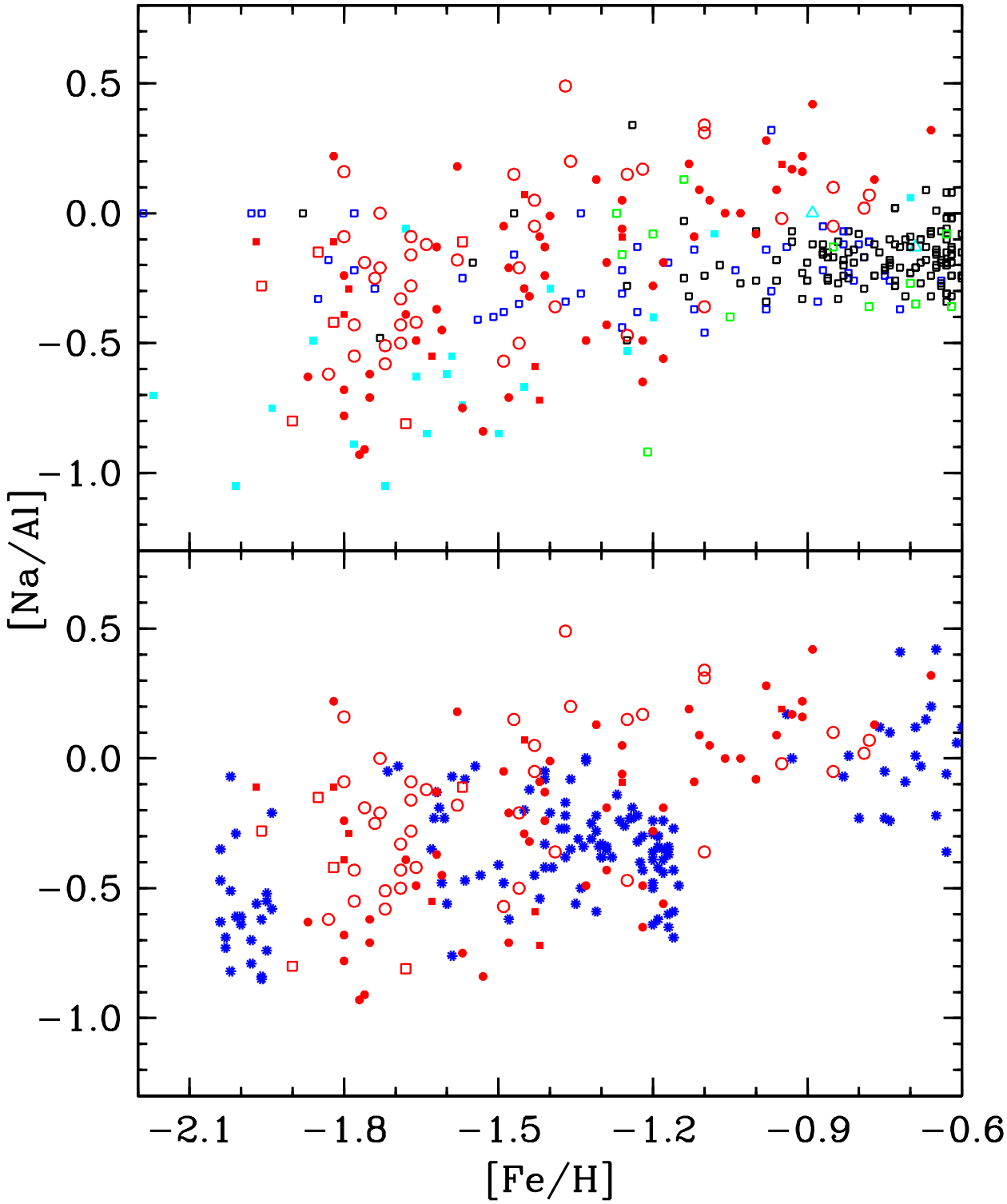

Fig. 14.— [Na/Al] ratios as a function of metallicity are shown for a variety of populations. The symbols in the top panel are the same as those in Figure 11 and the blue points in the bottom panel represent individual globular cluster stars.

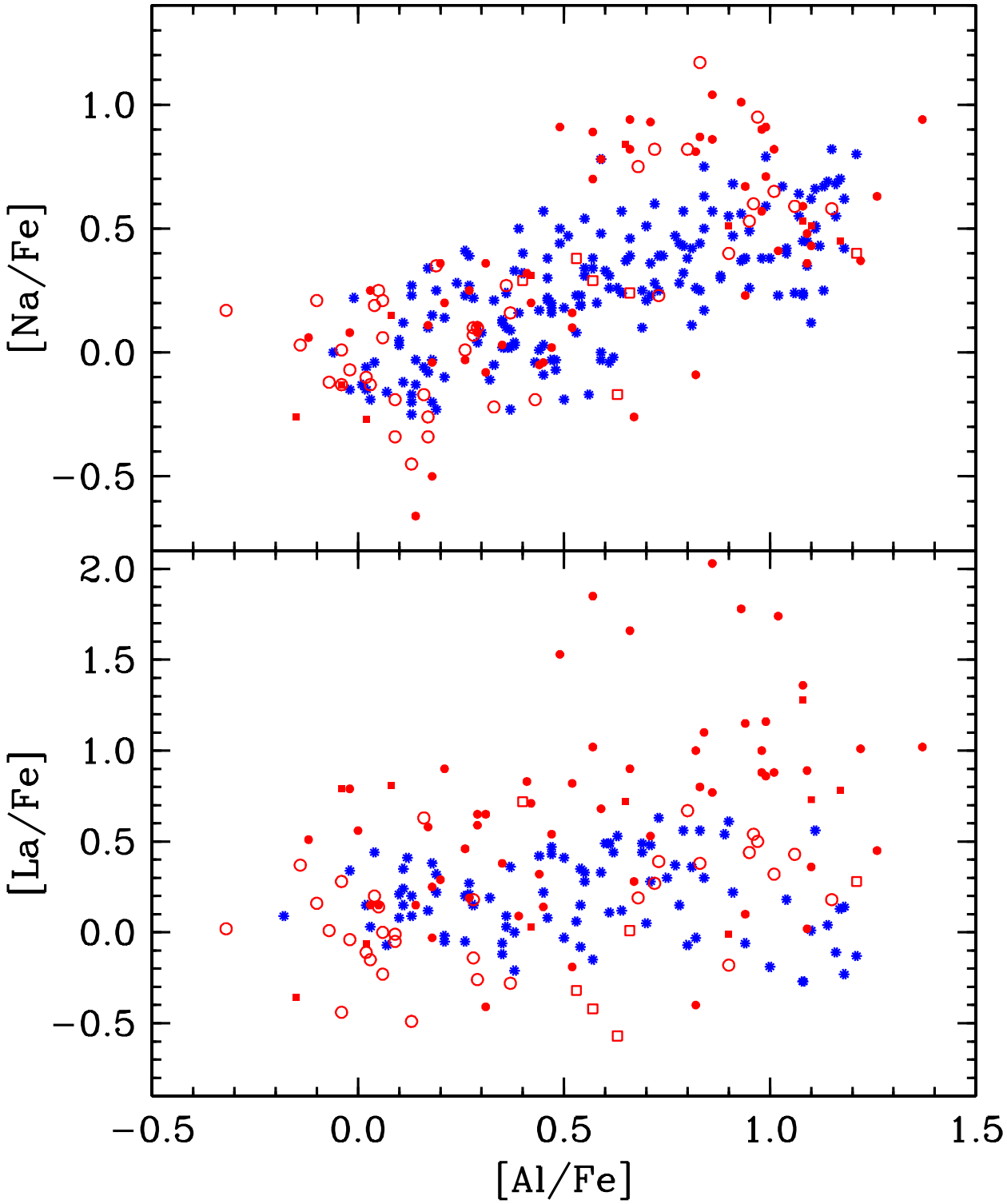

Fig. 15.— The top panel shows [Na/Fe] versus [Al/Fe] and compares ω Cen data to results from individual globular cluster stars. The bottom panel shows the same set of stars but plots [La/Fe] versus [Al/Fe]. The symbols are the same as those in Figure 14.

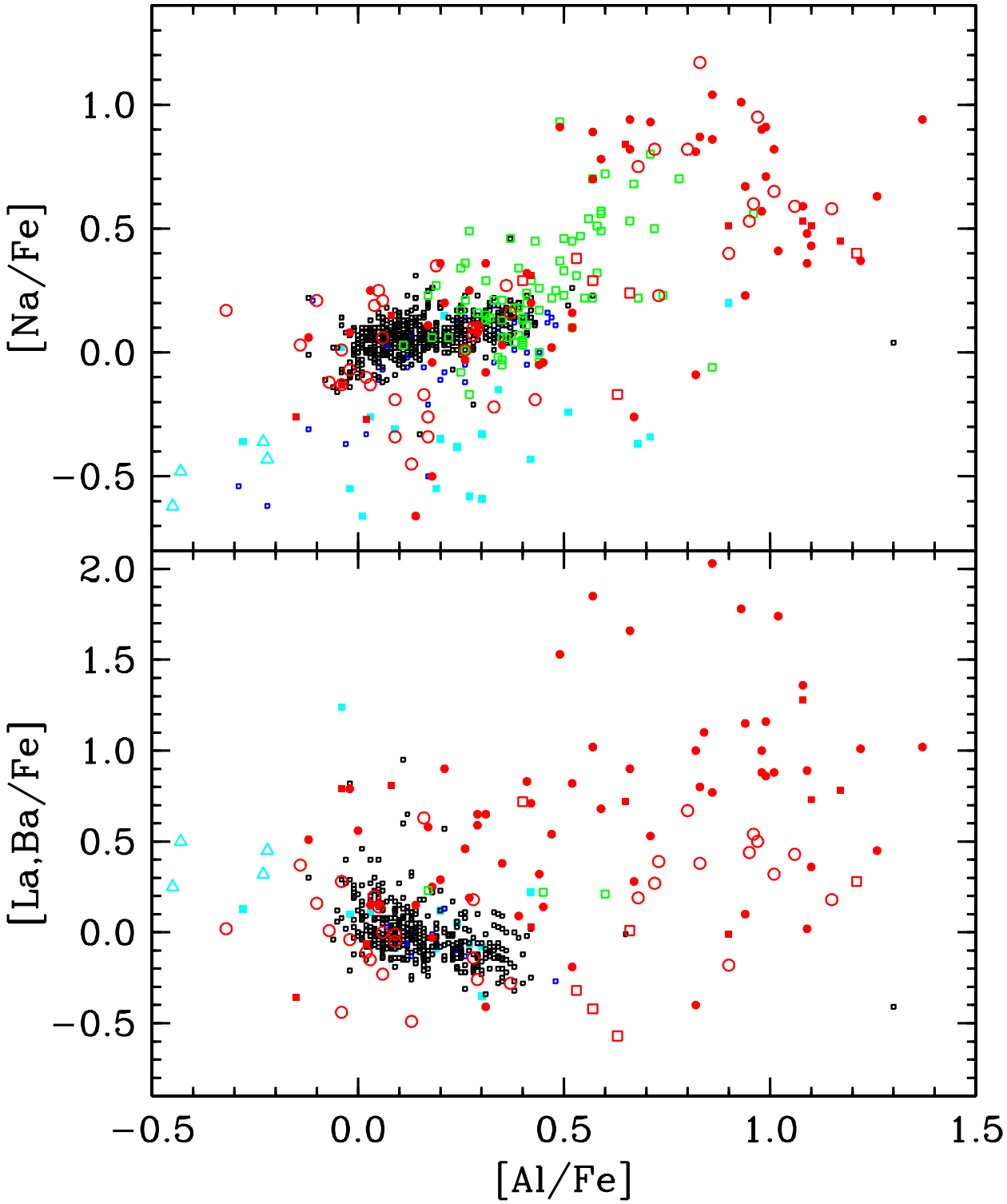

Fig. 16.— The top panel shows [Na/Fe] versus [Al/Fe] with data from this study and the literature. The bottom panel shows [La,Ba/Fe] versus [Al/Fe] where the Ba data are used as a tracer for the s–process in the disk and halo while La is used in all other cases. The symbols are the same as those in Figure 11.

Table 1. Photometry, Membership, and Model Atmosphere Parameters

Star LEID[a]	Alt. ROA[b]	V	B−V	J	H	K	M_V^0	Mem. Prob.[c]	T_{eff} (K)	log g (cm s^{-2})	[Fe/H] Avg.	V_t (km s^{-1})	S/N 6125 Å	S/N 6670 Å
9	370	12.529	1.250	10.382	9.755	9.627	−1.543	99	4505	1.20	−1.41	2.05	100	100
6017	240	12.233	1.420	9.717	8.982	8.808	−1.839	98	4145	0.85	−1.22	2.00	125	100
12013	394	12.579	1.319	10.242	9.560	9.402	−1.493	98	4305	1.10	−1.31	1.85	100	125
15023	234	12.182	1.166	9.964	9.352	9.231	−1.890	100	4455	1.05	−1.80	2.05	125	150
16015	213	12.127	1.122	9.979	9.373	9.210	−1.945	100	4510	1.05	−1.80	1.60	125	125
17015	325	12.430	1.156	10.235	9.610	9.497	−1.642	100	4470	1.15	−1.82	1.65	150	100
19062	464	12.803	1.144	10.601	10.001	9.872	−1.269	98	4470	1.30	−1.75	1.50	100	100
22037	307	12.339	1.186	10.178	9.559	9.402	−1.733	100	4485	1.10	−1.76	1.90	150	150
23061	296	12.337	1.188	10.158	9.472	9.390	−1.735	100	4460	1.10	−1.66	1.65	150	125
24027	5969	13.013	1.099	10.952	10.344	10.226	−1.059	100	4600	1.45	−1.57	1.80	125	75
24056	364	12.474	1.145	10.363	9.708	9.584	−1.598	100	4520	1.20	−1.80	1.65	150	125
25026	569	12.875	1.067	10.807	10.238	10.137	−1.197	100	4630	1.40	−1.83	1.65	75	125
26022	5788	13.095	1.071	11.071	10.486	10.380	−0.977	100	4660	1.50	−1.75	1.60	75	100
26086	295	12.787	1.313	10.330	9.650	9.464	−1.285	98	4205	1.10	−1.13	1.90	100	75
28092	5896	12.521	1.207	10.301	9.649	9.522	−1.551	100	4425	1.15	−1.61	1.70	50	50
30013	540	12.895	1.249	10.737	10.116	9.955	−1.177	100	4485	1.35	−1.33	1.80	100	75
32169	5510	13.331	1.173	10.975	10.289	10.128	−0.741	100	4285	1.40	−0.91	1.70	100	100
32171	251	12.189	1.383	9.897	9.176	9.051	−1.883	100	4325	0.95	−1.48	1.70	100	100
33099	175	12.100	1.483	9.615	8.848	8.691	−1.972	100	4155	0.80	−1.18	2.05	125	125
34029	243	12.107	1.452	9.635	8.878	8.719	−1.965	99	4170	0.80	−1.26	2.00	200	150
34225	557	13.017	1.229	10.608	9.932	9.820	−1.055	100	4270	1.25	−1.20	2.15	···	75
35172	237	12.414	1.399	10.043	9.310	9.127	−1.658	100	4245	1.00	−1.22	1.85	100	75

Table 1—Continued

Star LEID[a]	Alt. ROA[b]	V	B−V	J	H	K	M_V^0	Mem. Prob.[c]	T_{eff} (K)	log g (cm s^{-2})	[Fe/H] Avg.	V_t (km s^{-1})	S/N 6125 Å	S/N 6670 Å
35201	263	12.530	1.360	10.268	9.530	9.389	−1.542	100	4335	1.10	−1.20	1.90	100	100
36282	290	12.351	1.155	10.179	9.575	9.449	−1.721	100	4500	1.15	−1.82	1.85	100	100
38198	···	12.474	1.374	10.122	9.425	9.242	−1.598	100	4275	1.05	−1.53	1.95	150	150
38232	···	12.236	1.449	9.724	9.021	8.834	−1.836	100	4160	0.85	−1.45	2.00	175	175
39026	287	12.333	1.373	9.943	9.208	9.059	−1.739	100	4240	0.95	−1.49	1.95	175	175
39048	451	12.887	1.420	10.106	9.335	9.114	−1.185	99	3965	0.95	−0.98	2.00	100	125
39129	···	12.843	1.361	10.639	9.982	9.833	−1.229	100	4430	1.30	−1.32	1.85	···	75
39392	4579	13.413	1.194	11.108	10.440	10.265	−0.659	100	4330	1.45	−0.91	1.90	100	100
41033	463	12.900	1.258	10.257	9.503	9.330	−1.172	99	4060	1.05	−1.09	2.10	100	125
42508	600	13.041	1.137	10.783	10.144	9.990	−1.031	100	4390	1.35	−1.58	1.90	100	100
43061	357	12.602	1.431	9.744	8.973	8.780	−1.470	100	3930	0.80	−0.93	2.15	125	150
43389	···	12.856	1.301	10.387	9.686	9.500	−1.216	100	4190	1.10	−1.40	1.65	100	100
45358	···	13.067	1.449	10.552	9.798	9.637	−1.005	99	4145	1.15	−1.03	1.95	125	150
45485	3804	13.391	1.146	11.056	10.351	10.253	−0.681	99	4315	1.45	−1.06	1.75	100	100
46121	···	12.891	1.400	10.101	9.400	9.175	−1.181	100	3985	0.95	−0.96	1.85	125	125
47215	···	13.491	1.300	10.894	10.108	9.994	−0.581	100	4095	1.30	−0.77	1.85	100	125
48116	···	12.847	1.474	10.129	9.342	9.109	−1.225	100	3990	0.95	−0.86	1.75	150	···
48323	500	13.081	1.461	10.286	9.458	9.273	−0.991	100	3945	1.00	−0.75	1.80	100	···
49013	312	12.325	1.299	10.046	9.399	9.231	−1.747	99	4365	1.05	−1.61	2.00	150	150
49037	509	12.864	0.994	10.839	10.313	10.175	−1.208	100	4690	1.45	−1.77	1.50	100	100
51021	171	11.984	1.470	9.391	8.633	8.424	−2.088	100	4075	0.70	−1.41	1.90	150	150
51080	236	12.317	1.428	9.809	9.058	8.900	−1.755	100	4150	0.85	−1.48	2.00	125	150

Table 1—Continued

Star LEID[a]	Alt. ROA[b]	V	B−V	J	H	K	M_V^0	Mem. Prob.[c]	T_{eff} (K)	log g (cm s^{-2})	[Fe/H] Avg.	V_t (km s^{-1})	S/N 6125 Å	S/N 6670 Å
51132	421	12.874	1.365	10.267	9.503	9.375	−1.198	100	4090	1.05	−1.11	2.10	125	100
54022	2594	13.360	1.412	10.825	10.069	9.910	−0.712	100	4135	1.25	−0.66	1.90	100	100
54105	386	12.771	1.293	10.194	9.473	9.277	−1.301	100	4105	1.00	−1.18	2.05	100	100
55101	480	12.923	1.252	10.505	9.832	9.650	−1.149	100	4240	1.20	−1.00	1.90	100	100
55111	182	11.969	1.476	9.502	8.804	8.591	−2.103	100	4185	0.75	−1.44	2.00	150	200
55142	367	12.442	1.445	10.008	9.257	9.086	−1.630	100	4195	0.95	−1.12	2.10	100	125
56040	204	12.379	1.162	10.204	9.606	9.423	−1.693	100	4475	1.15	−1.76	2.05	150	175
57010	207	12.154	1.412	9.744	9.001	8.864	−1.918	99	4225	0.85	−1.62	2.00	175	175
59036	289	12.396	1.182	10.209	9.554	9.433	−1.676	100	4455	1.10	−1.75	1.90	175	150
59090	271	12.316	1.255	10.081	9.451	9.267	−1.756	100	4405	1.05	−1.64	1.85	100	100
59094	164	12.174	1.157	10.091	9.527	9.386	−1.898	97	4600	1.10	−1.85	1.50	75	···
60066	2118	13.086	1.253	11.067	10.470	10.330	−0.986	100	4640	1.50	−1.29	2.00	50	50
63021	1878	13.169	1.181	11.031	10.389	10.293	−0.903	100	4515	1.45	−1.42	1.60	75	75
65046	601	12.904	1.098	10.873	10.312	10.193	−1.168	100	4665	1.45	−1.69	1.45	100	···
66047	472	12.704	1.351	10.452	9.779	9.628	−1.368	100	4380	1.20	−1.26	1.75	75	75
66054	232	12.111	1.290	9.908	9.226	9.123	−1.961	100	4430	1.00	−1.71	2.00	···	75
69027	1471	13.365	1.399	10.944	10.229	10.050	−0.707	100	4225	1.35	−0.89	2.00	75	75
76038	316	12.535	1.411	10.009	9.238	9.049	−1.537	98	4120	0.95	−1.29	2.05	125	100
77025	194	12.197	1.339	9.861	9.171	9.008	−1.875	99	4300	0.95	−1.68	2.05	100	100
80029	218	12.273	1.293	9.949	9.248	9.111	−1.799	97	4310	1.00	−1.66	1.85	100	125
81018	217	12.282	1.174	10.015	9.377	9.244	−1.790	100	4395	1.05	−1.87	1.85	50	50
85027	264	12.370	1.260	10.035	9.358	9.217	−1.702	99	4315	1.00	−1.62	1.95	75	75

Table 1—Continued

Star LEID[a]	Alt. ROA[b]	V	B−V	J	H	K	M_V^0	Mem. Prob.[c]	T_{eff} (K)	log g (cm s^{-2})	[Fe/H] Avg.	V_t (km s^{-1})	S/N 6125 Å	S/N 6670 Å

[a]Identifier from van Leeuwen et al. (2000).

[b]Identifier from Woolley (1966).

[c]Membership probability from van Leeuwen et al. (2000).

Table 2a. Linelist and Equivalent Widths

λ (Å)	Element	E.P. (eV)	log gf	9	6017	12013	15023	16015	17015	19062	22037	23061	24027	24056
6003.01	Fe I	3.88	−1.07	···	···	···	···	···	···	···	40	···	···	46
6007.32	Ni I	1.68	−3.35	···	70	···	···	···	···	···	21	···	···	22
6007.97	Fe I	4.65	−0.70	···	53	···	···	···	···	···	···	···	19	···
6008.57	Fe I	3.88	−0.94	···	99	···	···	···	···	···	···	···	···	···
6015.25	Fe I	2.22	−4.66	···	17	12	···	···	···	···	···	···	···	···
6024.07	Fe I	4.55	−0.06	84	107	89	59	52	59	61	58	60	···	49
6027.06	Fe I	4.07	−1.14	47	68	63	25	15	24	35	22	28	57	20
6035.35	Fe I	4.29	−2.56	···	···	···	···	···	···	···	···	···	···	···
6056.01	Fe I	4.73	−0.44	52	51	43	23	22	18	36	16	26	30	···
6064.63	Ti I	1.05	−1.92	22	60	59	12	···	8	21	7	11	8	8
6065.49	Fe I	2.61	−1.51	152	189	169	132	114	127	116	119	131	117	111
6078.50	Fe I	4.79	−0.34	41	52	59	21	22	20	29	22	28	33	22
6079.02	Fe I	4.65	−1.06	···	···	30	7	···	···	9	···	9	13	···
6082.72	Fe I	2.22	−3.61	52	87	72	33	23	···	30	21	26	33	22
6084.11	Fe II	3.20	−3.87	23	···	18	9	13	···	9	···	14	···	9
6086.29	Ni I	4.26	−0.54	19	31	25	···	···	8	···	···	7	23	···
6089.57	Fe I	5.02	−0.92	13	···	···	···	9	8	···	···	8	···	···
6091.18	Ti I	2.27	−0.42	···	52	44	···	···	···	···	···	···	19	···
6094.38	Fe I	4.65	−1.66	···	···	7	···	···	···	···	···	8	···	···
6096.67	Fe I	3.98	−1.88	15	38	28	13	···	7	15	7	···	···	11
6102.18	Fe I	4.83	−0.37	36	72	63	24	19	22	28	26	25	28	24
6102.73	Ca I	1.88	−0.81	158	173	166	113	106	116	117	116	116	120	109

Table 2a—Continued

λ (Å)	Element	E.P. (eV)	log gf	9	6017	12013	15023	16015	17015	19062	22037	23061	24027	24056
6108.13	Ni I	1.68	−2.51	95	135	112	65	51	67	68	59	75	71	60
6111.08	Ni I	4.09	−0.89	13	···	25	···	8	···	13	···	···	17	···
6120.25	Fe I	0.91	−5.95	12	47	38	4	11	···	···	···	11	···	10
6121.01	Ti I	1.88	−1.32	···	18	13	···	···	···	···	···	···	···	···
6122.23	Ca I	1.89	−0.26	181	231	204	146	129	152	143	138	144	151	141
6126.22	Ti I	1.07	−1.42	48	105	85	19	19	22	26	25	24	27	18
6128.98	Ni I	1.68	−3.36	42	79	64	22	···	21	15	27	21	31	16
6146.24	Ti I	1.87	−1.51	···	···	12	···	···	···	···	···	···	···	···
6149.25	Fe II	3.89	−2.78	28	34	28	26	19	···	14	24	22	···	···
6151.62	Fe I	2.18	−3.33	67	95	86	43	40	44	44	41	48	52	45
6154.23	Na I	2.10	−1.57	···	50	34	···	···	···	···	···	···	20	···
6157.73	Fe I	4.07	−1.22	51	···	74	27	22	23	25	26	24	36	25
6160.75	Na I	2.10	−1.27	19	76	62	3	3	···	12	8	7	26	12
6161.30	Ca I	2.52	−1.28	58	108	99	25	25	29	38	31	37	60	32
6162.18	Ca I	1.90	−0.07	205	248	226	167	141	155	167	163	163	170	154
6165.36	Fe I	4.14	−1.51	27	35	39	11	···	15	23	18	18	17	13
6166.44	Ca I	2.52	−1.11	53	96	100	39	42	43	49	36	44	53	40
6169.04	Ca I	2.52	−0.69	84	123	118	50	59	57	67	54	60	67	62
6169.56	Ca I	2.52	−0.42	103	163	137	73	72	66	83	76	77	104	77
6173.34	Fe I	2.22	−2.89	103	129	120	71	57	76	71	73	75	82	70
6175.37	Ni I	4.09	−0.55	32	36	35	13	10	···	24	11	11	10	16
6176.82	Ni I	4.09	−0.42	34	45	55	26	15	21	26	16	17	···	18

Table 2a—Continued

λ (Å)	Element	E.P. (eV)	log gf	9	6017	12013	15023	16015	17015	19062	22037	23061	24027	24056
6177.25	Ni I	1.83	−3.53	20	47	35	···	10	11	11	14	···	···	14
6180.21	Fe I	2.73	−2.66	56	93	94	36	38	31	40	32	48	43	36
6186.72	Ni I	4.11	−0.96	···	10	16	8	8	···	···	···	9	···	···
6188.00	Fe I	3.94	−1.69	23	54	43	···	11	19	18	9	17	20	12
6200.32	Fe I	2.61	−2.41	100	119	118	67	60	59	74	62	71	73	64
6210.67	Sc I	0.00	−1.53	11	···	31	···	···	···	10	···	···	···	7
6219.29	Fe I	2.20	−2.42	130	···	152	107	84	99	106	104	105	96	91
6226.74	Fe I	3.88	−2.19	···	···	21	···	···	8	···	···	···	···	···
6229.23	Fe I	2.84	−3.00	44	62	56	21	18	18	21	12	28	17	···
6232.65	Fe I	3.65	−1.23	80	122	85	48	46	41	59	46	49	59	48
6546.24	Fe I	2.76	−1.65	131	···	131	107	91	87	94	98	106	103	98
6551.68	Fe I	0.99	−5.77	···	···	···	17	···	···	···	···	···	···	15
6554.23	Ti I	1.44	−1.16	21	76	71	···	···	···	···	···	···	···	···
6556.07	Ti I	1.46	−1.10	···	58	56	12	···	···	···	···	···	···	10
6559.57	Ti II	2.05	−2.30	38	39	39	51	36	35	42	38	···	32	41
6574.25	Fe I	0.99	−5.02	68	96	88	41	21	33	43	40	47	35	30
6586.31	Ni I	1.95	−2.81	57	77	76	24	···	34	25	28	34	···	34
6592.92	Fe I	2.73	−1.52	···	···	155	···	106	119	102	···	123	123	114
6593.88	Fe I	2.43	−2.42	···	154	145	93	78	96	83	92	93	98	83
6597.57	Fe I	4.79	−0.95	···	···	···	9	···	15	14	12	19	16	···
6604.60	Sc II	1.36	−1.48	61	···	···	41	···	50	···	40	···	42	45
6606.97	Ti II	2.06	−2.79	12	···	32	16	18	11	···	13	···	17	···

Table 2a—Continued

λ (Å)	Element	E.P. (eV)	log gf	9	6017	12013	15023	16015	17015	19062	22037	23061	24027	24056
6608.04	Fe I	2.28	−3.96	···	52	38	···	···	···	···	16	23	···	···
6609.12	Fe I	2.56	−2.69	78	104	97	···	50	50	59	62	62	66	61
6625.02	Fe I	1.01	−5.37	40	91	80	26	21	31	20	17	21	···	···
6627.54	Fe I	4.55	−1.58	13	13	23	···	···	···	···	···	···	···	9
6633.75	Fe I	4.79	−0.80	···	···	···	···	···	···	···	···	···	···	···
6643.63	Ni I	1.68	−2.01	132	···	155	115	81	102	116	110	111	99	110
6645.12	Eu II	1.37	+0.20	4	12	4	4	9	5	10	12	9	10	16
6646.96	Fe I	2.61	−3.96	···	24	···	8	···	···	···	···	···	···	···
6648.12	Fe I	1.01	−5.92	···	···	···	4	9	···	···	···	8	14	···
6677.99	Fe I	2.69	−1.35	160	185	162	130	115	110	125	112	127	129	118
6696.03	Al I	3.14	−1.57	synth	synth	synth	···	···	···	···	synth	···	synth	synth
6698.66	Al I	3.14	−1.89	···	synth	synth	synth	synth	···	···	synth	···	synth	···
6703.57	Fe I	2.76	−3.01	36	80	56	20	16	···	···	···	27	20	17
6710.32	Fe I	1.48	−4.83	38	91	68	18	···	16	···	17	26	···	22
6717.68	Ca I	2.71	−0.61	100	···	···	64	61	78	82	72	78	89	64
6726.67	Fe I	4.61	−1.07	22	···	30	···	···	···	14	···	···	···	9
6733.15	Fe I	4.64	−1.48	···	21	11	···	···	···	···	···	8	···	···
6739.52	Fe I	1.56	−4.79	···	···	42	10	···	···	28	···	···	17	···
6743.12	Ti I	0.90	−1.65	31	100	83	12	···	15	14	18	···	19	17
6774.27	La II	0.13	−1.75	7	92	33	9	13	8	25	5	7	18	6

Table 2b. Linelist and Equivalent Widths

λ (Å)	Element	E.P. (eV)	log gf	25026	26022	26086	28092	30013	32169	32171	33099	34029	34225	35172
6003.01	Fe I	3.88	−1.07	···	···	88	···	···	···	···	···	···	···	···
6007.32	Ni I	1.68	−3.35	18	···	67	16	···	···	50	57	···	···	···
6007.97	Fe I	4.65	−0.70	···	···	67	34	···	48	···	···	···	···	···
6008.57	Fe I	3.88	−0.94	40	···	121	···	···	···	···	···	···	···	···
6015.25	Fe I	2.22	−4.66	···	···	26	···	···	···	···	···	···	···	17
6024.07	Fe I	4.55	−0.06	56	45	113	66	89	126	···	110	97	···	113
6027.06	Fe I	4.07	−1.14	···	···	80	···	···	73	49	90	75	···	75
6035.35	Fe I	4.29	−2.56	···	···	···	···	···	···	···	···	···	···	···
6056.01	Fe I	4.73	−0.44	16	21	61	33	···	66	32	···	52	···	···
6064.63	Ti I	1.05	−1.92	14	···	96	···	31	79	24	85	75	···	66
6065.49	Fe I	2.61	−1.51	100	91	189	···	145	179	142	190	181	···	174
6078.50	Fe I	4.79	−0.34	15	···	64	···	40	77	49	···	61	···	54
6079.02	Fe I	4.65	−1.06	···	···	57	···	28	57	···	55	30	···	43
6082.72	Fe I	2.22	−3.61	14	17	76	···	66	84	···	86	93	···	78
6084.11	Fe II	3.20	−3.87	···	···	···	···	···	···	19	···	22	···	···
6086.29	Ni I	4.26	−0.54	···	8	32	···	30	49	30	30	26	···	26
6089.57	Fe I	5.02	−0.92	···	···	···	···	···	41	14	33	···	···	30
6091.18	Ti I	2.27	−0.42	···	11	67	···	21	47	19	61	53	···	50
6094.38	Fe I	4.65	−1.66	···	···	···	···	···	···	···	···	···	···	···
6096.67	Fe I	3.98	−1.88	···	···	38	···	···	42	19	···	34	···	···
6102.18	Fe I	4.83	−0.37	21	23	81	23	48	87	39	81	56	···	65
6102.73	Ca I	1.88	−0.81	98	95	213	115	156	183	143	185	184	···	189

Table 2b—Continued

λ (Å)	Element	E.P. (eV)	log gf	25026	26022	26086	28092	30013	32169	32171	33099	34029	34225	35172
6108.13	Ni I	1.68	−2.51	35	58	129	76	102	122	105	139	···	···	125
6111.08	Ni I	4.09	−0.89	···	11	33	···	17	48	20	37	···	···	37
6120.25	Fe I	0.91	−5.95	···	···	54	···	16	46	···	52	43	···	42
6121.01	Ti I	1.88	−1.32	···	···	45	···	···	40	···	33	28	···	30
6122.23	Ca I	1.89	−0.26	145	134	245	150	175	248	172	233	233	···	228
6126.22	Ti I	1.07	−1.42	···	16	112	30	70	114	72	114	115	···	97
6128.98	Ni I	1.68	−3.36	13	···	61	···	44	75	48	74	72	···	69
6146.24	Ti I	1.87	−1.51	···	···	43	···	···	···	···	···	27	···	···
6149.25	Fe II	3.89	−2.78	15	···	···	···	···	···	···	···	28	···	···
6151.62	Fe I	2.18	−3.33	20	39	109	78	76	···	65	102	98	···	95
6154.23	Na I	2.10	−1.57	···	5	112	···	···	108	30	74	50	···	68
6157.73	Fe I	4.07	−1.22	14	28	···	···	···	···	···	···	···	···	···
6160.75	Na I	2.10	−1.27	···	17	123	18	62	110	43	92	68	···	92
6161.30	Ca I	2.52	−1.28	17	···	136	58	90	132	74	119	117	···	117
6162.18	Ca I	1.90	−0.07	134	147	265	183	202	253	199	257	247	···	248
6165.36	Fe I	4.14	−1.51	···	···	67	···	38	71	33	50	49	···	48
6166.44	Ca I	2.52	−1.11	29	42	114	33	82	122	76	118	107	···	104
6169.04	Ca I	2.52	−0.69	50	63	153	65	98	149	94	139	129	···	135
6169.56	Ca I	2.52	−0.42	64	82	174	74	104	161	108	156	152	···	156
6173.34	Fe I	2.22	−2.89	53	49	145	84	116	134	103	153	128	···	143
6175.37	Ni I	4.09	−0.55	7	19	36	···	···	43	18	44	34	···	36
6176.82	Ni I	4.09	−0.42	10	···	63	14	35	50	36	44	47	···	56

Table 2b—Continued

λ (Å)	Element	E.P. (eV)	log gf	25026	26022	26086	28092	30013	32169	32171	33099	34029	34225	35172
6177.25	Ni I	1.83	−3.53	···	···	50	···	32	68	20	56	44	···	37
6180.21	Fe I	2.73	−2.66	22	28	109	52	64	113	70	100	102	···	90
6186.72	Ni I	4.11	−0.96	···	···	16	···	···	···	···	17	20	···	···
6188.00	Fe I	3.94	−1.69	···	···	75	···	42	71	31	62	54	···	50
6200.32	Fe I	2.61	−2.41	39	60	120	73	86	125	96	127	123	···	120
6210.67	Sc I	0.00	−1.53	···	···	66	···	···	59	24	67	49	···	52
6219.29	Fe I	2.20	−2.42	83	83	···	118	117	161	123	160	160	···	152
6226.74	Fe I	3.88	−2.19	7	···	32	15	···	54	···	···	30	···	···
6229.23	Fe I	2.84	−3.00	···	···	69	···	43	78	33	98	63	···	61
6232.65	Fe I	3.65	−1.23	···	37	121	82	96	110	82	127	98	···	104
6546.24	Fe I	2.76	−1.65	73	77	···	···	134	···	126	···	···	···	···
6551.68	Fe I	0.99	−5.77	···	···	···	···	···	···	···	···	51	···	···
6554.23	Ti I	1.44	−1.16	17	···	97	···	···	···	36	···	79	···	69
6556.07	Ti I	1.46	−1.10	···	···	···	···	27	···	28	···	96	···	62
6559.57	Ti II	2.05	−2.30	···	28	35	···	30	···	29	···	72	49	···
6574.25	Fe I	0.99	−5.02	30	19	···	70	···	103	72	118	112	···	115
6586.31	Ni I	1.95	−2.81	34	20	77	63	51	66	50	82	81	65	81
6592.92	Fe I	2.73	−1.52	104	108	186	115	151	···	139	210	177	182	···
6593.88	Fe I	2.43	−2.42	76	64	146	98	···	146	124	174	158	156	164
6597.57	Fe I	4.79	−0.95	···	···	···	···	···	···	17	···	32	···	···
6604.60	Sc II	1.36	−1.48	···	···	61	···	···	···	···	85	···	73	66
6606.97	Ti II	2.06	−2.79	···	13	···	···	···	···	···	···	···	···	···

Table 2b—Continued

λ (Å)	Element	E.P. (eV)	log gf	25026	26022	26086	28092	30013	32169	32171	33099	34029	34225	35172
6608.04	Fe I	2.28	−3.96	···	···	63	···	···	48	24	59	58	···	···
6609.12	Fe I	2.56	−2.69	44	···	···	67	77	125	73	114	121	···	107
6625.02	Fe I	1.01	−5.37	17	17	···	···	···	106	52	120	···	94	···
6627.54	Fe I	4.55	−1.58	···	···	···	···	···	36	10	21	20	14	27
6633.75	Fe I	4.79	−0.80	···	···	···	···	···	···	···	···	···	···	···
6643.63	Ni I	1.68	−2.01	97	90	188	116	143	145	140	189	156	149	162
6645.12	Eu II	1.37	+0.20	11	11	10	54	10	28	22	34	20	36	16
6646.96	Fe I	2.61	−3.96	···	···	45	···	15	26	10	37	28	34	42
6648.12	Fe I	1.01	−5.92	···	···	···	···	···	···	···	···	66	···	···
6677.99	Fe I	2.69	−1.35	103	111	200	147	···	···	150	232	192	···	191
6696.03	Al I	3.14	−1.57	synth	synth	synth	···	synth	synth	synth	synth	synth	synth	synth
6698.66	Al I	3.14	−1.89	···	synth	synth	···	synth	synth	synth	synth	synth	synth	synth
6703.57	Fe I	2.76	−3.01	25	···	74	29	···	···	54	···	74	77	76
6710.32	Fe I	1.48	−4.83	···	···	···	31	61	···	56	···	84	···	···
6717.68	Ca I	2.71	−0.61	62	67	···	99	···	···	106	···	152	···	···
6726.67	Fe I	4.61	−1.07	10	···	···	···	···	···	···	···	30	···	···
6733.15	Fe I	4.64	−1.48	···	···	19	···	···	29	···	27	16	26	···
6739.52	Fe I	1.56	−4.79	13	···	···	30	33	···	···	···	62	61	···
6743.12	Ti I	0.90	−1.65	···	···	111	···	65	97	47	129	123	88	99
6774.27	La II	0.13	−1.75	7	7	73	51	86	75	112	91	68	90	93

Table 2c. Linelist and Equivalent Widths

λ (Å)	Element	E.P. (eV)	log gf	35201	36282	38198	38232	39026	39048	39129	39392	41033	42508	43061
6003.01	Fe I	3.88	−1.07	···	···	···	···	73	···	···	···	···	···	···
6007.32	Ni I	1.68	−3.35	···	···	···	···	···	···	···	···	96	···	···
6007.97	Fe I	4.65	−0.70	···	···	···	···	···	58	···	···	66	···	···
6008.57	Fe I	3.88	−0.94	···	···	···	···	···	···	···	···	131	···	···
6015.25	Fe I	2.22	−4.66	23	···	···	···	11	36	···	28	34	···	···
6024.07	Fe I	4.55	−0.06	108	61	89	90	87	141	···	130	134	91	···
6027.06	Fe I	4.07	−1.14	71	···	51	74	53	111	···	93	96	33	···
6035.35	Fe I	4.29	−2.56	···	···	···	···	···	···	···	···	···	···	19
6056.01	Fe I	4.73	−0.44	···	19	46	45	50	65	···	66	67	30	72
6064.63	Ti I	1.05	−1.92	57	···	29	65	57	140	···	83	112	15	146
6065.49	Fe I	2.61	−1.51	177	117	155	167	162	207	···	196	203	135	224
6078.50	Fe I	4.79	−0.34	60	29	49	55	50	77	···	77	80	38	84
6079.02	Fe I	4.65	−1.06	48	···	16	29	27	···	···	58	62	17	66
6082.72	Fe I	2.22	−3.61	83	21	67	83	69	···	···	76	···	38	122
6084.11	Fe II	3.20	−3.87	···	···	···	19	18	···	···	···	···	14	···
6086.29	Ni I	4.26	−0.54	39	14	28	28	22	38	···	39	37	19	···
6089.57	Fe I	5.02	−0.92	22	···	···	···	···	···	···	43	···	···	···
6091.18	Ti I	2.27	−0.42	43	···	26	43	34	117	···	64	82	···	105
6094.38	Fe I	4.65	−1.66	···	···	12	9	9	29	···	22	23	7	28
6096.67	Fe I	3.98	−1.88	···	···	15	34	24	58	···	53	51	15	···
6102.18	Fe I	4.83	−0.37	63	18	48	58	48	···	···	80	···	40	···
6102.73	Ca I	1.88	−0.81	168	114	163	177	162	248	···	204	220	130	265

Table 2c—Continued

λ (Å)	Element	E.P. (eV)	log gf	35201	36282	38198	38232	39026	39048	39129	39392	41033	42508	43061
6108.13	Ni I	1.68	−2.51	121	62	108	119	109	155	···	128	148	89	150
6111.08	Ni I	4.09	−0.89	32	···	21	23	15	···	···	40	44	10	48
6120.25	Fe I	0.91	−5.95	34	···	22	32	34	87	···	56	76	10	90
6121.01	Ti I	1.88	−1.32	···	···	···	19	···	···	···	36	56	···	95
6122.23	Ca I	1.89	−0.26	210	149	196	210	211	···	···	253	283	172	355
6126.22	Ti I	1.07	−1.42	97	19	83	106	87	183	···	116	156	48	168
6128.98	Ni I	1.68	−3.36	64	···	55	60	59	93	···	87	83	28	102
6146.24	Ti I	1.87	−1.51	···	···	···	17	···	···	···	42	56	···	50
6149.25	Fe II	3.89	−2.78	···	···	20	17	22	···	···	···	···	···	···
6151.62	Fe I	2.18	−3.33	84	38	83	105	89	123	···	104	117	70	132
6154.23	Na I	2.10	−1.57	70	···	28	14	17	149	···	108	121	7	127
6157.73	Fe I	4.07	−1.22	···	18	74	78	66	···	···	···	···	56	···
6160.75	Na I	2.10	−1.27	87	14	43	36	35	137	···	129	127	29	154
6161.30	Ca I	2.52	−1.28	107	24	87	88	88	···	···	127	···	61	···
6162.18	Ca I	1.90	−0.07	233	153	205	236	219	362	···	277	307	182	366
6165.36	Fe I	4.14	−1.51	41	···	39	37	33	···	···	65	74	27	68
6166.44	Ca I	2.52	−1.11	98	34	84	97	91	170	···	120	142	60	156
6169.04	Ca I	2.52	−0.69	124	48	101	121	116	···	···	145	168	84	185
6169.56	Ca I	2.52	−0.42	134	···	122	138	125	209	···	158	185	108	···
6173.34	Fe I	2.22	−2.89	120	69	109	128	109	152	···	148	161	96	175
6175.37	Ni I	4.09	−0.55	32	16	31	31	···	54	···	47	53	17	50
6176.82	Ni I	4.09	−0.42	43	···	39	42	48	61	···	51	72	···	62

Table 2c—Continued

λ (Å)	Element	E.P. (eV)	log gf	35201	36282	38198	38232	39026	39048	39129	39392	41033	42508	43061
6177.25	Ni I	1.83	−3.53	36	···	34	44	26	69	···	60	64	···	···
6180.21	Fe I	2.73	−2.66	86	37	78	93	84	115	···	111	108	62	131
6186.72	Ni I	4.11	−0.96	···	···	···	15	12	31	···	24	47	···	34
6188.00	Fe I	3.94	−1.69	45	11	34	41	42	73	···	68	69	18	76
6200.32	Fe I	2.61	−2.41	118	63	109	114	98	141	···	121	134	70	149
6210.67	Sc I	0.00	−1.53	39	···	18	31	28	161	···	69	100	···	143
6219.29	Fe I	2.20	−2.42	156	102	125	153	148	···	···	174	···	121	189
6226.74	Fe I	3.88	−2.19	···	···	···	20	18	51	···	40	28	13	43
6229.23	Fe I	2.84	−3.00	62	19	46	63	57	···	···	88	93	30	106
6232.65	Fe I	3.65	−1.23	109	44	97	100	93	135	···	106	125	67	128
6546.24	Fe I	2.76	−1.65	···	···	···	155	···	···	···	···	···	117	···
6551.68	Fe I	0.99	−5.77	···	···	···	32	28	···	···	52	···	···	···
6554.23	Ti I	1.44	−1.16	···	···	···	66	59	153	···	···	···	19	145
6556.07	Ti I	1.46	−1.10	59	···	49	75	73	···	···	···	···	···	155
6559.57	Ti II	2.05	−2.30	···	···	···	46	49	···	···	60	···	28	47
6574.25	Fe I	0.99	−5.02	94	···	···	106	86	146	66	119	138	51	162
6586.31	Ni I	1.95	−2.81	77	···	65	72	73	···	52	77	86	···	100
6592.92	Fe I	2.73	−1.52	···	108	···	189	168	208	162	196	205	132	···
6593.88	Fe I	2.43	−2.42	150	95	133	140	137	193	130	159	187	97	199
6597.57	Fe I	4.79	−0.95	···	···	···	33	17	···	···	48	···	···	···
6604.60	Sc II	1.36	−1.48	64	37	···	72	···	82	57	···	···	···	···
6606.97	Ti II	2.06	−2.79	···	···	···	···	33	···	···	···	···	···	···

Table 2c—Continued

λ (Å)	Element	E.P. (eV)	log gf	35201	36282	38198	38232	39026	39048	39129	39392	41033	42508	43061
6608.04	Fe I	2.28	−3.96	44	···	···	67	42	86	25	58	70	···	···
6609.12	Fe I	2.56	−2.69	100	58	98	102	86	···	81	111	129	77	173
6625.02	Fe I	1.01	−5.37	87	···	63	97	66	···	55	108	···	···	···
6627.54	Fe I	4.55	−1.58	25	9	···	16	13	32	···	···	28	12	29
6633.75	Fe I	4.79	−0.80	···	···	···	···	···	···	···	···	···	···	···
6643.63	Ni I	1.68	−2.01	162	92	151	161	155	186	136	150	174	133	188
6645.12	Eu II	1.37	+0.20	32	7	24	16	12	39	12	34	16	12	28
6646.96	Fe I	2.61	−3.96	29	···	16	22	21	56	19	36	39	···	55
6648.12	Fe I	1.01	−5.92	···	10	37	45	40	105	···	···	···	···	109
6677.99	Fe I	2.69	−1.35	196	129	···	180	172	231	164	209	215	156	247
6696.03	Al I	3.14	−1.57	synth	synth	synth	synth	synth	synth	synth	synth	synth	synth	synth
6698.66	Al I	3.14	−1.89	synth	···	synth	synth	···	synth	···	synth	synth	···	synth
6703.57	Fe I	2.76	−3.01	···	34	48	60	59	95	57	81	···	25	123
6710.32	Fe I	1.48	−4.83	···	···	52	68	55	127	61	···	···	32	139
6717.68	Ca I	2.71	−0.61	···	57	103	···	120	···	···	···	···	103	···
6726.67	Fe I	4.61	−1.07	···	···	22	22	32	···	···	···	···	11	···
6733.15	Fe I	4.64	−1.48	···	···	8	13	6	27	18	40	24	···	30
6739.52	Fe I	1.56	−4.79	···	10	41	51	···	95	···	···	···	···	···
6743.12	Ti I	0.90	−1.65	89	···	56	88	···	187	···	119	153	44	171
6774.27	La II	0.13	−1.75	71	12	71	47	49	155	37	52	87	30	98

Table 2d. Linelist and Equivalent Widths

λ (Å)	Element	E.P. (eV)	log gf	43389	45358	45485	46121	47215	48116	48323	49013	49037	51021	51080
6003.01	Fe I	3.88	−1.07	82	···	···	···	···	···	···	···	···	···	···
6007.32	Ni I	1.68	−3.35	···	···	···	91	···	···	···	···	···	···	···
6007.97	Fe I	4.65	−0.70	37	···	···	···	···	84	60	···	···	49	···
6008.57	Fe I	3.88	−0.94	89	···	···	···	···	···	···	···	···	90	···
6015.25	Fe I	2.22	−4.66	···	···	22	···	32	···	···	8	···	···	···
6024.07	Fe I	4.55	−0.06	101	117	114	105	144	129	134	71	50	···	102
6027.06	Fe I	4.07	−1.14	64	74	85	90	···	93	95	53	19	62	79
6035.35	Fe I	4.29	−2.56	···	···	···	···	···	···	···	···	···	···	···
6056.01	Fe I	4.73	−0.44	45	67	59	65	80	66	71	40	14	50	58
6064.63	Ti I	1.05	−1.92	66	106	67	130	121	140	146	23	8	69	68
6065.49	Fe I	2.61	−1.51	157	192	175	198	204	200	206	142	···	164	170
6078.50	Fe I	4.79	−0.34	56	76	···	69	82	76	92	42	21	42	49
6079.02	Fe I	4.65	−1.06	28	···	42	47	···	67	···	15	···	28	31
6082.72	Fe I	2.22	−3.61	74	96	89	120	117	122	···	50	17	81	81
6084.11	Fe II	3.20	−3.87	18	···	···	20	···	···	···	···	···	···	···
6086.29	Ni I	4.26	−0.54	19	37	34	43	53	47	50	···	···	22	22
6089.57	Fe I	5.02	−0.92	···	···	···	···	···	···	···	···	···	···	···
6091.18	Ti I	2.27	−0.42	52	82	69	86	110	106	113	16	···	47	53
6094.38	Fe I	4.65	−1.66	9	···	16	19	22	31	27	···	···	···	···
6096.67	Fe I	3.98	−1.88	34	45	···	48	54	42	64	12	7	28	30
6102.18	Fe I	4.83	−0.37	55	89	82	···	···	···	102	48	21	56	59
6102.73	Ca I	1.88	−0.81	162	219	195	216	237	256	257	137	98	184	175

Table 2d—Continued

λ (Å)	Element	E.P. (eV)	log gf	43389	45358	45485	46121	47215	48116	48323	49013	49037	51021	51080
6108.13	Ni I	1.68	−2.51	111	137	120	142	141	140	152	92	44	124	120
6111.08	Ni I	4.09	−0.89	20	48	37	44	55	51	52	12	···	22	26
6120.25	Fe I	0.91	−5.95	37	58	37	75	78	84	93	16	···	52	39
6121.01	Ti I	1.88	−1.32	33	49	20	95	99	···	···	14	···	32	31
6122.23	Ca I	1.89	−0.26	206	285	···	318	338	397	409	159	137	236	227
6126.22	Ti I	1.07	−1.42	98	···	97	161	157	181	185	38	···	118	109
6128.98	Ni I	1.68	−3.36	55	85	80	90	100	101	109	43	11	71	67
6146.24	Ti I	1.87	−1.51	···	···	···	65	81	···	···	···	···	19	···
6149.25	Fe II	3.89	−2.78	13	···	···	22	···	···	···	···	16	24	···
6151.62	Fe I	2.18	−3.33	96	119	104	114	119	114	···	74	29	104	95
6154.23	Na I	2.10	−1.57	30	107	81	68	126	137	137	···	···	24	21
6157.73	Fe I	4.07	−1.22	···	···	···	···	···	···	···	37	17	77	···
6160.75	Na I	2.10	−1.27	44	130	113	84	128	151	139	15	4	33	35
6161.30	Ca I	2.52	−1.28	101	···	112	···	···	···	···	62	20	98	103
6162.18	Ca I	1.90	−0.07	224	311	239	314	336	383	378	188	150	233	234
6165.36	Fe I	4.14	−1.51	47	62	47	···	87	···	89	30	10	38	39
6166.44	Ca I	2.52	−1.11	90	141	105	144	132	179	163	66	29	101	107
6169.04	Ca I	2.52	−0.69	117	153	131	149	173	179	177	87	45	132	124
6169.56	Ca I	2.52	−0.42	140	189	160	175	···	196	194	102	78	132	143
6173.34	Fe I	2.22	−2.89	117	144	132	150	154	···	159	103	42	128	125
6175.37	Ni I	4.09	−0.55	27	63	49	60	46	70	52	···	···	31	33
6176.82	Ni I	4.09	−0.42	53	71	69	77	82	54	66	28	17	51	49

Table 2d—Continued

λ (Å)	Element	E.P. (eV)	log gf	43389	45358	45485	46121	47215	48116	48323	49013	49037	51021	51080
6177.25	Ni I	1.83	−3.53	34	54	56	61	66	83	67	32	11	46	33
6180.21	Fe I	2.73	−2.66	83	122	···	118	123	125	116	61	20	104	93
6186.72	Ni I	4.11	−0.96	···	28	···	46	29	41	51	17	···	21	16
6188.00	Fe I	3.94	−1.69	40	65	55	80	66	79	79	36	···	55	48
6200.32	Fe I	2.61	−2.41	106	128	116	133	···	···	148	92	52	120	121
6210.67	Sc I	0.00	−1.53	···	88	59	107	···	147	150	17	···	···	44
6219.29	Fe I	2.20	−2.42	134	···	···	···	···	···	···	131	77	155	150
6226.74	Fe I	3.88	−2.19	21	···	28	54	47	···	50	12	···	19	23
6229.23	Fe I	2.84	−3.00	61	88	57	87	91	···	···	41	···	63	58
6232.65	Fe I	3.65	−1.23	93	133	116	110	122	115	131	88	35	96	···
6546.24	Fe I	2.76	−1.65	···	···	···	···	···	···	···	···	···	···	···
6551.68	Fe I	0.99	−5.77	···	···	···	86	···	···	···	···	···	50	···
6554.23	Ti I	1.44	−1.16	···	···	62	147	···	···	···	24	16	81	62
6556.07	Ti I	1.46	−1.10	···	···	78	142	···	···	···	···	···	103	88
6559.57	Ti II	2.05	−2.30	···	41	42	49	···	···	···	50	···	61	47
6574.25	Fe I	0.99	−5.02	89	123	95	132	131	···	···	59	···	122	···
6586.31	Ni I	1.95	−2.81	54	98	70	···	88	···	···	62	···	95	98
6592.92	Fe I	2.73	−1.52	···	···	163	···	···	···	···	···	···	166	170
6593.88	Fe I	2.43	−2.42	···	176	140	···	···	···	···	112	67	153	153
6597.57	Fe I	4.79	−0.95	34	···	···	···	68	···	···	···	11	···	26
6604.60	Sc II	1.36	−1.48	45	···	···	77	···	···	···	62	···	···	···
6606.97	Ti II	2.06	−2.79	···	···	···	56	···	···	···	···	···	33	···

Table 2d—Continued

λ (Å)	Element	E.P. (eV)	log gf	43389	45358	45485	46121	47215	48116	48323	49013	49037	51021	51080
6608.04	Fe I	2.28	−3.96	44	70	46	80	···	···	···	···	···	66	52
6609.12	Fe I	2.56	−2.69	89	131	109	131	···	···	···	91	50	132	111
6625.02	Fe I	1.01	−5.37	94	120	86	···	···	···	···	57	···	86	83
6627.54	Fe I	4.55	−1.58	19	32	27	25	38	···	···	···	···	21	17
6633.75	Fe I	4.79	−0.80	···	···	···	···	···	···	···	···	···	···	···
6643.63	Ni I	1.68	−2.01	···	159	161	190	164	···	···	134	75	159	151
6645.12	Eu II	1.37	+0.20	21	23	9	···	24	···	···	14	7	22	21
6646.96	Fe I	2.61	−3.96	···	···	43	43	61	···	···	9	···	24	18
6648.12	Fe I	1.01	−5.92	···	73	···	82	83	···	···	21	···	52	51
6677.99	Fe I	2.69	−1.35	171	202	177	208	···	···	···	164	···	180	···
6696.03	Al I	3.14	−1.57	synth	synth	synth	synth	synth	···	···	synth	synth	synth	synth
6698.66	Al I	3.14	−1.89	synth	synth	synth	synth	synth	···	···	···	···	···	synth
6703.57	Fe I	2.76	−3.01	63	···	64	80	93	···	···	34	17	67	75
6710.32	Fe I	1.48	−4.83	59	104	82	107	122	···	···	42	13	65	64
6717.68	Ca I	2.71	−0.61	···	···	···	···	···	···	···	81	60	···	···
6726.67	Fe I	4.61	−1.07	26	···	···	···	···	···	···	···	···	34	24
6733.15	Fe I	4.64	−1.48	···	22	···	21	···	···	···	···	···	···	···
6739.52	Fe I	1.56	−4.79	38	···	···	···	···	···	···	25	···	57	48
6743.12	Ti I	0.90	−1.65	···	···	82	183	164	···	···	40	···	121	100
6774.27	La II	0.13	−1.75	64	161	75	91	101	···	···	18	10	41	55

Table 2e. Linelist and Equivalent Widths

λ (Å)	Element	E.P. (eV)	log gf	51132	54022	54105	55101	55111	55142	56040	57010	59036	59090	59094
6003.01	Fe I	3.88	−1.07	···	···	···	101	···	···	···	···	···	49	···
6007.32	Ni I	1.68	−3.35	···	···	···	···	···	···	···	···	···	···	···
6007.97	Fe I	4.65	−0.70	53	···	···	···	···	···	···	···	···	···	···
6008.57	Fe I	3.88	−0.94	114	···	···	···	···	···	···	···	···	···	···
6015.25	Fe I	2.22	−4.66	22	···	···	25	···	···	···	7	···	···	···
6024.07	Fe I	4.55	−0.06	123	135	120	119	91	···	56	82	74	65	39
6027.06	Fe I	4.07	−1.14	85	112	84	88	54	···	31	51	27	45	···
6035.35	Fe I	4.29	−2.56	···	···	···	···	···	···	···	···	···	···	···
6056.01	Fe I	4.73	−0.44	75	84	58	62	45	···	25	48	26	32	···
6064.63	Ti I	1.05	−1.92	111	112	100	78	54	103	9	47	13	13	···
6065.49	Fe I	2.61	−1.51	202	200	191	···	168	203	122	164	132	131	92
6078.50	Fe I	4.79	−0.34	73	···	···	73	46	73	23	39	···	33	···
6079.02	Fe I	4.65	−1.06	58	71	58	62	26	···	9	22	···	13	···
6082.72	Fe I	2.22	−3.61	110	122	110	88	77	102	21	67	29	36	···
6084.11	Fe II	3.20	−3.87	···	···	···	···	17	···	···	···	···	···	···
6086.29	Ni I	4.26	−0.54	40	51	34	41	18	47	7	22	15	13	···
6089.57	Fe I	5.02	−0.92	···	···	···	40	···	···	···	···	···	···	···
6091.18	Ti I	2.27	−0.42	88	108	68	75	30	67	···	30	···	12	···
6094.38	Fe I	4.65	−1.66	15	29	23	23	···	20	···	8	···	···	···
6096.67	Fe I	3.98	−1.88	46	59	51	38	28	40	···	26	10	9	···
6102.18	Fe I	4.83	−0.37	92	104	81	77	63	84	27	52	34	32	···
6102.73	Ca I	1.88	−0.81	221	248	219	199	···	···	110	156	131	136	81

Table 2e—Continued

λ (Å)	Element	E.P. (eV)	log gf	51132	54022	54105	55101	55111	55142	56040	57010	59036	59090	59094
6108.13	Ni I	1.68	−2.51	149	152	135	128	119	148	63	106	73	73	···
6111.08	Ni I	4.09	−0.89	52	···	40	···	18	···	11	···	···	14	···
6120.25	Fe I	0.91	−5.95	56	75	59	···	38	64	···	36	12	16	···
6121.01	Ti I	1.88	−1.32	64	99	32	34	17	44	···	16	···	9	···
6122.23	Ca I	1.89	−0.26	304	364	260	245	216	264	142	194	162	159	115
6126.22	Ti I	1.07	−1.42	162	173	126	116	98	138	23	81	26	35	···
6128.98	Ni I	1.68	−3.36	86	107	92	80	65	94	24	59	23	34	···
6146.24	Ti I	1.87	−1.51	···	···	45	46	···	···	···	···	···	···	···
6149.25	Fe II	3.89	−2.78	···	28	···	···	26	30	23	···	···	25	···
6151.62	Fe I	2.18	−3.33	124	120	112	···	94	111	43	91	57	58	29
6154.23	Na I	2.10	−1.57	118	153	104	108	20	106	···	12	16	15	···
6157.73	Fe I	4.07	−1.22	···	···	···	···	71	···	28	72	45	42	···
6160.75	Na I	2.10	−1.27	143	143	110	121	30	121	···	29	28	16	···
6161.30	Ca I	2.52	−1.28	···	···	···	···	84	···	33	79	46	51	···
6162.18	Ca I	1.90	−0.07	316	344	267	257	224	286	157	212	189	166	136
6165.36	Fe I	4.14	−1.51	75	90	72	66	49	59	10	28	15	19	···
6166.44	Ca I	2.52	−1.11	147	155	130	122	97	136	34	79	46	45	26
6169.04	Ca I	2.52	−0.69	159	171	141	158	111	152	53	105	68	73	39
6169.56	Ca I	2.52	−0.42	190	205	180	166	134	169	83	121	86	95	60
6173.34	Fe I	2.22	−2.89	133	155	149	144	128	149	80	113	84	83	44
6175.37	Ni I	4.09	−0.55	58	63	53	41	29	49	20	34	13	22	···
6176.82	Ni I	4.09	−0.42	68	76	54	53	46	57	17	40	27	25	···

Table 2e—Continued

λ (Å)	Element	E.P. (eV)	log gf	51132	54022	54105	55101	55111	55142	56040	57010	59036	59090	59094
6177.25	Ni I	1.83	−3.53	61	72	51	45	30	60	15	32	15	13	···
6180.21	Fe I	2.73	−2.66	131	119	110	106	78	107	42	78	45	51	28
6186.72	Ni I	4.11	−0.96	22	30	16	33	···	20	···	17	7	···	···
6188.00	Fe I	3.94	−1.69	69	88	59	77	30	79	14	38	16	16	15
6200.32	Fe I	2.61	−2.41	150	149	124	129	114	135	69	111	68	83	50
6210.67	Sc I	0.00	−1.53	103	137	78	56	···	80	···	27	11	14	···
6219.29	Fe I	2.20	−2.42	···	174	168	···	156	···	95	140	106	112	81
6226.74	Fe I	3.88	−2.19	34	···	22	···	···	···	···	···	···	···	···
6229.23	Fe I	2.84	−3.00	88	102	78	77	58	87	···	41	24	25	···
6232.65	Fe I	3.65	−1.23	129	155	113	128	90	134	54	83	59	59	···
6546.24	Fe I	2.76	−1.65	···	···	···	···	···	···	···	135	112	121	···
6551.68	Fe I	0.99	−5.77	···	···	···	···	···	···	···	38	···	···	···
6554.23	Ti I	1.44	−1.16	···	161	···	92	59	···	···	44	28	29	···
6556.07	Ti I	1.46	−1.10	117	127	···	···	80	106	···	54	···	16	···
6559.57	Ti II	2.05	−2.30	44	···	···	50	59	···	32	50	35	28	···
6574.25	Fe I	0.99	−5.02	132	···	115	113	99	120	43	92	44	42	···
6586.31	Ni I	1.95	−2.81	83	95	78	84	70	···	35	63	···	38	···
6592.92	Fe I	2.73	−1.52	200	225	200	203	166	204	···	143	···	128	···
6593.88	Fe I	2.43	−2.42	179	···	169	169	141	157	96	138	100	···	···
6597.57	Fe I	4.79	−0.95	···	···	···	···	···	···	···	21	···	11	···
6604.60	Sc II	1.36	−1.48	···	···	···	···	···	66	44	···	67	44	···
6606.97	Ti II	2.06	−2.79	···	···	···	···	14	···	···	26	···	···	···

Table 2e—Continued

λ (Å)	Element	E.P. (eV)	log gf	51132	54022	54105	55101	55111	55142	56040	57010	59036	59090	59094
6608.04	Fe I	2.28	−3.96	73	77	···	···	48	···	···	45	···	···	···
6609.12	Fe I	2.56	−2.69	···	152	128	122	117	···	62	112	59	74	···
6625.02	Fe I	1.01	−5.37	···	···	···	···	90	···	···	70	···	37	···
6627.54	Fe I	4.55	−1.58	31	39	19	···	13	···	···	7	···	···	···
6633.75	Fe I	4.79	−0.80	···	···	···	···	···	···	···	···	···	···	···
6643.63	Ni I	1.68	−2.01	170	193	166	156	150	161	105	151	111	131	···
6645.12	Eu II	1.37	+0.20	26	34	18	18	8	42	9	12	12	8	···
6646.96	Fe I	2.61	−3.96	···	67	36	38	22	···	···	20	···	···	···
6648.12	Fe I	1.01	−5.92	86	···	···	···	51	···	···	32	···	10	···
6677.99	Fe I	2.69	−1.35	209	228	228	196	182	···	127	179	132	137	···
6696.03	Al I	3.14	−1.57	synth	synth	synth	synth	synth	synth	synth	synth	synth	···	···
6698.66	Al I	3.14	−1.89	synth	synth	synth	synth	synth	synth	···	synth	synth	···	···
6703.57	Fe I	2.76	−3.01	80	87	96	95	60	97	17	51	···	···	···
6710.32	Fe I	1.48	−4.83	112	···	114	···	63	···	···	45	25	···	···
6717.68	Ca I	2.71	−0.61	···	···	···	···	···	···	73	118	92	83	···
6726.67	Fe I	4.61	−1.07	···	···	···	···	···	···	7	15	···	···	···
6733.15	Fe I	4.64	−1.48	19	28	25	29	12	23	···	···	···	···	···
6739.52	Fe I	1.56	−4.79	···	···	89	···	44	···	17	35	···	···	···
6743.12	Ti I	0.90	−1.65	141	158	138	116	91	128	21	65	26	34	···
6774.27	La II	0.13	−1.75	155	161	88	90	44	111	14	62	10	23	···

Table 2f. Linelist and Equivalent Widths

λ (Å)	Element	E.P. (eV)	log gf	60066	63021	65046	66047	66054	69027	76038	77025	80029	81018	85027
6003.01	Fe I	3.88	−1.07	···	···	···	···	···	···	···	81	···	···	···
6007.32	Ni I	1.68	−3.35	···	···	···	···	···	···	···	···	···	···	···
6007.97	Fe I	4.65	−0.70	···	···	···	···	···	···	···	···	···	···	···
6008.57	Fe I	3.88	−0.94	···	···	···	···	···	···	···	···	···	···	···
6015.25	Fe I	2.22	−4.66	···	···	···	···	···	···	13	···	11	···	···
6024.07	Fe I	4.55	−0.06	74	71	39	89	···	···	106	72	76	···	62
6027.06	Fe I	4.07	−1.14	···	61	···	56	···	···	81	···	43	42	45
6035.35	Fe I	4.29	−2.56	···	···	···	···	···	···	···	···	···	···	···
6056.01	Fe I	4.73	−0.44	···	40	···	54	···	···	48	39	31	21	32
6064.63	Ti I	1.05	−1.92	26	24	···	52	···	121	84	29	14	13	20
6065.49	Fe I	2.61	−1.51	···	132	98	156	···	186	181	149	138	121	153
6078.50	Fe I	4.79	−0.34	···	34	30	57	···	74	55	46	36	31	36
6079.02	Fe I	4.65	−1.06	18	17	···	22	···	79	41	22	13	···	···
6082.72	Fe I	2.22	−3.61	···	···	···	73	···	95	105	60	52	22	54
6084.11	Fe II	3.20	−3.87	···	···	···	···	···	···	10	15	···	···	···
6086.29	Ni I	4.26	−0.54	···	15	···	17	···	33	33	15	14	···	13
6089.57	Fe I	5.02	−0.92	11	14	···	···	···	···	···	···	15	···	10
6091.18	Ti I	2.27	−0.42	25	18	···	31	···	102	69	15	12	···	···
6094.38	Fe I	4.65	−1.66	···	···	···	···	···	···	···	···	···	···	···
6096.67	Fe I	3.98	−1.88	···	18	···	···	···	46	33	22	···	···	22
6102.18	Fe I	4.83	−0.37	42	41	···	60	···	105	76	43	44	19	41
6102.73	Ca I	1.88	−0.81	134	122	95	167	···	219	195	145	134	137	152

Table 2f—Continued

λ (Å)	Element	E.P. (eV)	log gf	60066	63021	65046	66047	66054	69027	76038	77025	80029	81018	85027
6108.13	Ni I	1.68	−2.51	95	96	40	103	···	164	147	94	90	···	100
6111.08	Ni I	4.09	−0.89	···	17	···	···	···	···	30	9	···	···	14
6120.25	Fe I	0.91	−5.95	17	···	···	32	···	68	57	18	15	···	13
6121.01	Ti I	1.88	−1.32	···	···	···	15	···	58	62	8	14	···	13
6122.23	Ca I	1.89	−0.26	167	161	124	211	···	288	267	176	169	···	179
6126.22	Ti I	1.07	−1.42	62	44	···	···	···	164	144	59	49	21	58
6128.98	Ni I	1.68	−3.36	45	44	10	59	···	88	85	44	48	28	46
6146.24	Ti I	1.87	−1.51	···	···	···	···	···	···	39	···	···	···	···
6149.25	Fe II	3.89	−2.78	27	···	···	25	···	25	31	13	19	···	21
6151.62	Fe I	2.18	−3.33	···	55	···	82	···	137	115	76	72	43	68
6154.23	Na I	2.10	−1.57	···	···	···	33	···	131	37	10	13	18	20
6157.73	Fe I	4.07	−1.22	···	55	24	···	···	···	···	54	51	···	58
6160.75	Na I	2.10	−1.27	82	36	···	45	···	125	50	17	10	···	19
6161.30	Ca I	2.52	−1.28	89	62	20	94	···	···	122	58	61	35	65
6162.18	Ca I	1.90	−0.07	217	199	145	225	···	341	281	185	176	179	194
6165.36	Fe I	4.14	−1.51	51	20	19	42	···	67	59	20	23	···	27
6166.44	Ca I	2.52	−1.11	78	73	39	98	···	153	130	63	70	66	69
6169.04	Ca I	2.52	−0.69	115	95	44	133	···	173	141	89	86	66	95
6169.56	Ca I	2.52	−0.42	108	109	80	133	···	201	173	108	106	90	111
6173.34	Fe I	2.22	−2.89	113	91	···	110	···	172	129	105	100	72	92
6175.37	Ni I	4.09	−0.55	···	28	···	21	···	···	49	19	20	···	16
6176.82	Ni I	4.09	−0.42	50	36	18	···	···	78	70	27	34	31	34

Table 2f—Continued

λ (Å)	Element	E.P. (eV)	log gf	60066	63021	65046	66047	66054	69027	76038	77025	80029	81018	85027
6177.25	Ni I	1.83	−3.53	40	···	···	···	···	62	60	21	···	24	16
6180.21	Fe I	2.73	−2.66	90	61	40	91	···	···	109	66	59	65	65
6186.72	Ni I	4.11	−0.96	···	16	···	···	···	24	33	···	···	···	···
6188.00	Fe I	3.94	−1.69	39	34	···	43	···	79	61	30	29	···	···
6200.32	Fe I	2.61	−2.41	99	95	57	106	···	138	125	105	89	61	88
6210.67	Sc I	0.00	−1.53	···	18	···	32	···	···	68	18	···	···	···
6219.29	Fe I	2.20	−2.42	···	109	83	···	···	165	165	129	124	118	133
6226.74	Fe I	3.88	−2.19	···	···	···	32	···	48	31	21	14	···	···
6229.23	Fe I	2.84	−3.00	···	36	···	65	···	77	81	33	31	···	45
6232.65	Fe I	3.65	−1.23	75	···	36	···	···	126	116	75	70	48	74
6546.24	Fe I	2.76	−1.65	···	114	···	158	···	···	162	129	137	98	144
6551.68	Fe I	0.99	−5.77	···	···	···	···	···	···	···	23	···	···	···
6554.23	Ti I	1.44	−1.16	···	···	···	···	···	···	96	32	···	···	···
6556.07	Ti I	1.46	−1.10	···	···	···	51	···	···	108	38	···	···	···
6559.57	Ti II	2.05	−2.30	···	45	···	42	···	···	58	38	···	34	···
6574.25	Fe I	0.99	−5.02	51	52	···	···	53	···	123	81	67	···	90
6586.31	Ni I	1.95	−2.81	···	···	···	75	···	94	104	···	65	49	74
6592.92	Fe I	2.73	−1.52	···	121	···	164	141	186	199	154	152	···	···
6593.88	Fe I	2.43	−2.42	···	···	···	130	99	···	160	132	118	85	123
6597.57	Fe I	4.79	−0.95	···	···	···	···	···	···	23	12	···	···	···
6604.60	Sc II	1.36	−1.48	···	···	···	46	···	···	···	46	58	···	55
6606.97	Ti II	2.06	−2.79	···	22	···	···	21	···	43	21	···	···	···

Table 2f—Continued

λ (Å)	Element	E.P. (eV)	log gf	60066	63021	65046	66047	66054	69027	76038	77025	80029	81018	85027
6608.04	Fe I	2.28	−3.96	···	···	···	57	24	···	···	25	34	···	34
6609.12	Fe I	2.56	−2.69	···	···	···	89	61	137	122	···	89	51	74
6625.02	Fe I	1.01	−5.37	···	44	···	···	24	···	···	49	41	···	49
6627.54	Fe I	4.55	−1.58	···	···	···	···	···	···	31	···	···	···	···
6633.75	Fe I	4.79	−0.80	···	···	···	···	···	···	···	···	···	···	···
6643.63	Ni I	1.68	−2.01	135	···	···	···	113	180	185	142	137	119	142
6645.12	Eu II	1.37	+0.20	20	13	···	14	9	16	18	10	7	17	11
6646.96	Fe I	2.61	−3.96	···	13	···	25	···	···	33	11	···	···	···
6648.12	Fe I	1.01	−5.92	···	14	···	36	···	···	49	22	19	11	25
6677.99	Fe I	2.69	−1.35	···	141	···	···	138	229	···	175	···	125	165
6696.03	Al I	3.14	−1.57	synth	synth	···	synth	synth	synth	synth	synth	synth	synth	synth
6698.66	Al I	3.14	−1.89	synth	synth	···	synth	synth	synth	synth	synth	synth	synth	···
6703.57	Fe I	2.76	−3.01	···	44	···	53	···	100	73	40	39	···	47
6710.32	Fe I	1.48	−4.83	···	40	···	···	27	···	74	38	33	35	42
6717.68	Ca I	2.71	−0.61	···	101	···	···	···	···	···	···	101	···	···
6726.67	Fe I	4.61	−1.07	···	···	···	···	13	···	35	···	24	···	15
6733.15	Fe I	4.64	−1.48	···	···	···	27	···	···	26	···	···	···	13
6739.52	Fe I	1.56	−4.79	24	···	···	···	···	···	68	46	27	···	···
6743.12	Ti I	0.90	−1.65	···	41	···	79	29	137	141	47	50	26	···
6774.27	La II	0.13	−1.75	63	44	···	26	···	129	65	36	24	21	48

Table 3. Derived Abundances

Star LEID	[FeI/H]	[FeII/H]	[Fe/H] Avg.	[NaI/Fe]	[AlI/Fe]	[CaI/Fe]	[ScI/Fe]	[ScII/Fe]	[Sc/Fe] Avg.	[TiI/Fe]	[TiII/Fe]	[Ti/Fe] Avg.	[NiI/Fe]	[LaII/Fe]	[EuII/Fe]
9	−1.47	−1.34	−1.41	−0.08	+0.06	+0.26	−0.07	+0.21	+0.07	+0.08	−0.03	+0.03	−0.06	−0.41	−0.41
6017	−1.41	−1.03	−1.22	+0.36	+1.01	+0.20	···	···	···	−0.07	−0.13	−0.10	−0.21	+0.89	−0.16
12013	−1.37	−1.24	−1.31	+0.36	+0.24	+0.40	−0.10	···	−0.10	+0.21	+0.20	+0.21	−0.03	+0.29	−0.46
15023	−1.87	−1.73	−1.80	−0.50	+0.18	+0.20	···	+0.12	+0.12	+0.04	+0.38	+0.21	−0.04	−0.03	−0.21
16015	−1.83	−1.76	−1.80	−0.66	+0.13	+0.30	···	···	···	+0.16	+0.30	+0.23	−0.10	+0.15	+0.18
17015	−1.82	···	−1.82	···	···	+0.38	···	+0.39	+0.39	+0.09	+0.23	+0.16	−0.07	−0.07	+0.02
19062	−1.70	−1.80	−1.75	+0.07	···	+0.46	+0.27	···	+0.27	+0.21	+0.45	+0.33	+0.04	+0.58	+0.27
22037	−1.88	−1.63	−1.76	−0.09	+0.82	+0.23	···	+0.11	+0.11	+0.07	+0.23	+0.15	−0.11	−0.40	+0.30
23061	−1.71	−1.60	−1.66	−0.29	···	+0.24	···	···	···	+0.08	···	+0.08	−0.17	−0.29	+0.11
24027	−1.57	···	−1.57	+0.43	+1.18	+0.44	···	+0.18	+0.18	+0.23	+0.24	+0.23	+0.03	+0.36	+0.25
24056	−1.78	−1.82	−1.80	+0.16	+0.40	+0.38	+0.19	+0.32	+0.25	+0.10	+0.42	+0.26	+0.04	−0.19	+0.54
25026	−1.80	−1.86	−1.83	···	+0.39	+0.36	···	···	···	+0.60	···	+0.60	−0.02	+0.09	+0.45
26022	−1.75	···	−1.75	+0.23	+0.94	+0.47	···	···	···	+0.41	+0.29	+0.35	+0.08	+0.10	+0.43
26086	−1.13	···	−1.13	+1.04	+0.86	+0.50	−0.03	+0.07	+0.02	+0.31	−0.11	+0.10	−0.09	+0.77	−0.17
28092	−1.61	···	−1.61	+0.10	···	+0.24	···	···	···	+0.04	···	+0.04	−0.18	+0.88	···
30013	−1.33	···	−1.33	+0.59	+1.08	+0.37	···	···	···	+0.23	−0.08	+0.07	+0.00	+1.36	+0.04
32169	−0.91	···	−0.91	+0.82	+0.66	+0.39	···	···	···	+0.10	···	+0.10	−0.07	+0.90	+0.34
32171	−1.57	−1.38	−1.48	+0.41	+1.12	+0.36	+0.04	···	+0.04	+0.05	−0.12	−0.03	−0.06	+1.74	+0.39
33099	−1.18	···	−1.18	+0.57	+1.13	+0.25	−0.14	+0.31	+0.08	+0.16	···	+0.16	−0.13	+0.88	+0.40
34029	−1.37	−1.15	−1.26	+0.36	+0.31	+0.36	−0.21	···	−0.21	+0.20	+0.48	+0.34	−0.16	+0.65	+0.14
34225	−1.20	···	−1.20	···	+0.84	···	···	+0.31	+0.31	−0.08	+0.21	+0.06	−0.34	+1.10	+0.61
35172	−1.22	···	−1.22	+0.67	+1.16	+0.46	−0.01	+0.18	+0.08	+0.15	···	+0.15	−0.05	+1.15	+0.08
35201	−1.20	···	−1.20	+0.71	+0.99	+0.34	−0.01	+0.16	+0.07	+0.21	···	+0.21	−0.05	+0.86	+0.49
36282	−1.82	···	−1.82	+0.25	+0.03	+0.27	···	+0.14	+0.14	+0.17	···	+0.17	−0.02	+0.15	+0.11
38198	−1.54	−1.51	−1.53	+0.37	+1.22	+0.36	−0.21	···	−0.21	+0.17	···	+0.17	+0.04	+1.01	+0.49
38232	−1.49	−1.41	−1.45	−0.03	+0.26	+0.31	−0.28	+0.33	+0.02	+0.20	+0.19	+0.19	−0.05	+0.46	+0.18
39026	−1.54	−1.43	−1.49	+0.11	+0.17	+0.40	−0.09	···	−0.09	+0.32	+0.36	+0.34	−0.06	+0.58	+0.06
39048	−0.98	···	−0.98	+0.94	+0.66	+0.47	+0.40	+0.22	+0.31	+0.41	···	+0.41	−0.04	+1.66	+0.42
39129	−1.32	···	−1.32	···	+0.00	···	···	+0.24	+0.24	···	···	···	−0.16	+0.56	+0.14
39392	−0.91	···	−0.91	+0.93	+0.71	+0.37	+0.08	···	+0.08	+0.29	+0.27	+0.28	−0.10	+0.53	+0.46
41033	−1.09	···	−1.09	+0.87	+0.83	+0.32	−0.08	···	−0.08	+0.27	···	+0.27	+0.01	+0.80	+0.04
42508	−1.68	−1.48	−1.58	+0.06	−0.12	+0.31	···	···	···	+0.07	+0.07	+0.07	−0.09	+0.51	+0.29
43061	−0.93	···	−0.93	+0.78	+0.61	+0.32	−0.07	···	−0.07	+0.09	−0.02	+0.03	−0.12	+0.68	+0.15
43389	−1.41	−1.39	−1.40	+0.20	+0.21	+0.42	···	+0.04	+0.04	+0.41	···	+0.41	−0.08	+0.90	+0.39

Table 3—Continued

Star LEID	[FeI/H]	[FeII/H]	[Fe/H] Avg.	[NaI/Fe]	[AlI/Fe]	[CaI/Fe]	[ScI/Fe]	[ScII/Fe]	[Sc/Fe] Avg.	[TiI/Fe]	[TiII/Fe]	[Ti/Fe] Avg.	[NiI/Fe]	[LaII/Fe]	[EuII/Fe]
45358	−1.03	···	−1.03	+0.86	+0.86	+0.43	−0.04	···	−0.04	+0.29	+0.00	+0.15	+0.00	+2.03	+0.22
45485	−1.06	···	−1.06	+0.81	+0.82	+0.41	+0.11	···	+0.11	+0.13	+0.10	+0.11	+0.06	+1.00	−0.12
46121	−1.07	−0.85	−0.96	+0.08	−0.02	+0.21	−0.23	+0.16	−0.04	+0.33	+0.36	+0.34	+0.04	+0.79	···
47215	−0.77	···	−0.77	+0.70	+0.57	+0.26	···	···	···	+0.39	···	+0.39	−0.04	+1.02	+0.15
48116	−0.86	···	−0.86	+0.98	···	+0.56	+0.30	···	+0.30	+0.53	···	+0.53	+0.07	···	···
48323	−0.75	···	−0.75	+0.71	···	+0.33	+0.15	···	+0.15	+0.40	···	+0.40	+0.04	···	···
49013	−1.61	···	−1.61	−0.04	+0.41	+0.26	+0.09	+0.33	+0.21	+0.17	+0.37	+0.27	+0.03	+0.14	+0.27
49037	−1.77	−1.77	−1.77	−0.26	+0.67	+0.45	···	···	···	+0.48	···	+0.48	+0.00	+0.28	+0.26
51021	−1.50	−1.31	−1.41	−0.04	+0.21	+0.30	···	···	···	+0.21	+0.39	+0.30	−0.06	+0.25	+0.24
51080	−1.48	···	−1.48	+0.08	+0.29	+0.42	−0.08	···	−0.08	+0.32	+0.24	+0.28	+0.00	+0.59	+0.33
51132	−1.11	···	−1.11	+1.01	+0.93	+0.42	+0.03	···	+0.03	+0.30	+0.06	+0.18	+0.00	+1.78	+0.31
54022	−0.69	−0.63	−0.66	+0.89	+0.57	+0.32	+0.19	···	+0.19	+0.28	···	+0.28	−0.07	+1.85	+0.24
54105	−1.18	···	−1.18	+0.82	+1.01	+0.34	−0.10	···	−0.10	+0.23	···	+0.23	−0.07	+0.88	+0.13
55101	−1.00	···	−1.00	+0.90	+0.98	+0.32	−0.21	···	−0.21	+0.20	+0.07	+0.14	−0.15	+1.00	+0.05
55111	−1.52	−1.36	−1.44	+0.03	+0.35	+0.29	···	···	···	+0.16	+0.13	+0.14	−0.14	+0.38	−0.22
55142	−1.13	−1.10	−1.12	+0.91	+0.99	+0.42	+0.05	+0.00	+0.03	+0.30	···	+0.30	−0.06	+1.16	+0.51
56040	−1.86	−1.65	−1.76	···	+0.05	+0.17	···	+0.14	+0.14	+0.13	+0.13	+0.13	−0.06	+0.15	+0.14
57010	−1.62	···	−1.62	+0.10	+0.47	+0.39	−0.03	···	−0.03	+0.27	+0.39	+0.33	+0.04	+0.82	+0.13
59036	−1.75	···	−1.75	+0.48	+1.10	+0.44	+0.28	+0.54	+0.41	+0.26	+0.21	+0.24	−0.01	+0.02	+0.33
59090	−1.73	−1.54	−1.64	+0.19	···	+0.28	+0.17	+0.06	+0.12	+0.13	−0.05	+0.04	−0.09	+0.26	+0.01
59094	−1.85	···	−1.85	···	···	+0.25	···	···	···	···	···	···	···	···	···
60066	−1.24	−1.34	−1.29	+0.94	+1.37	+0.44	···	···	···	+0.47	···	+0.47	+0.16	+1.02	+0.41
63021	−1.42	···	−1.42	+0.32	+0.41	+0.44	+0.27	···	+0.27	+0.24	+0.33	+0.29	+0.07	+0.83	+0.26
65046	−1.69	···	−1.69	···	···	+0.31	···	···	···	···	···	···	−0.19	···	···
66047	−1.24	−1.27	−1.26	+0.25	+0.32	+0.51	+0.06	−0.04	+0.01	+0.20	+0.10	+0.15	−0.17	+0.19	+0.08
66054	−1.71	···	−1.71	···	+1.02	···	···	···	···	+0.13	+0.32	+0.23	−0.17	···	+0.09
69027	−0.86	−0.92	−0.89	+0.91	+0.49	+0.48	···	···	···	+0.45	···	+0.45	+0.00	+1.53	+0.05
76038	−1.32	−1.25	−1.29	+0.11	+0.29	+0.46	−0.07	···	−0.07	+0.38	+0.46	+0.42	+0.13	+0.65	+0.16
77025	−1.65	−1.71	−1.68	+0.02	+0.41	+0.27	+0.02	+0.10	+0.06	+0.19	+0.27	+0.23	−0.06	+0.54	+0.11
80029	−1.66	−1.65	−1.66	−0.05	+0.44	+0.33	···	+0.31	+0.31	+0.15	···	+0.15	−0.01	+0.32	−0.05
85027	−1.64	−1.59	−1.62	+0.20	+0.33	+0.34	···	+0.22	+0.22	+0.25	···	+0.25	−0.05	+0.71	+0.13

Table 4. Abundance Sensitivity to Model Atmosphere Parameters

Element	$\Delta T_{eff}\pm100$ (K)	Δlog g±0.30 (cm s^{-2})	Δ[M/H]±0.30 (dex)	$\Delta V_t\pm0.30$ (km s^{-1})
		[Fe/H]≈–2.0		
Fe I	± 0.14	∓ 0.01	∓ 0.04	∓ 0.06
Fe II	∓ 0.02	± 0.11	± 0.06	∓ 0.01
Na I	± 0.08	∓ 0.03	∓ 0.03	± 0.00
Al I	± 0.07	∓ 0.02	∓ 0.03	∓ 0.02
Ca I	± 0.12	∓ 0.04	∓ 0.06	∓ 0.10
Ti I	± 0.19	∓ 0.03	∓ 0.05	∓ 0.01
Ti II	∓ 0.04	± 0.12	± 0.08	∓ 0.03
Sc I	± 0.21	∓ 0.01	∓ 0.06	± 0.00
Sc II	± 0.02	± 0.11	± 0.07	∓ 0.04
Ni I	± 0.14	± 0.01	∓ 0.03	∓ 0.04
La II	± 0.05	± 0.12	± 0.08	± 0.00
Eu II	± 0.01	± 0.11	± 0.07	± 0.00
		[Fe/H]≈–1.5		
Fe I	± 0.09	± 0.04	± 0.01	∓ 0.08
Fe II	∓ 0.06	± 0.15	± 0.08	∓ 0.01
Na I	± 0.09	∓ 0.02	∓ 0.02	∓ 0.01
Al I	± 0.08	∓ 0.01	∓ 0.02	∓ 0.01
Ca I	± 0.14	∓ 0.03	∓ 0.04	∓ 0.15
Ti I	± 0.19	± 0.00	∓ 0.04	∓ 0.04
Ti II	∓ 0.05	± 0.13	± 0.09	∓ 0.03
Sc I	± 0.24	± 0.01	∓ 0.02	∓ 0.01
Sc II	∓ 0.02	± 0.13	± 0.10	∓ 0.06
Ni I	± 0.05	± 0.05	± 0.03	∓ 0.06
La II	± 0.03	± 0.13	± 0.10	∓ 0.03
Eu II	∓ 0.02	± 0.13	± 0.10	± 0.00
		[Fe/H]≈–1.0		
Fe I	± 0.08	± 0.06	± 0.02	∓ 0.11
Fe II	∓ 0.13	± 0.18	± 0.11	∓ 0.03
Na I	± 0.11	∓ 0.01	∓ 0.04	∓ 0.08

Table 4—Continued

Element	$\Delta T_{eff}\pm100$ (K)	Δlog g±0.30 (cm s^{-2})	Δ[M/H]±0.30 (dex)	$\Delta V_t\pm0.30$ (km s^{-1})
Al I	$\pm$ 0.10	$\pm$ 0.00	$\mp$ 0.03	$\mp$ 0.08
Ca I	$\pm$ 0.15	$\mp$ 0.04	$\mp$ 0.02	$\mp$ 0.17
Ti I	$\pm$ 0.19	$\pm$ 0.00	$\mp$ 0.04	$\mp$ 0.08
Ti II	$\mp$ 0.05	$\pm$ 0.14	$\pm$ 0.10	$\mp$ 0.13
Sc I	$\pm$ 0.24	$\pm$ 0.01	$\mp$ 0.03	$\mp$ 0.04
Sc II	$\mp$ 0.02	$\pm$ 0.14	$\pm$ 0.11	$\mp$ 0.04
Ni I	$\pm$ 0.04	$\pm$ 0.07	$\pm$ 0.05	$\mp$ 0.09
La II	$\pm$ 0.05	$\pm$ 0.14	$\pm$ 0.09	$\mp$ 0.19
Eu II	$\mp$ 0.02	$\pm$ 0.13	$\pm$ 0.11	$\mp$ 0.01
		[Fe/H]$\approx$–0.5		
Fe I	$\pm$ 0.02	$\pm$ 0.05	$\pm$ 0.07	$\mp$ 0.14
Fe II	$\mp$ 0.19	$\pm$ 0.14	$\pm$ 0.17	$\mp$ 0.04
Na I	$\pm$ 0.10	$\mp$ 0.04	$\pm$ 0.00	$\mp$ 0.13
Al I	$\pm$ 0.09	$\mp$ 0.01	$\mp$ 0.01	$\mp$ 0.10
Ca I	$\pm$ 0.14	$\mp$ 0.06	$\pm$ 0.02	$\mp$ 0.15
Ti I	$\pm$ 0.16	$\pm$ 0.02	$\mp$ 0.01	$\mp$ 0.16
Ti II	$\pm$ 0.06	$\pm$ 0.15	$\pm$ 0.11	$\pm$ 0.14
Sc I	$\pm$ 0.21	$\pm$ 0.04	$\mp$ 0.02	$\mp$ 0.14
Sc II	$\pm$ 0.02	$\pm$ 0.16	$\pm$ 0.13	$\pm$ 0.05
Ni I	$\pm$ 0.00	$\pm$ 0.08	$\pm$ 0.09	$\mp$ 0.11
La II	$\pm$ 0.03	$\pm$ 0.11	$\pm$ 0.12	$\mp$ 0.26
Eu II	$\mp$ 0.02	$\pm$ 0.12	$\pm$ 0.12	$\mp$ 0.01

Table 5. Literature References for Figures 11–16

Object	Reference
Thin/Thick Disk	Bensby et al. (2003)
Thin/Thick Disk	Bensby et al. (2005)
Thin/Thick Disk	Fulbright et al. (2000)
Thin/Thick Disk	Fulbright et al. (2007)
Thin/Thick Disk	Reddy et al. (2003)
Thin/Thick Disk	Simmerer et al. (2004)
Halo	Fulbright et al. (2000)
Halo	Reddy et al. (2006)
Halo	Simmerer et al. (2004)
Bulge	McWilliam & Rich (1994)
Bulge	Fulbright et al. (2007)
Bulge	Lecureur et al. (2007)
Dwarf Spheroidals	Shetrone et al. (2001)
Dwarf Spheroidals	Shetrone et al. (2003)
Sagittarius Dwarf	Sbordone et al. (2007)
Globular Cluster (M4)	Ivans et al. (1999)
Globular Cluster (M5)	Ivans et al. (2001)
Globular Cluster (M13)	Sneden et al. (2004)
Globular Cluster (M13)	Johnson et al. (2005)
Globular Cluster (M15[a])	Sneden et al. (1997)
Globular Cluster (M68[a])	Lee et al. (2005)
Globular Cluster (M71)	Ramírez & Cohen (2002)
Globular Cluster (M80)	Cavallo et al. (2004)
Globular Cluster (47 Tuc)	Carretta et al. (2004)
Globular Cluster (47 Tuc)	James et al. (2004)
Globular Cluster (NGC 288)	Shetrone & Keane (2000)
Globular Cluster (NGC 362)	Shetrone & Keane (2000)

[a]These two clusters have had their measured [Fe/H] values shifted by +0.2 dex to fit in Figures 11–14. These shifts were not applied to the displayed [X/Fe] abundances.